



**Australian Government**  
**Bureau of Meteorology**

**The Centre for Australian Weather and Climate Research**  
A partnership between CSIRO and the Bureau of Meteorology



# Large-scale indicators of Australian East Coast Lows and associated extreme weather events

Andrew J. Dowdy, Graham A. Mills and Bertrand Timbal

**CAWCR Technical Report No. 037**

June 2011



[www.cawcr.gov.au](http://www.cawcr.gov.au)





# Large-scale indicators of Australian East Coast Lows and associated extreme weather events

Andrew J. Dowdy, Graham A. Mills and Bertrand Timbal

*The Centre for Australian Weather and Climate Research  
- a partnership between CSIRO and the Bureau of Meteorology*

**CAWCR Technical Report No. 037**

June 2011

ISSN: 1836-019X

National Library of Australia Cataloguing-in-Publication entry

Author: Andrew J. Dowdy, Graham A. Mills and Bertrand Timbal

Title: Large-scale indicators of Australian East Coast Lows and associated extreme weather events

ISBN: 978-1-921826-36-8 (Electronic Resource)

Series: CAWCR technical report; 37

Notes: Included bibliography references and index

Subjects: Climatic extremes--Australia--Observations.

Lows (Meteorology)--Environmental aspects--Pacific Coast (Australia)

Pacific Coast (Australia)--Climate--Observations.

Other Authors / Contributors: Day, K.A. (Editor)

Dewey Number: 551.6994

Enquiries should be addressed to:

A. Dowdy  
Centre for Australian Weather and Climate Research  
Bureau of Meteorology, GPO Box 1289, Melbourne, VIC, 3001  
A.Dowdy@bom.gov.au

## Copyright and Disclaimer

© 2011 CSIRO and the Bureau of Meteorology. To the extent permitted by law, all rights are reserved and no part of this publication covered by copyright may be reproduced or copied in any form or by any means except with the written permission of CSIRO and the Bureau of Meteorology.

CSIRO and the Bureau of Meteorology advise that the information contained in this publication comprises general statements based on scientific research. The reader is advised and needs to be aware that such information may be incomplete or unable to be used in any specific situation. No reliance or actions must therefore be made on that information without seeking prior expert professional, scientific and technical advice. To the extent permitted by law, CSIRO and the Bureau of Meteorology (including each of its employees and consultants) excludes all liability to any person for any consequences, including but not limited to all losses, damages, costs, expenses and any other compensation, arising directly or indirectly from using this publication (in part or in whole) and any information or material contained in it.

## Contents

List of Figures .....	ii
List of Tables .....	vi
Abstract.....	1
<b>1 Introduction .....</b>	<b>2</b>
<b>2 Data and methodology – objective identification of upper closed lows and associated extreme weather events .....</b>	<b>5</b>
<b>3 What constitutes an ECL event? .....</b>	<b>6</b>
<b>4 Spatial variability of the diagnostics.....</b>	<b>12</b>
4.1 Preferred positions of extreme values of the diagnostics .....	13
4.2 Extreme values of the diagnostics for days on which ECLs occurred.....	16
<b>5 Quantitative performance measures of the diagnostics.....</b>	<b>20</b>
5.1 Defining and matching events .....	21
5.2 Domain selection for ECL events .....	22
5.3 Domain selection for high impact events.....	25
5.4 Optimum performance statistics for ECL events .....	31
5.5 Optimum performance statistics for high impact events.....	33
<b>6 Seasonal variation .....</b>	<b>35</b>
<b>7 Conclusion and future directions .....</b>	<b>41</b>
<b>Acknowledgments .....</b>	<b>42</b>
<b>References.....</b>	<b>42</b>
<b>Appendix A - Preferred positions of extreme values of the diagnostics.....</b>	<b>45</b>
<b>Appendix B - Extreme values of the diagnostics.....</b>	<b>51</b>
B.1 Extreme values of the diagnostics for days on which ECLs occurred .....	51
B.2 Extreme values of the diagnostics for days on which strong wind events occurred..	57
B.3 Extreme values of the diagnostics for days on which heavy localised rainfall events occurred.....	66
B.4 Extreme values of the diagnostics for days on which heavy widespread rainfall events occurred.....	75
<b>Appendix C - Graphical performance measures.....</b>	<b>84</b>
<b>Appendix D - Tabular performance measures .....</b>	<b>90</b>

## LIST OF FIGURES

<b>Fig. 1</b>	The Pasha Bulker was grounded at Newcastle on 8 June 2007 (top left panel). Large-scale observed conditions at the time of the storm: geopotential height (non shaded red contours) and wind speed (shaded greyscale contours) at 300 hPa (top right panel), 400 hPa wind (shown as wind barbs) and isentropic potential vorticity (contour lines) overlaid on contrast-enhanced satellite imagery in the water-vapour channel (the dark areas correspond to dry air in the upper troposphere) (bottom left panel) and the simulation of low level wind speed and MSLP (bottom right panel). ....	3
<b>Fig. 2</b>	Time series during 2006 at 500 hPa of the three diagnostic quantities (the maximum magnitude within a geographic region): geostrophic vorticity (upper panel), isentropic potential vorticity (middle panel) and the forcing term (lower panel). Observed ECL events are shown as vertical dashed lines. The 90th percentile of each diagnostic quantity is shown by the horizontal dashed lines. ....	7
<b>Fig. 3</b>	An example of an event defined as a “hit” on 6 September 2006. Upper left – AWAP rainfall analysis for the 24-hours to 9am on 7 September 2006. Upper right shows the National Meteorological and Oceanographic Centre (NMOC) mean sea level pressure (MSLP) analysis for 1800 UTC 6 September 2006, while the lower panels show the IPV/wind (right) and the height/wind fields at 300 hPa (left) from the ERA Interim dataset for 1200 UTC 6 September 2006. ....	8
<b>Fig. 4</b>	As for Fig. 3, but for 13 November 2006 as an example of a “false alarm”. ....	9
<b>Fig. 5</b>	As for Fig. 3, but for 5 November 2006 as an example of a “miss”. ....	10
<b>Fig. 6</b>	Number of times that the minimum value of the 400 hPa geostrophic vorticity in the area displayed occurred at a particular location, using 6-hourly data from 1989-2006 (upper left) and normalised by the latitudinal average to remove latitudinal gradients (upper right). Number of times that the geostrophic vorticity exceeds its 90th percentile (lower left) and normalised by the average for that latitude to remove latitudinal gradients (lower right). X- and Y-axes show latitude and longitude, respectively. ....	14
<b>Fig. 7</b>	As for Fig. 6, but for IPV. ....	15
<b>Fig. 8</b>	As for Fig. 6, but for the forcing term. ....	16
<b>Fig. 9</b>	Number of times that the minimum value of the 400 hPa geostrophic vorticity in the area displayed occurred at a particular location, using all ECL event days, at six different time lags (from -4 days to +1 day) with respect to the ECL event day. X and Y axes show latitude and longitude, respectively. ....	18
<b>Fig. 10</b>	As for Fig. 9, but for isentropic potential vorticity. ....	19
<b>Fig. 11</b>	As for Fig. 9, but for the forcing term. ....	20
<b>Fig. 12</b>	CSI for different diagnostic box positions, for ECL events, with a 1-day running mean applied to the diagnostic. The different panels correspond to geostrophic vorticity (left column), IPV (middle column) and the forcing term (right column) at 500 hPa (upper row), 400 hPa (middle row) and 300 hPa (lower row). The x and y axis represent the longitude and latitude, respectively, of the centre of the diagnostic box (which has geographic dimensions of 15 degrees in longitude and 10.5 degrees in latitude). ....	23

<b>Fig. 13</b>	As for Fig. 12, but with a 2-day running mean applied to the diagnostic time series. ....	24
<b>Fig. 14</b>	As for Fig. 12, but for strong wind event days, with a 1-day running mean applied to the diagnostic.....	26
<b>Fig. 15</b>	As for Fig. 12, but for strong wind event days with a 2-day running mean applied to the diagnostic.....	27
<b>Fig. 16</b>	As for Fig. 12, but for days on which the maximum localised rainfall in the eastern seaboard was above 50 mm, with a 1-day running mean applied to the diagnostic.....	28
<b>Fig. 17</b>	As for Fig. 12, but for days on which the maximum localised rainfall in the eastern seaboard was above 50 mm, with a 2-day running mean applied to the diagnostic.....	29
<b>Fig. 18</b>	As for Fig. 12, but for days on which the total rainfall in the eastern seaboard was above its 90th percentile.....	30
<b>Fig. 19</b>	As for Fig. 12, but for days on which the total rainfall in the eastern seaboard was above its 90th percentile, with a 2-day running mean applied to the diagnostic.....	31
<b>Fig. 20</b>	Number of times that the minimum value of the 400 hPa geostrophic vorticity in the area displayed occurred at a particular location, using all ECL event days that occurred during summer (November-April), at six different time lags (from -4 days to +1 day) with respect to the ECL event day. X and Y axes show latitude and longitude, respectively. ....	36
<b>Fig. 21</b>	As for Fig. 20, but only using data for winter (May-October).....	37
<b>Fig. 22</b>	As for Fig. 13, but only using data for summer (November-April). ....	38
<b>Fig. 23</b>	As for Fig. 13, but only using data for winter (May-October).....	39
<b>Fig. A1</b>	As for Fig. 6, but for the 300 hPa geostrophic vorticity.....	45
<b>Fig. A2</b>	As for Fig. 6, but for the 500 hPa geostrophic vorticity.....	46
<b>Fig. A3</b>	As for Fig. 6, but for the 300 hPa IPV. ....	47
<b>Fig. A4</b>	As for Fig. 6, but for the 500 hPa IPV. ....	48
<b>Fig. A5</b>	As for Fig. 6, but for the 300 hPa forcing term.....	49
<b>Fig. A6</b>	As for Fig. 6, but for the 500 hPa forcing term.....	50
<b>Fig. B1</b>	As for Fig. 9, but for the 300 hPa geostrophic vorticity.....	51
<b>Fig. B2</b>	As for Fig. 9, but for the 500 hPa geostrophic vorticity.....	52
<b>Fig. B3</b>	As for Fig. 9, but for the 300 hPa IPV. ....	53
<b>Fig. B4</b>	As for Fig. 9, but for the 500 hPa IPV. ....	54
<b>Fig. B5</b>	As for Fig. 9, but for the 300 hPa forcing term.....	55
<b>Fig. B6</b>	As for Fig. 9, but for the 500 hPa forcing term.....	56

<b>Fig. B7</b>	As for Fig. 9, but for the 300 hPa geostrophic vorticity as an indicator of strong wind events. ....	57
<b>Fig. B8</b>	As for Fig. 9, but for the 400 hPa geostrophic vorticity as an indicator of strong wind events. ....	58
<b>Fig. B9</b>	As for Fig. 9, but for the 500 hPa geostrophic vorticity as an indicator of strong wind events. ....	59
<b>Fig. B10</b>	As for Fig. 9, but for the 300 hPa IPV as an indicator of strong wind events. ....	60
<b>Fig. B11</b>	As for Fig. 9, but for the 400 hPa IPV as an indicator of strong wind events. ....	61
<b>Fig. B12</b>	As for Fig. 9, but for the 500 hPa IPV as an indicator of strong wind events. ....	62
<b>Fig. B13</b>	As for Fig. 9, but for the 300 hPa forcing term as an indicator of strong wind events. ....	63
<b>Fig. B14</b>	As for Fig. 9, but for the 400 hPa forcing term as an indicator of strong wind events. ....	64
<b>Fig. B15</b>	As for Fig. 9, but for the 500 hPa forcing term as an indicator of strong wind events. ....	65
<b>Fig. B16</b>	As for Fig. 9, but for the 300 hPa geostrophic vorticity as an indicator of heavy localised rain events. ....	66
<b>Fig. B17</b>	As for Fig. 9, but for the 400 hPa geostrophic vorticity as an indicator of heavy localised rain events. ....	67
<b>Fig. B18</b>	As for Fig. 9, but for the 500 hPa geostrophic vorticity as an indicator of heavy localised rain events. ....	68
<b>Fig. B19</b>	As for Fig. 9, but for the 300 hPa IPV as an indicator of heavy localised rain events. ....	69
<b>Fig. B20</b>	As for Fig. 9, but for the 400 hPa IPV as an indicator of heavy localised rain events. ....	70
<b>Fig. B21</b>	As for Fig. 9, but for the 500 hPa IPV as an indicator of heavy localised rain events. ....	71
<b>Fig. B22</b>	As for Fig. 9, but for the 300 hPa forcing term as an indicator of heavy localised rain events. ....	72
<b>Fig. B23</b>	As for Fig. 9, but for the 400 hPa forcing term as an indicator of heavy localised rain events. ....	73
<b>Fig. B24</b>	As for Fig. 9, but for the 500 hPa forcing term as an indicator of heavy localised rain events. ....	74
<b>Fig. B25</b>	As for Fig. 9, but for the 300 hPa geostrophic vorticity as an indicator of heavy widespread rain events. ....	75
<b>Fig. B26</b>	As for Fig. 9, but for the 400 hPa geostrophic vorticity as an indicator of heavy widespread rain events. ....	76
<b>Fig. B27</b>	As for Fig. 9, but for the 500 hPa geostrophic vorticity as an indicator of heavy widespread rain events. ....	77
<b>Fig. B28</b>	As for Fig. 9, but for the 300 hPa IPV as an indicator of heavy widespread rain events. ....	78

<b>Fig. B29</b> As for Fig. 9, but for the 400 hPa IPV as an indicator of heavy widespread rain events. ....	79
<b>Fig. B30</b> As for Fig. 9, but for the 500 hPa IPV as an indicator of heavy widespread rain events. ....	80
<b>Fig. B31</b> As for Fig. 9, but for the 300 hPa forcing term as an indicator of heavy widespread rain events. ....	81
<b>Fig. B32</b> As for Fig. 9, but for the 400 hPa forcing term as an indicator of heavy widespread rain events. ....	82
<b>Fig. B33</b> As for Fig. 9, but for the 500 hPa forcing term as an indicator of heavy widespread rain events. ....	83
<b>Fig. C1</b> As for Fig. 13, but for strong wind events during summer. ....	84
<b>Fig. C2</b> As for Fig. 13, but for strong wind events during winter. ....	85
<b>Fig. C3</b> As for Fig. 13, but for heavy localised rainfall events during summer. ....	86
<b>Fig. C4</b> As for Fig. 13, but for heavy localised rainfall events during winter. ....	87
<b>Fig. C5</b> As for Fig. 13, but for heavy widespread rainfall events during summer. ....	88
<b>Fig. C6</b> As for Fig. 13, but for heavy widespread rainfall events during winter. ....	89

## LIST OF TABLES

<b>Table 1</b>	The correspondence between different event type pair combinations, including the ECL database, the strong wind event set, and the two heavy rain event sets. The values in the brackets represent the percentage fraction of the total number of type 1 events. ....	12
<b>Table 2</b>	Summary of diagnostic performance for ECL events, with a 2-day running mean applied to the diagnostic time series. The maximum CSI value is shown, with its corresponding number of hits, misses and false alarms. The latitude and longitude values shown represent the centre of the geographic box that produced the maximum CSI value for each diagnostic and pressure level. ....	32
<b>Table 3</b>	As for Table 2, but for extreme wind events.....	34
<b>Table 4</b>	As for Table 2, but for extreme localised rainfall.....	34
<b>Table 5</b>	As for Table 2, but for extreme widespread rainfall events.....	35
<b>Table 6</b>	As for Table 2, but only using data only for winter. ....	40
<b>Table 7</b>	As for Table 2, but only using data only for summer.....	40
<b>Table D1</b>	As for Table 2, but for strong wind events only using data for summer.....	90
<b>Table D2</b>	As for Table 2, but for strong wind events only using data for winter. ....	90
<b>Table D3</b>	As for Table 2, but for heavy localised rainfall events only using data for summer. .	91
<b>Table D4</b>	As for Table 2, but for heavy localised rainfall events only using data for winter. ....	91
<b>Table D5</b>	As for Table 2, but for heavy widespread rainfall events only using data for summer.....	92
<b>Table D6</b>	As for Table 2, but for heavy widespread rainfall events only using data for winter. ....	92

## **ABSTRACT**

Extra-tropical cyclones that develop near the east coast of Australia often have severe consequences such as flash flooding and damaging winds and seas, as well as beneficial consequences such as being responsible for heavy rainfall events that contribute significantly to total rainfall and runoff. There is subjective evidence that the development of most major events, commonly known as East Coast Lows, is associated with the movement of a high amplitude upper-tropospheric trough system over eastern Australia. This report examines a number of large-scale diagnostic quantities in the upper troposphere associated with east-coast cyclogenesis, based on the ECMWF interim reanalyses. Climatologies of these diagnostic quantities are examined and compared with a database of observed East Coast Low events in order to test this hypothesis. With a view to future impact-based studies, the diagnostics are also compared with severe weather events such as extreme rainfall and wind speeds. Diagnostic quantities based on geostrophic vorticity and isentropic potential vorticity are shown to provide a good indication of the likely occurrence of east-coast cyclogenesis, as well as associated impacts such as extreme rainfall events. Results are examined in relation to seasonal and geographic variations. The potential application of these diagnostics to global climate model simulations of past and future climates is also discussed.

# 1 INTRODUCTION

The term East Coast Low (ECL) is generally used in Australia to refer to a low-pressure system with closed cyclonic circulation at sea level that forms and/or intensifies in a maritime environment within the vicinity of the east coast of Australia (e.g. Speer et al. 2009), although it should also be noted that a range of secondary criteria are used in different studies. The most intense of these systems have many of the characteristics of the subtropical cyclones described by Simpson (1952) and Otkin and Martin (2004).

The hurricane-force winds, heavy rain and large seas and swells associated with many ECLs can cause major socio-economic impacts on eastern Australia. The extreme winds sometimes generated by ECLs pose a major hazard to marine activities and on-shore infrastructure, and large ocean waves combined with storm-surge can cause severe coastal erosion. The extreme rainfall events associated with ECLs frequently cause significant flash flooding near the coast, as well as major flooding in river systems with their headwaters in the Great Dividing Range. An example of such an ECL is that which occurred in early June 2007 near the city of Newcastle in New South Wales (NSW). This event caused extensive flooding, the grounding of the bulk coal-carrying ship the Pasha Bulker, ten deaths and insurance claims of around \$1.4 billion making it one of the most costly natural disasters in Australia's history.

ECLs do also, however, have beneficial outcomes. They are a critical source of rainfall for catchments east of the Great Dividing Range: e.g. Sydney's Warragamba catchment tends to replenish in bursts linked to extreme rainfall events such as ECLs (Pepler and Rakich 2010). The water supply implications of ECLs are not limited only to the coast, as large events can bring significant falls to the headwaters of western flowing rivers, particularly in the northeast of NSW.

Mills et al. (2010) present a detailed diagnostic analysis of the precursor environment and the mesoscale evolution of the Pasha Bulker storm, and some features of their analysis are shown in Fig. 1. Associated with that ECL were very heavy rainfall in a band extending inland from the NSW coast, a marked upper-tropospheric cut-off low and a strong jet streak over eastern Australia (top right panel), very strong patterns of Isentropic Potential Vorticity (IPV) and of IPV advection seen in NWP fields and confirmed by Water-Vapour (6.7  $\mu\text{m}$ ) channel satellite imagery (lower left panel), and storm-force low-level winds on the south side of the low (lower right panel). In that study, the authors also examined the synoptic-scale upper-tropospheric evolution that preceded the development of the intense surface low-pressure development for 11 other of the most damaging ECLs (Bureau of Meteorology - NSW Regional Forecasting Centre). The authors showed that for all of these lows a very similar evolution of the upper-tropospheric fields in their pre-development phase was evident, and suggested the following sequence of events in the upper-troposphere that can lead to the development of such ECLs.

- 48 to 72 hours prior to the explosive development, an upper-tropospheric split-jet, or blocking pattern, with a positively tilted trough or cut-off low over south-eastern Australia is established.
- The upstream trough over the Indian Ocean amplifies, followed by downstream amplification of the ridge south of Australia.
- The next stage of this energy-dispersion process is the development of a southerly jet streak on the western side of the positively tilted trough over eastern Australia.

- As this southerly jet streak propagates towards the apex of the trough (lower latitudes), the trough/cut-off low deepens and begins to negatively tilt (towards the northeast) and move towards the coast.
- The northwesterly jet on the northeast flank of the upper cut-off low strengthens, becomes highly focussed, and a region of very strong cyclonic shear near its exit becomes located very close to the centre of the upper cut-off low. In this regard the pattern is very similar to that described by Risbey et al. (2009) for cut-off lows that lead to the heavier rainfall events over the cropping areas of southeastern Australia. The consequence of this evolution is a focussing of IPV advection on the northeast side of the cut-off low, which forces pressure falls at the surface.
- If/where low-level ingredients (such as baroclinicity, lesser static stability, more rapid growth rates, etc.) are suitable, explosive development (i.e. rapid intensification) of an ECL occurs.

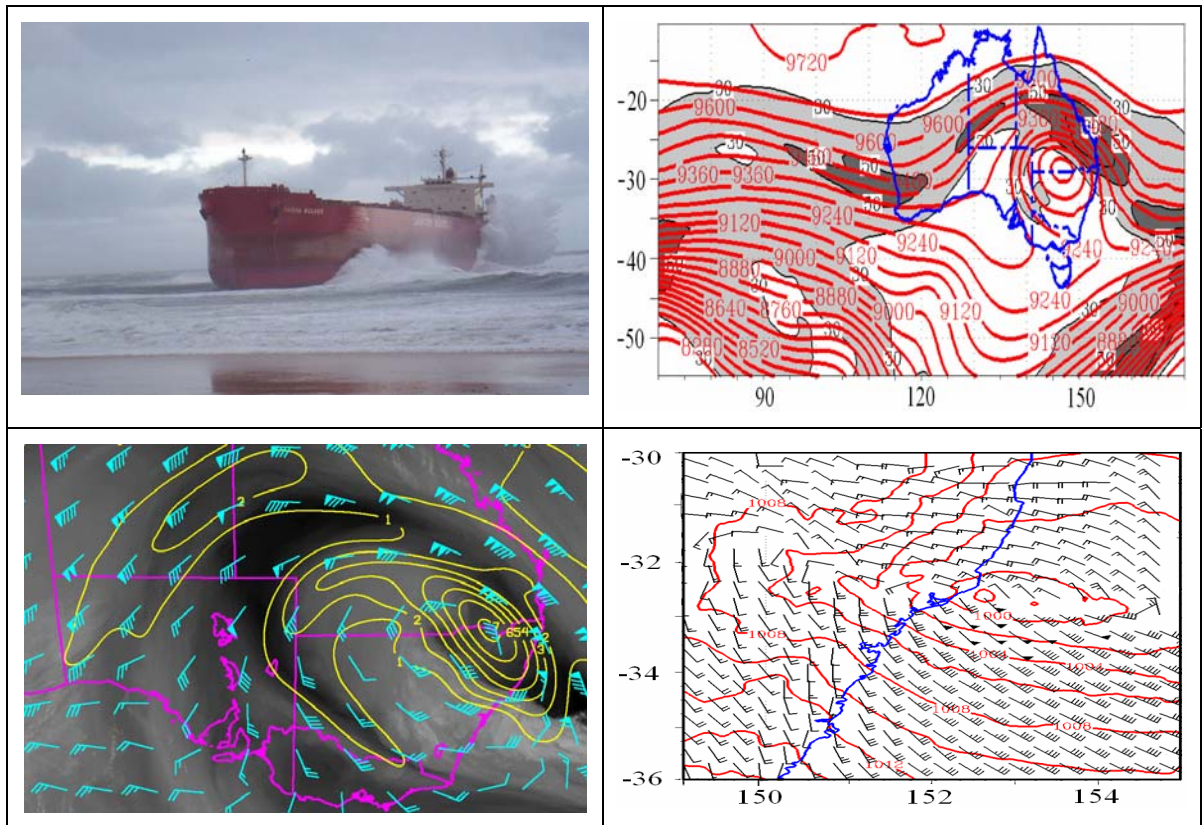


**Fig. 1** The Pasha Bulker was grounded at Newcastle on 8 June 2007 (top left panel). Large-scale observed conditions at the time of the storm: geopotential height (non shaded red contours) and wind speed (shaded greyscale contours) at 300 hPa (top right panel), 400 hPa wind (shown as wind barbs) and isentropic potential vorticity (contour lines) overlaid on contrast-enhanced satellite imagery in the water-vapour channel (the dark areas correspond to dry air in the upper troposphere) (bottom left panel) and the simulation of low level wind speed and MSLP (bottom right panel).

While these events were selected prior to the development of this hypothesis, and all selected events were included in their analysis, the authors did note that this pattern was based on a selected set of major events. They also note that a broader climatological study would be needed to determine how generally applicable this model was to ECL development, and also to test for

frequency of null cases – how often does this upper-tropospheric evolution occur without an ECL development?

There is a relatively limited body of work on the climatology of ECLs. Hopkins and Holland (1990) presented a climatology of Australian east-coast cyclones from 1958 to 1992 based on MSLP analyses and rainfall observations, while Speer et al. (2009) recently produced a climatology of maritime cyclones in the vicinity of the east coast of Australia based on a synoptic typology using data from 1970 to 2006. These climatologies are purely surface-based, using semi-objective classification of MSLP analyses together with, in some cases, measures of observed coastal impacts such as rainfall or wind. While some studies have qualitatively described the upper-tropospheric wave/jet structures of particular events and noted the association with large-amplitude upper trough systems (Holland et al. 1987, Qi et al. 2006), hitherto no systematic studies of upper-tropospheric patterns associated with ECL occurrence have been presented.

For individual events, accurate forecasts of the precise locations and intensities of weather associated with ECLs are essential for community preparedness. For longer term planning, understanding of the climatological distribution of the surface lows and of the environments in which they occur, including interannual variability and long-term trends, is necessary if changes in their occurrence are to be assessed under future climate change scenarios. This knowledge is essential for planning mitigation of flooding and coastal erosion, and for water resources planning.

The region with the most uncertain future rainfall projections for the whole of Australia is Eastern Australia, centred on NSW (CSIRO and Bureau of Meteorology 2007). The high level of uncertainty in projections for this region is largely due to current General Circulation Model (GCM) simulations having model resolutions that are too coarse to resolve these frequently quite small-scale, albeit intense, ECL systems (Kuwano-Yoshida and Asuma 2008). However, if the hypothesis that large scale upper-tropospheric cut-off low developments are strongly associated with ECL developments, then changes in the environmental or dynamic influences associated with the large-scale upper-tropospheric evolutions may be identifiable in current or future climate change projections, and changes in the frequency of such upper-tropospheric cut-off lows (perhaps including large amplitude troughs) over eastern Australia might be used as a proxy for changes in frequency of ECL formation in coarse-resolution GCM simulations.

Before applying such an analysis to GCM simulations, the hypothesis developed above needs to be tested on reanalysis data, and this report presents the first stages of such a study. Using ERA-Interim reanalyses (Uppala et al. 2008), a 1989-2006 climatology of upper cut-off lows in Australian longitudes is developed, and compared with ECL occurrence during that period. Based on the considerations described above, a number of diagnostic quantities that might be used to identify upper-cut-off lows in reanalysis data were selected, including geostrophic vorticity, IPV, and a forcing term based on the advection by the geostrophic winds of the gradient of quasi-geostrophic potential vorticity (Bluestein 1992). The analysis includes determining the best geographic region over which to apply the diagnostics. A systematic comparison of these reanalysis event diagnostics with the ECL events in the Speer et al. (2009) database (hereafter referred to as the ‘ECL database’) is presented in this report. With a view to future impact-based studies, the diagnostics are also compared with severe weather event impact definitions based on extreme rainfall and high wind speed occurrences.

Chapter 2 reviews techniques by which upper-tropospheric lows can be identified from reanalysis data sets. An initial comparison is made between these diagnostic quantities and the ECL database events in Chapter 3, including a discussion on the relative merits of an impacts-based definition of an ECL event. The spatial variability of the diagnostics is presented in

Chapter 4. This is followed by a quantitative assessment of how well the diagnostics can predict the occurrence of an ECL (Chapter 5), including optimizing the geographic region over which the diagnostic is applied, and the seasonal variation in the results is examined (Chapter 6). These results are summarized and discussed in Chapter 7, where future research directions are also discussed.

## 2 DATA AND METHODOLOGY – OBJECTIVE IDENTIFICATION OF UPPER CLOSED LOWS AND ASSOCIATED EXTREME WEATHER EVENTS

As the basis for our climatology of the diagnostic quantities examined in this study, the publicly released ECMWF interim reanalysis dataset with 1.5° latitude-longitude grid is used (Uppala et al. 2008) (hereafter referred to as the ERA-Interim dataset). Six-hourly analyses from the ERA-Interim dataset are used in this study from 1989 (marking the start of the ECMWF interim reanalysis dataset) until the end of 2006 (which is currently the end of the ECL database).

The ECL database (Speer et al. 2009) is used to identify the occurrence of an ECL. It contains entries listing periods during which there was a closed surface low between 20°S and 40°S and between the NSW coastline and 160°E. While secondary criteria, such as severe wind speeds or rainfall, may be included in the database for some events, this study did not use this information, with ECL events being defined here by simply classing the period from the start to the end of each individual low as a single event. In order to assess the ability of the diagnostic quantities to identify strong wind speed and heavy rainfall events, the ERA-Interim dataset is also used to define strong wind speed events, while the Australian Water Availability Project (AWAP) rainfall analyses (Jones et al. 2009) are used to identify heavy rainfall events. These rainfall analyses have a 0.05° grid spacing in both latitude and longitude.

Three diagnostics are calculated at several levels from the ERA-Interim dataset at 6-hourly intervals and used in this study. The first diagnostic quantity is geostrophic vorticity,  $\xi$ , at the 500, 400, and 300 hPa pressure surfaces (Equation 1). Higher levels were not used as it was felt that these would lie above the tropopause for some of the year, and many of the major ECL presented in Mills et al. (2010) occur during the winter when the tropopause is generally lower (seasonal aspects will be addressed in later sections).

$$\xi = \frac{1}{f} \nabla^2 \Phi \quad (1)$$

where  $f$  is the Coriolis Parameter and  $\nabla^2 \Phi$  is the Laplacian of geopotential.

There are a very large number of climatologies of upper and surface cyclones reported in the literature. Prior to the availability of reanalysis data sets (Kalnay et al. 1996, Uppala et al. 2005) these were at least partly subjective and involved assessment of contoured analyses. Using reanalysis data sets, though, a number of objective climatologies have been published. These generally seek a local minimum in the geopotential height field, subject to threshold magnitudes of this local minimum relative to surrounding gridpoints, and often include secondary criteria such as the requirement for the zonal wind direction to reverse on the poleward side of the height minimum, or that the low system be “cold-cored”. The former of these criteria ensures that the low centre is “cut off” from the westerly mid-latitude winds, while the latter excludes systems originating in the tropics. Examples of such climatologies are presented in Pook et al.

(2006), Nieto et al. (2005) and Ndarana and Waugh (2010). Sinclair (1997), Keable et al. (2002) and Fuenzalida et al. (2005) also examined parameters such as the Laplacian of the geopotential height or the geostrophic vorticity, and again secondary criteria are often used.

The second diagnostic quantity examined in this study is the Isentropic Potential Vorticity (IPV) calculated on these same pressure surfaces. Cut-off lows are often accompanied by substantial tropopause depressions, and the conservative characteristics of IPV (Hoskins et al. 1985) make this an attractive quantity to use. However, it must be remembered that (1) the arguments about tropopause heights (above) can be interpreted in terms of the dynamic tropopause which can be defined in terms of a particular value of IPV, (2) IPV is not conserved along pressure surfaces as it is for adiabatic flow on isentropic surfaces, and (3) it is not the IPV anomaly itself that leads to lower-tropospheric development, but rather the differential advection of IPV (Hoskins et al. 1985, p911-912).

This last point led Mills et al. (2010) to calculate the forcing term of the pseudo-potential vorticity form of the quasi-geostrophic height tendency equation (following Bluestein, 1992, Eqn 5.8.15), hereafter referred to as the “forcing term”, and overlay this field on IPV and upper wind patterns in their case study, and for the case study of the Pasha Bulker storm this diagnostic subjectively appeared to provide a more focused relationship with low level development than did the patterns of IPV. Accordingly, this forcing term is calculated as the third diagnostic quantity used here in this study, providing a measure of the differential advection of vorticity and being sensitive to spatial variations in static stability.

A particular decision made in this study was not to impose any additional criteria to select only closed lows, as some of the cases shown in Mills et al. (2010) had open troughs, although these were high amplitude troughs, and frequently showed very strong cyclonic shear on their northeast flank. Thus they would be expected to show maxima in the absolute magnitude of the three diagnostic quantities described above, although they would not necessarily be classed as cut-off lows. Dynamically, though, the forcings should be equivalent.

For each 6-hourly reanalysis, the value of each of these three diagnostic quantities was calculated at each reanalysis gridpoint between latitudes 15°S and 48°S, and longitudes 129°E and 174°E, with this area selected on the basis of the synoptic assessments presented in Mills et al. (2010). The extreme value of a diagnostic (i.e. minimum for geostrophic vorticity and IPV, since vorticity is negative for low pressure systems in the Southern Hemisphere, and maximum for the forcing term) within a specific geographic region is then used to examine the usefulness of the diagnostic in representing the occurrence of significant ECL events and associated severe weather events. The question of what threshold constitutes a significant event is of course open, and is addressed in the following section.

### **3 WHAT CONSTITUTES AN ECL EVENT?**

In the first instance, the ECL database (Speer et al. 2009), as described in the previous section, is compared with the diagnostic quantities. In order to determine the best way to match these ECL events with extreme values in the diagnostic quantities described above, we first plotted time-series of the extreme value (positive value for the forcing term and negative value for geostrophic vorticity and IPV) of these diagnostics in the geographic region from 141°E to 156°E and 25°S to 36°S (the specification of this geographic region is examined in detail in later sections of this study).

Such a time series for the calendar year 2006 is shown in Fig. 2, with the periods of ECL events shown as dashed vertical lines, with the longer duration events (e.g. events which lasted for

multiple days) appearing as wider lines. A 2-day running mean has been applied to each of the time series.

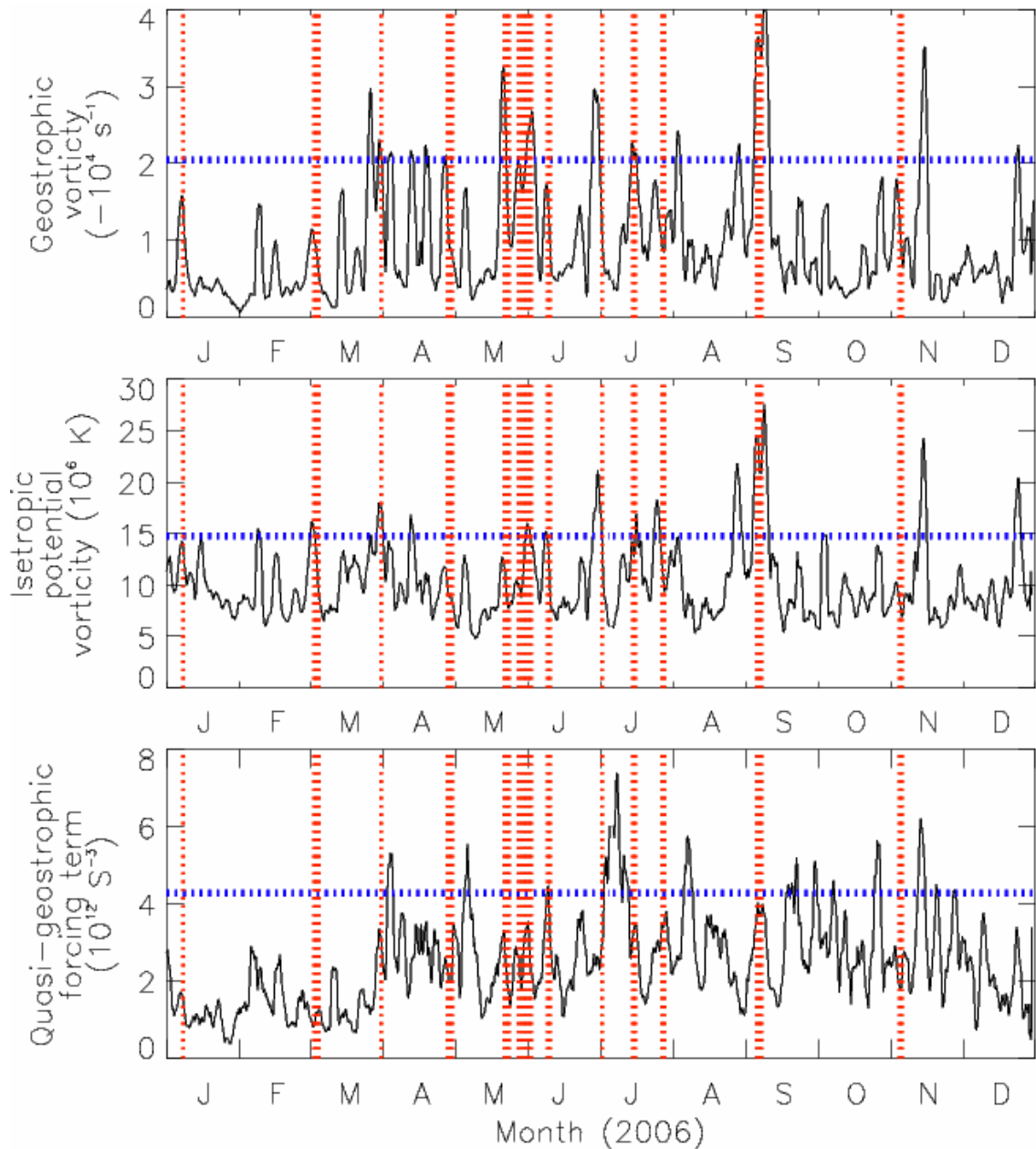


**Fig. 2** Time series during 2006 at 500 hPa of the three diagnostic quantities (the maximum magnitude within a geographic region): geostrophic vorticity (upper panel), isentropic potential vorticity (middle panel) and the forcing term (lower panel). Observed ECL events are shown as vertical dashed lines. The 90th percentile of each diagnostic quantity is shown by the horizontal dashed lines.

A visual assessment of this plot, and those for the other years in the sequence, suggested that the 90<sup>th</sup> percentile of each diagnostic, calculated for the period 1989-2006, provides a reasonable hit rate and false alarm rate (more quantitative contingency tables will be presented in a later section), and these 90<sup>th</sup> percentile values are shown as the horizontal dotted lines in Fig. 2. It is seen that there is a qualitatively good agreement between maxima in the diagnostic quantities and the ECL events, with the geostrophic vorticity and the IPV diagnostics appearing to better discriminate events than does the forcing term. However, there are significant numbers of

misses or false alarms. A closer examination of the hits, misses and false alarms was conducted on a case-by-case basis to better understand this behaviour and examples are presented in the following paragraphs.

The event of 6 September 2006 is an example of a “hit” in that it is correctly identified by the diagnostic quantities. In this case, all three diagnostics are above their 90<sup>th</sup> percentiles. Wind gusts of 109 km hr<sup>-1</sup> at Nobbys Head (Newcastle) and 96 km hr<sup>-1</sup> at Sydney Airport were recorded for this event. In Fig. 3 it is seen from the AWAP rainfall analysis (Fig. 3) that there was very heavy rainfall in the Sydney region. There was a surface low with several closed isobars just off the NSW coastline. An involted upper trough pattern is apparent, with a closed cyclonic circulation evident in the wind field over southeastern NSW, and a very marked IPV centre is apparent just a little northwest of the centre of the upper low. This offset is a result of the strong shear on the cyclonic side of the jet stream and is common to many of the major events described in Mills et al. (2010). This ECL event is an example of one that fits the conceptual model of upper-tropospheric precursors of a major impact ECL development.

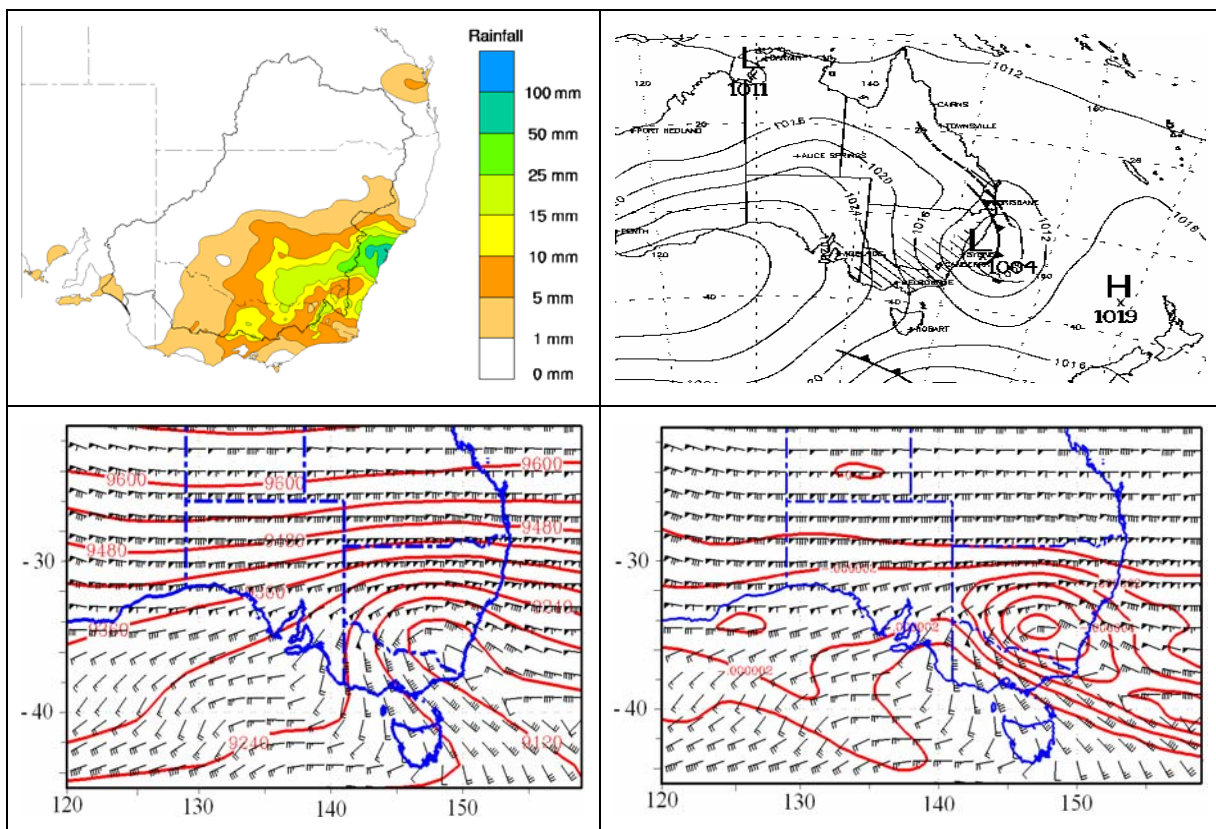


**Fig. 3** An example of an event defined as a “hit” on 6 September 2006. Upper left – AWAP rainfall analysis for the 24-hours to 9am on 7 September 2006. Upper right shows the National Meteorological and Oceanographic Centre (NMOC) mean sea level pressure (MSLP) analysis for 1800 UTC 6 September 2006, while the lower panels show the IPV/wind (right) and the height/wind fields at 300 hPa (left) from the ERA Interim dataset for 1200 UTC 6 September 2006.

During November 2006 there are two events worth discussing. On November 5 2006 there is an ECL event that is not identified by the diagnostics (i.e. a “miss”) since the diagnostics are not above their 90<sup>th</sup> percentiles. On 13 November 2006 there is a very strong signal in the diagnostics (with all three diagnostics being above their 90<sup>th</sup> percentile) even though the ECL database does not list an event occurring at this time (i.e. a “false alarm”).

First looking at the false alarm case on 13 November 2006 (Fig. 4), there was rainfall over a broad area of far eastern Victoria and over the Alpine areas of southeastern NSW, and an open trough is evident off the NSW coast in the MSLP analysis. Pressures in this open area were only just above 1000 hPa. To the west of this trough was a very strong pressure gradient, and mean wind speeds of above 25 knots for over 9 hours, with peak gusts of 48 knots, were observed on parts of the southern NSW coastline on the afternoon of 13 November. The 300 hPa geopotential height and IPV fields show an active open trough, with a very strong northwesterly jet on its eastern flank, and a centre of cyclonic IPV just to the eastern side of the axis of the trough. Although classified as a false alarm based on the ECL database, clearly on this occasion the upper-level diagnostics were useful in identifying the likely occurrence of severe weather characteristics of ECLs.

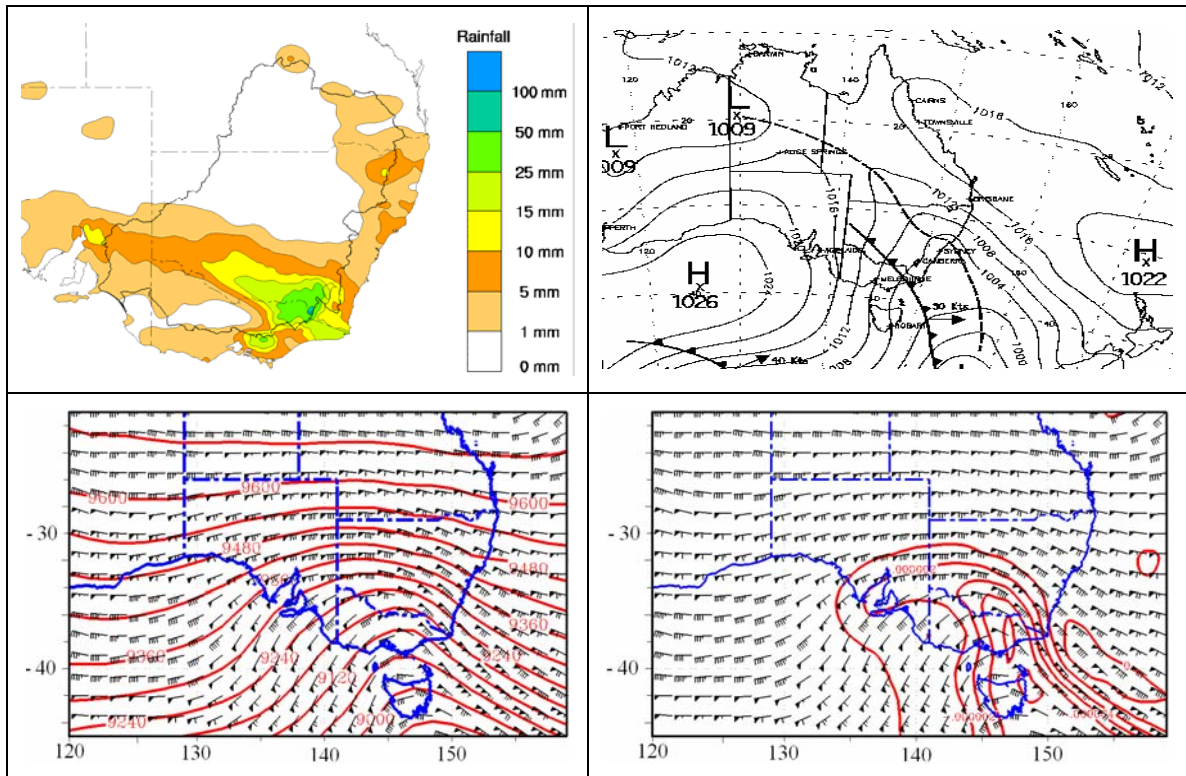


**Fig. 4** As for Fig. 3, but for 13 November 2006 as an example of a “false alarm”.

The situation for the “missed event”, on 5 November 2006, is shown in Fig. 5. There was rainfall along the NSW seaboard, although not as significant as that further south in the case described in the preceding paragraph. The MSLP analysis shows a low with a central pressure of some 1010 hPa, and given that the upper-tropospheric diagnostics “missed” this event, it is not surprising that the 300 hPa trough and IPV patterns are much weaker than those shown in Figs. 3 and 4. The upper-tropospheric response does not suggest the occurrence of a very significant event, and this is reasonably consistent with the observed rainfall and the very shallow nature of the MSLP low.

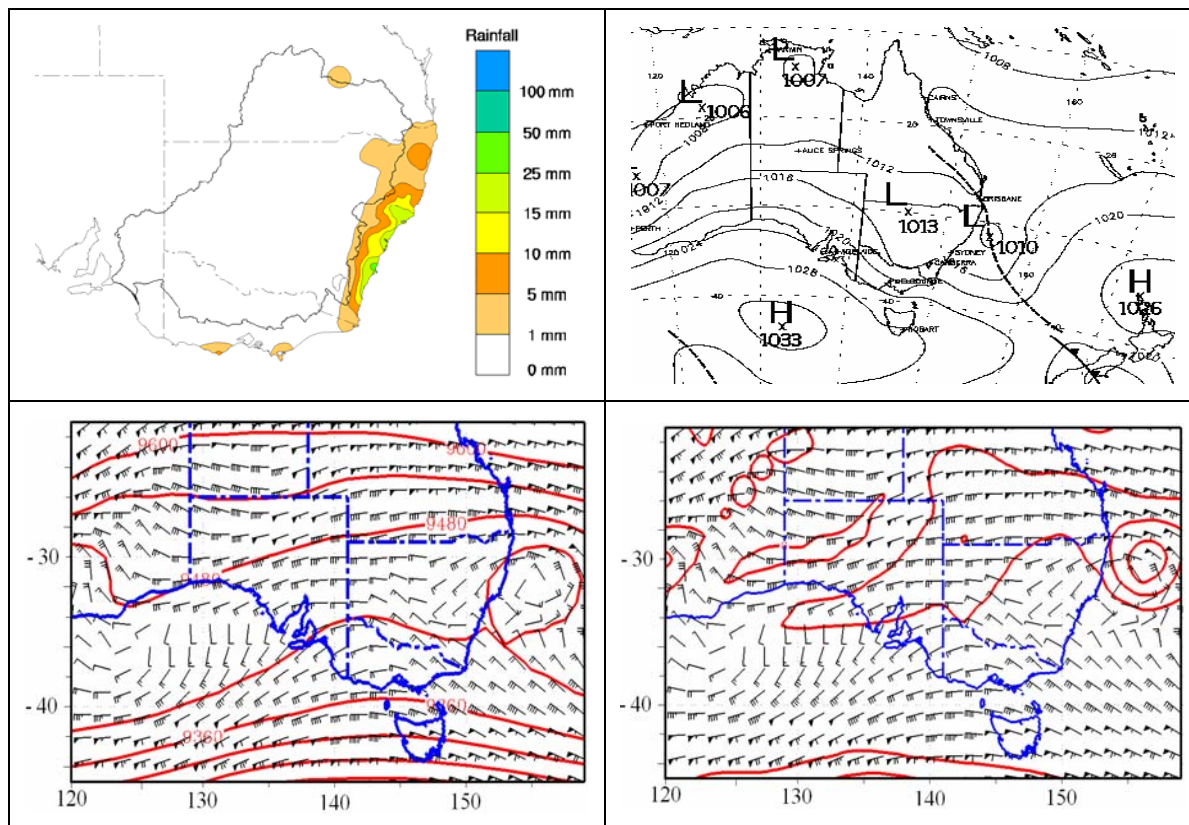


**Fig. 5** As for Fig. 3, but for 5 November 2006 as an example of a “miss”.

The above examples of a hit, false alarm and miss show that the definition of an ECL event, and associated extreme weather events, is somewhat subjective. The event that developed from an easterly dip (5 November 2006) appeared in the ECL database, but that which formed in a westerly trough (13 November 2006) did not. However the impacts of rainfall and of wind were greater for the event which was not included in the ECL database, and which had the stronger signal in the upper-tropospheric forcing diagnostics. This shows that the use of a database that is populated using subjective criteria may be problematic, and results using these definitions should consider the criteria used carefully.

Consequently, this report also examines the diagnostics using impacts-based event definitions (wind speed and rainfall). The model of a classic ECL such as the Pasha Bulker or the Sygna (Bridgeman 1986) storms provides the conceptual foundation of this study, with such ECLs typically showing gale-to-storm force winds from the southeastern quadrant on the southern side of the low, and very heavy rainfall on the seaward side of the Great Dividing Range in this strong southeasterly flow.

A strong wind event is determined by calculating the wind speed normal to the coastline (approximated as 30° east of north) at each gridpoint in the ERA Interim dataset for the geographic area from 150°E to 153°E and from 37.5°S to 27.5°S (i.e. a rectangle with a southwest corner from about the Victoria/New South Wales coastal border up to a northeast corner of about Brisbane). Then, using each 6-hourly analysis, an event day (using Local Time) is defined if at any point in that area the coast-normal wind speed exceeded 10 m s<sup>-1</sup> in any of the four 6-hourly analyses for that day. A single wind event was then defined for each contiguous period of event days, so that in common with the ECL data base, events could vary in duration.

Two definitions for heavy rainfall events were developed, each based on grid-average rainfall from the AWAP rainfall analyses (Jones et al. 2009). Each of these criteria is based on a definition of the eastern seaboard as the area between the watershed of the Great Dividing Range and the NSW coastline (Timbal 2010). The first type of rainfall event is simply defined as any day when the maximum individual gridpoint rainfall in the eastern seaboard exceeded 50 mm. This event type is referred to hereafter as a localized heavy rain event. A second type of rainfall event was defined as those days on which the integrated rainfall over the entire eastern seaboard exceeded a threshold amount chosen to be 50,000 mm – approximately its 90<sup>th</sup> percentile value. This event type is referred to hereafter as a widespread heavy rain event. Each of these rainfall event definitions have their flaws, as the first may be contaminated by isolated convective events not driven by ECLs, while the second could be generated by a range of synoptic situations that produce moderate, but very widespread rainfall rather than the typical ECL signature seen in Fig. 3, but equally each has strengths that will become more evident further into this report.

Thus four possible databases, the ECL database, the strong wind event set, and the two heavy rain event sets (localized and widespread) are available to compare with the large-scale indicators of ECL development. Some considerable overlap between these sets would be expected – indeed the value of this exercise would be greatly reduced if this were not to be the case. However, the examples in Figs 3-5 show that there will not always be a 1-to-1 correspondence between ECL, heavy rain and strong wind events, and so before analysing the relations between upper-low diagnostics and event occurrence, a comparison between these different sets of events is worthwhile.

Table 1 shows the correspondence between different pairs of event types. A match is counted if one event type occurs within one day of the other event type. The number of unmatched events of each type is also shown. As a measure of their correspondence, the Critical Success Index (Donaldson et al. 1975) is shown (calculated as the number of matched events divided by the sum of the number of matched events and the number of unmatched events of both types).

First comparing the ECL database events with the events-based definitions, it is seen that only about a quarter of the ECL events also have strong winds associated, but that only about a third of the strong wind events are unmatched to the ECL database. More than 50 per cent of the ECL events also have localized heavy rainfall, but only 38 per cent of the localized heavy rainfall events are associated with ECL events. Some 45 per cent of ECL events are matched by widespread heavy rain events, but again only 49 per cent of widespread heavy rain events are matched with ECL events.

Matching the strong wind events with the two definitions of rainfall event shows that most strong wind events also have both local and widespread heavy rain, but that only about 21 per cent of local heavy rain events, and about 27 per cent of widespread heavy rain events, match strong wind events. Finally, the best correspondence is between the two rain event types. It can be seen that it is quite likely for both widespread and local heavy rain to occur on the same day, that it is not common for widespread heavy rain to occur without there also being heavy local rain, but that it is very common for heavy local rain to occur without there also being widespread heavy rain.

These comparisons clearly show that defining an “ECL event” in an objective way is complex, and suggests that a single definition or a single diagnostic may not be the optimum solution. In sections 4-6 to follow, further discussion of these issues will be presented.

**Table 1** The correspondence between different event type pair combinations, including the ECL database, the strong wind event set, and the two heavy rain event sets. The values in the brackets represent the percentage fraction of the total number of type 1 events.

Event type 1	Event type 2	Matched event	Type 1 YES Type 2 NO	Type 1 NO Type 2 YES	CSI
ECL database	Strong wind	85 (23%)	281 (77%)	34 (9%)	0.21
	Localised heavy rain	195 (54%)	171 (47%)	325 (89%)	0.28
	Widespread heavy rain	163 (45%)	203 (55%)	168 (46%)	0.31
Strong wind	Localised heavy rain	110 (93%)	8 (7%)	411 (348%)	0.21
	Widespread heavy rain	94 (80%)	24 (20%)	244 (207%)	0.26
Localised heavy rain	Widespread heavy rain	297 (56%)	230 (44%)	41 (8%)	0.52

## 4 SPATIAL VARIABILITY OF THE DIAGNOSTICS

Having presented the upper-tropospheric diagnostics used in this study, and introduced the several ways to define an ECL event, we will now focus on the geographical area relevant to the Eastern Seaboard where ECLs are observed. The aim of this study is to determine whether or not there is sufficient relationship between the diagnostic indicators of upper tropospheric cold-core cyclones that are used in this study and subsequent (explosive) surface cyclogenesis in order for extreme values in the diagnostics in GCM model output to be used as a proxy for ECL occurrence. In order to do this we now need to examine the spatial variation of maxima in the diagnostics, to

- determine whether or not there is any predisposition of upper-tropospheric cyclones to occur in particular geographic areas,
- determine whether or not there is a relation between extreme values of these diagnostics in particular areas and the development of ECLs, and
- determine the area to use for calculation of the diagnostic quantities so that they provide the optimal indication of upper cut-off low events as a proxy for ECL events.

These points will be addressed in this section. Then in following sections, and using the optimal target area, the performance of these diagnostic indicators of upper cut-off lows as indicators of ECL development (using the various definitions of ECL) will be addressed, and some analysis of seasonal behaviour will be discussed.

## 4.1 Preferred positions of extreme values of the diagnostics

Figures 6 to 8 show the spatial distributions of the positions of the maximum values at 400 hPa of the three diagnostics, with similar figures for the 300 hPa and 500 hPa levels shown in Appendix A. The upper left panels of these figures show the number of times that the maximum value in the area displayed occurred at a particular location. The upper right panels show this same information, but normalised by the average for that latitude, so as to remove the latitudinal gradient. The lower left panels show the number of times that the diagnostic exceeds a threshold value set to the 90<sup>th</sup> percentile of the maximum value of each diagnostic at any grid point within a central region (from 141-156°E in longitude and 36-25°S in latitude). The rationale is to evaluate the possibility that multiple locations at any one time have diagnostic values above the 90<sup>th</sup> percentile value. The lower right panels show this same information, but normalised by the average for that latitude so as to remove the latitudinal gradient. The tendency for the diagnostic to show large values near the edges of the geographic area shown is an artefact caused by the influence of weather phenomena located slightly outside of the geographic area, and is not considered in the following discussion of these figures. Contour plots, such as Figs 6 to 8, are smoothed in this study using a 3x3 running mean to reduce the small-scale spatial variability that is unlikely to be representative of the underlying large-scale climatology that is the focus of this study.

The distribution for geostrophic vorticity extrema is shown in Fig. 6. Looking first at the upper-left panel, there is a maximum in frequency over southeastern Australia, with axes of higher frequency extending northwards just inland of the east coast of Australia, and also an east-west maximum along approximately 38°S through the Tasman Sea. When multiple centres are included (lower left panel) rather more centres are selected as expected (note the colour scales are different), but the spatial patterns are largely similar. When normalised by the mean number for each latitude band (right-hand panels) the centre of highest frequency becomes focussed in latitudes between 20 and 36°S, and around 150°E, with the centre of greatest frequency just north of the NSW border.

The plots for IPV centre distributions (Fig. 7) are rather similar in broad aspects, but the low-latitude region of highest frequency of centres is equatorward and west of that of the geostrophic vorticity. Spatial variations for the forcing term (Fig. 8) are harder to interpret, although less pronounced maxima do correspond to the maxima in Figs. 6 and 7.

Plots for the same quantities shown in Figs 6-8, but for 500 and 300 hPa, are shown in Appendix A (Figs A1 to A6). Spatial features are broadly similar in these plots as to the case for 400 hPa.

Many of these features can be attributed to the large-scale circulation of the southern hemisphere, with the southern maxima associated with the mid-latitude westerlies, and the maxima in the Tasman Sea associated with the tendency for blocking to occur in these longitudes (Karoly and Vincent 1998). Most pertinent to this study is the indication that there is a tendency for preferred frequency of upper cut-off lows over central northern NSW and central southern Queensland. This is consistent with the results presented in Ndarana and Waugh (2010), and following the arguments in Risbey et al. (2009) might be attributed in part to this region lying under the poleward exit of the mean position of the wintertime subtropical jet, the strength and position of which is determined by the cold continent, with some contribution from the higher latitude blocking that tends to be more frequent in New Zealand longitudes.

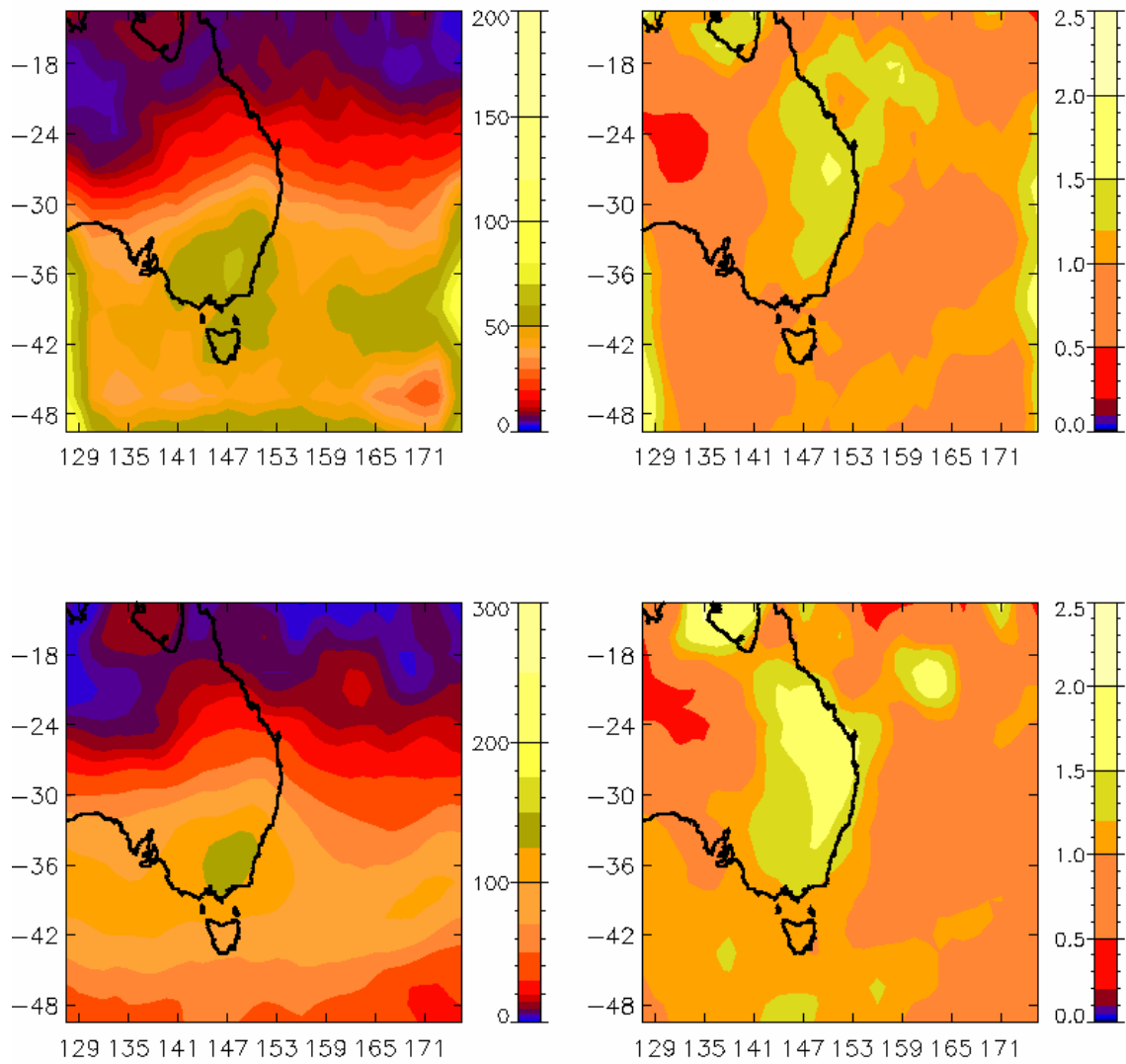


**Fig. 6** Number of times that the minimum value of the 400 hPa geostrophic vorticity in the area displayed occurred at a particular location, using 6-hourly data from 1989-2006 (upper left) and normalised by the latitudinal average to remove latitudinal gradients (upper right). Number of times that the geostrophic vorticity exceeds its 90th percentile (lower left) and normalised by the average for that latitude to remove latitudinal gradients (lower right). X- and Y-axes show longitude and latitude, respectively.

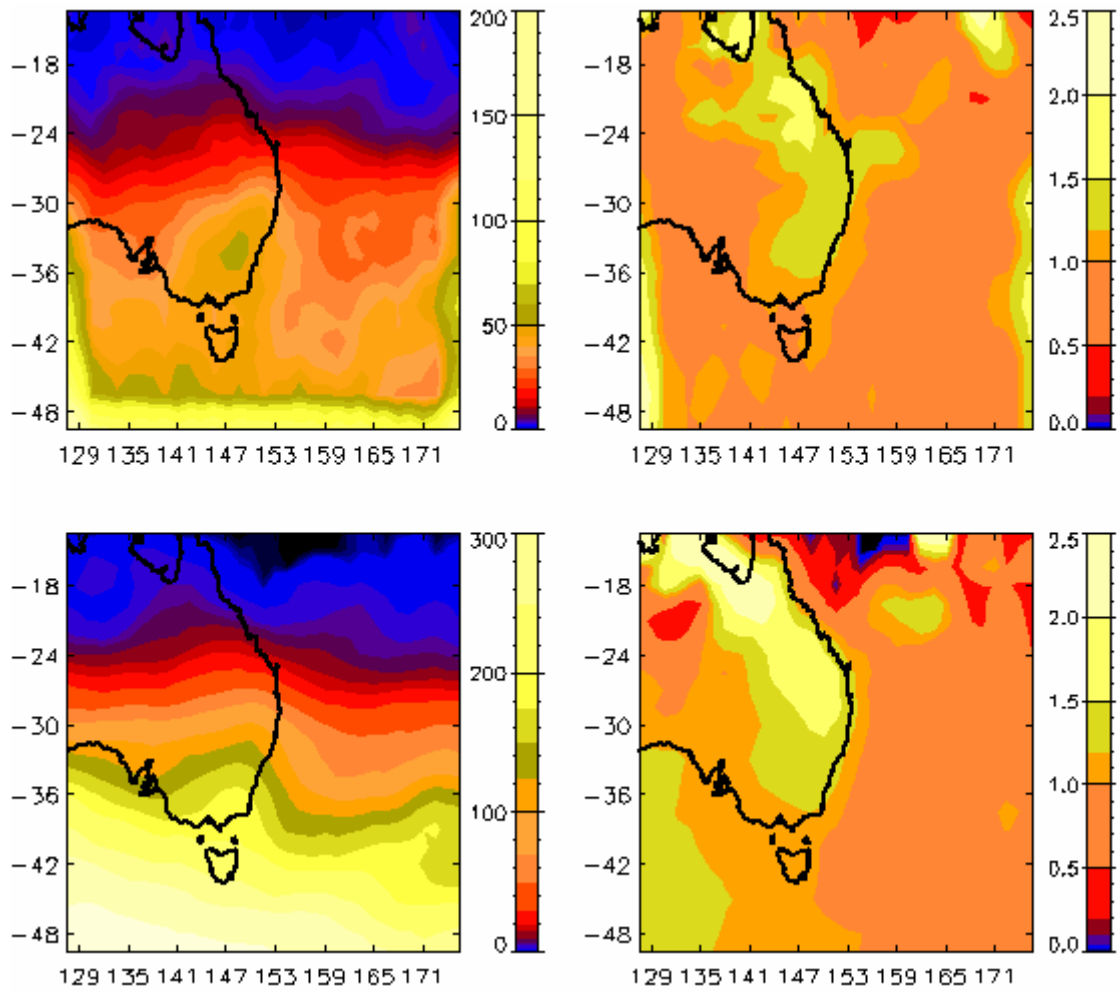


**Fig. 7** As for Fig. 6, but for IPV.

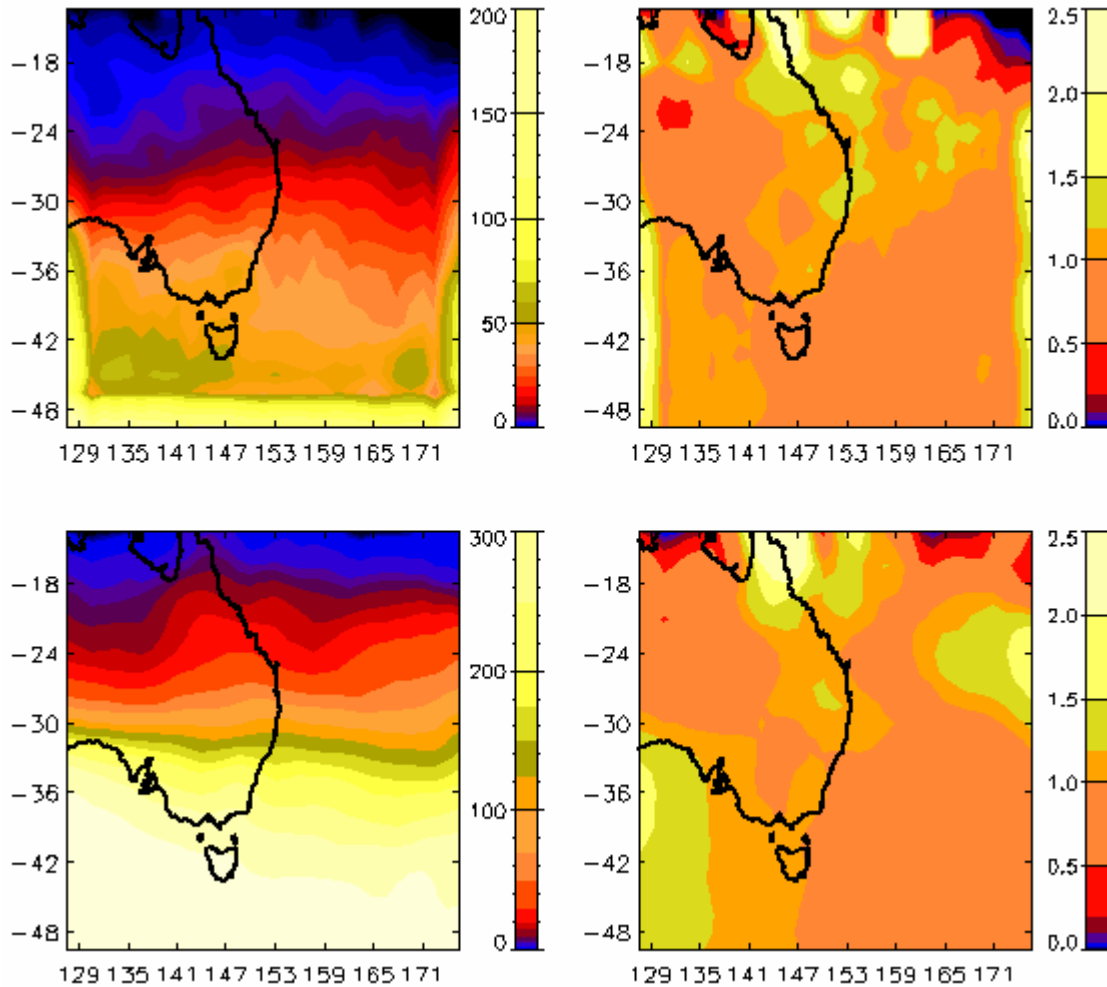


**Fig. 8** As for Fig. 6, but for the forcing term.

## 4.2 Extreme values of the diagnostics for days on which ECLs occurred

In the previous section the spatial location of diagnostic maxima was examined using data at 6-hourly intervals through the period from 1989 to 2006. In this section, maxima of the diagnostics are examined only for times in which ECL events occurred.

For every individual day of each ECL event, the position of the extreme value of a diagnostic (i.e. the maximum for the forcing term and minimum for the two vorticity terms) within the area surrounding eastern Australia was calculated (using the same area as used in the previous section). The number of times that the extreme diagnostic value within the area shown occurred at a particular location (i.e. reanalysis grid point) is shown Fig. 9 for the 400 hPa geostrophic vorticity diagnostic. The different panels in Fig. 9 represent different time lags of the diagnostic quantity with respect to the day of an ECL event, for daily intervals from 4 days before to 1 day after each ECL event day. The rationale of the different time lags is to see how the results change in time from a period before the ECL event until a period after the ECL event. Figures 10 and 11 repeat Fig. 9, but for IPV and the forcing term. Figures 9-11 are repeated for 300

and 500 hPa (see Appendix B). Appendix B also contains plots similar to Figs 9-11 for the heavy rain and high winds “impact events”. Particularly for the geostrophic vorticity and the IPV diagnostics, very similar patterns for the ECL events are seen, with significant centres of high frequency seen close to the NSW coastline at lag zero.

The temporal evolution of the diagnostics indicate clearly that the highest spatial concentration of maximal occurrence values is observed on ECL event days. There is a clear region of preference where the highest value of each diagnostic in the entire region tends to occur on ECL event days. This region is located over the central coastal region of NSW for the geostrophic vorticity and for the IPV terms, and elongated a little further towards the southwest for the forcing term. However, it is also worth noting that the centre of most frequent maxima occurrence becomes very clearly defined from two days before to one day after the peak intensity of the ECL, with the centre moving eastward with time. Given that there are some 669 individual ECL event days (from 366 ECL events that can be longer than one day in length) in this ECL data-base, this result across so many cases is a very strong indication that the hypothesised model by Mills et al. (2010) of ECL development being preceded by the development of a large-amplitude upper cut-off low is broadly applicable to the development of these ECLs, not just to the selected case studies presented in Mills et al. (2010).

It is also interesting that while there appears to be no particular preferred region for maxima of the forcing term in the general climate (Fig. 8), there is a clear preferred region for such maxima for the ECL events, suggesting that these upper-tropospheric cut-off lows have a structure such that surface development is more likely. This remains a topic for more detailed research, but may well be related to the prevalence of strong jet streaks, and strong cyclonic shear, on the northeast flank of these developing systems (Mills et al. 2010, Risbey et al. 2009).

These results provide a strong indication that the approach proposed, that indicators of upper cut-off lows over eastern Australia might be used as a proxy for the presence of ECL developments in GCM model output, has potential. However, this section did not investigate cases where extreme diagnostic values occur at times when no ECL event is observed. In the next section we assess the sensitivity of the diagnostics to choice of target area – that is, we attempt to define a smaller target area than that shown in Figs 6-11, and then provide quantitative assessment of the approach by comparing the number of upper-low identifications with the number of events in the ECL and the impacts data sets – including taking into consideration the number of ‘hits’, ‘misses’ and ‘false alarms’ that occur.

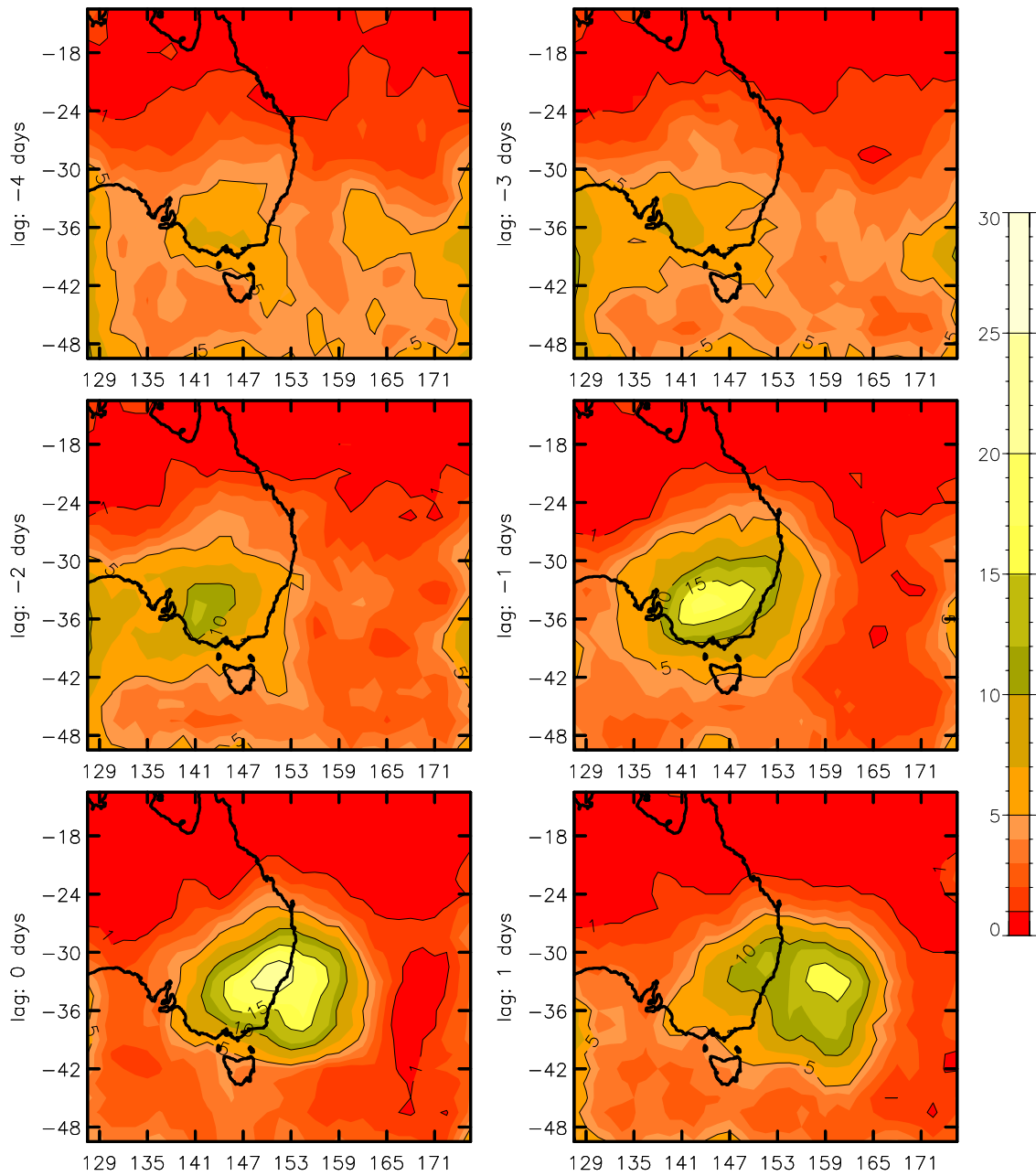


**Fig. 9** Number of times that the minimum value of the 400 hPa geostrophic vorticity in the area displayed occurred at a particular location, using all ECL event days, at six different time lags (from -4 days to +1 day) with respect to the ECL event day. X and Y axes show latitude and longitude, respectively.

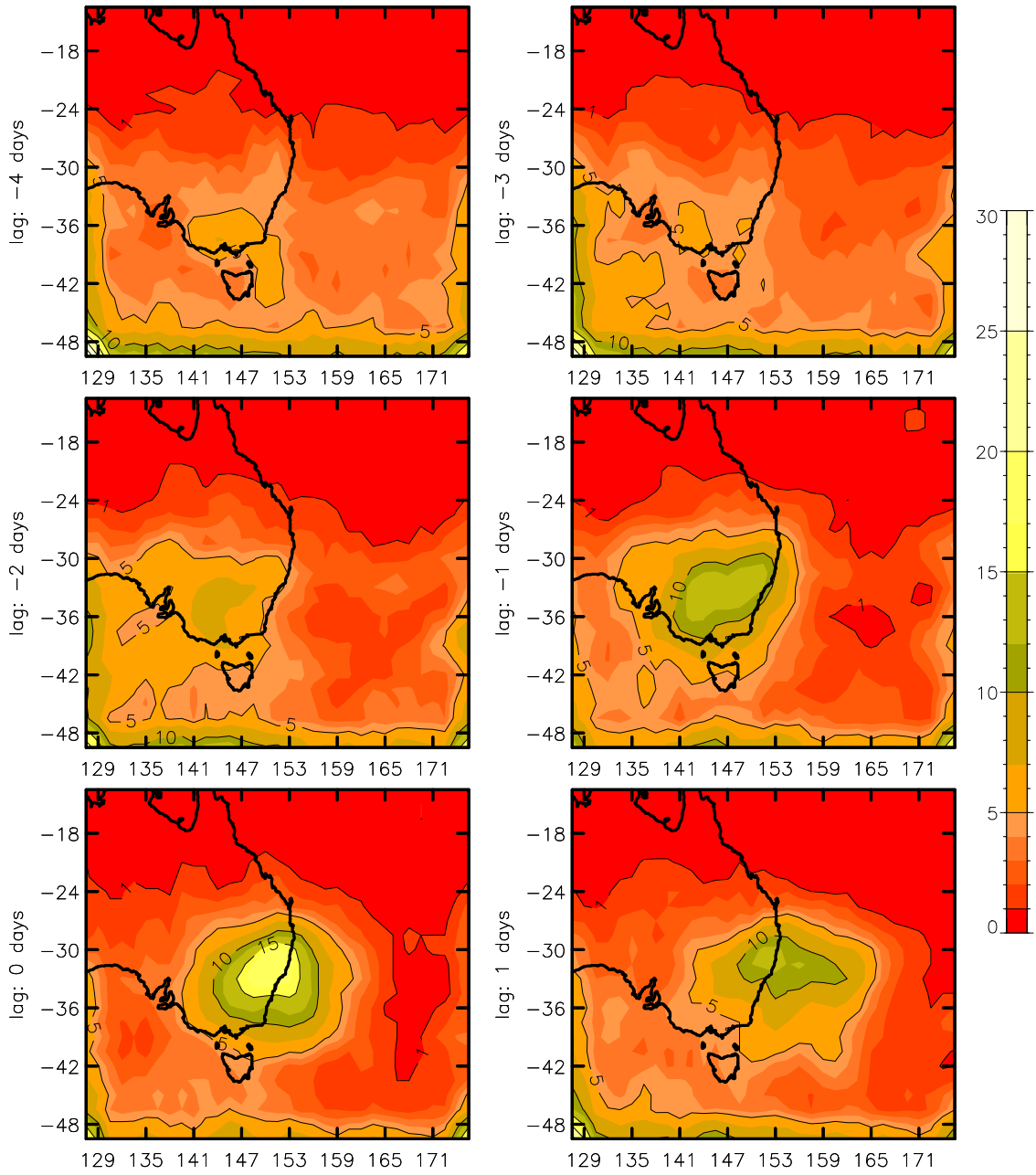


**Fig. 10** As for Fig. 9, but for isentropic potential vorticity.

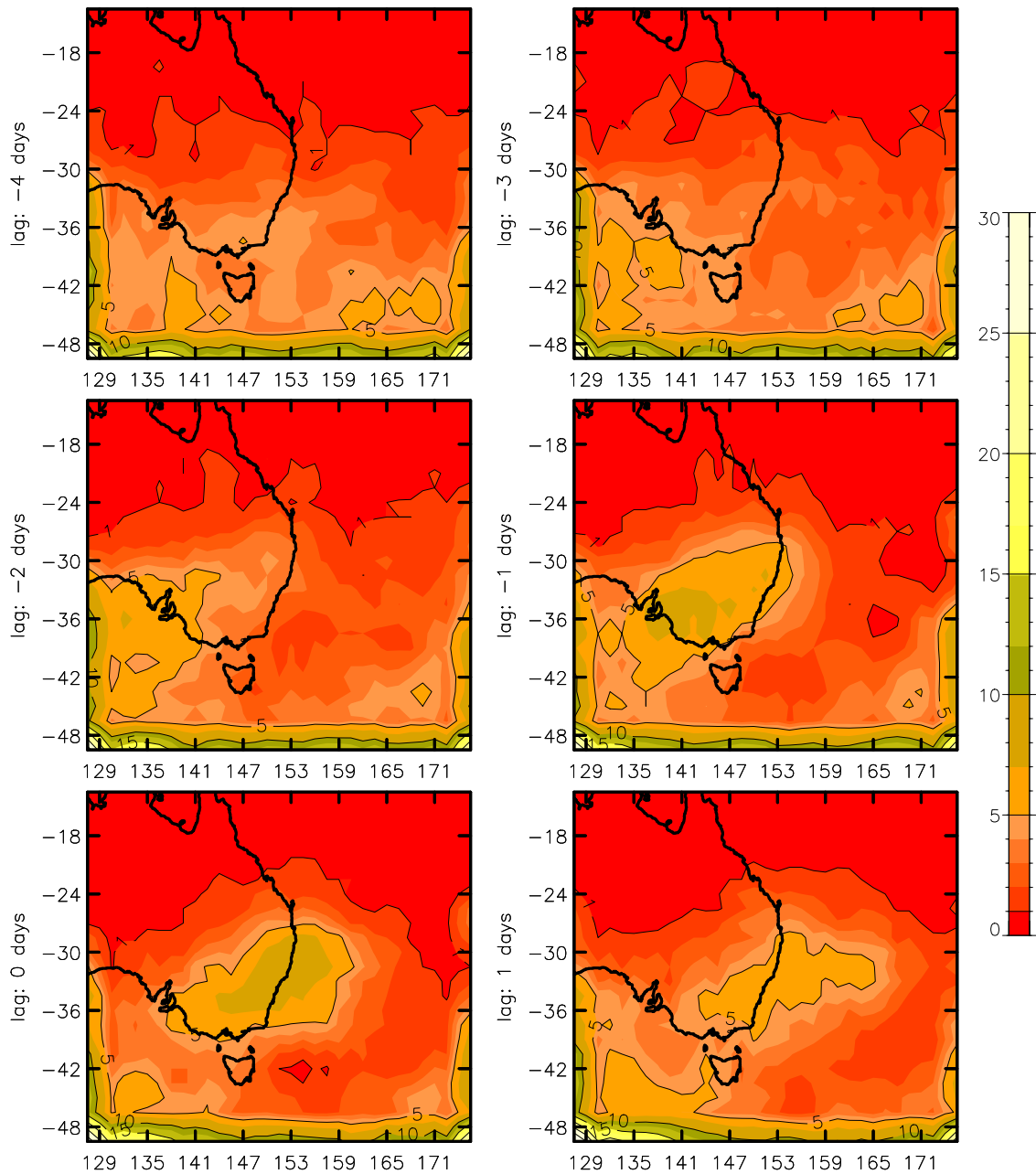


**Fig. 11** As for Fig. 9, but for the forcing term.

## 5 QUANTITATIVE PERFORMANCE MEASURES OF THE DIAGNOSTICS

In the previous section it was shown that there is considerable correspondence between the presence of significant upper-tropospheric cyclonic vorticity centres and subsequent ECL development. However, if this relationship is to be applied to GCM data to infer likely frequencies of ECL in these climate simulations, then it is important that the frequency of hits, misses, and false alarms that result from this approach be documented. Such contingency tables are first used to determine both the optimum region over which to seek diagnostic extrema and the degree of temporal filtering to be applied to the diagnostic 6-hourly time series. There is

also the matter of matching variable-length ECL or impact events with the maxima in the diagnostic time series.

A number of statistics commonly used in forecast verification are used including the Probability of Detection (POD), the False Alarm Ratio (FAR) and the Critical Success Index (CSI, also termed the Critical Success Score, CSS). The CSI rewards hits, while also penalising both misses and false alarms, and represents the fraction of observed and predicted events that are correctly predicted. These statistics were calculated with the target box incrementally moved by 1 reanalysis gridpoint to determine the target zone that was optimal for identifying ECL events, or impact events, while the verification statistics provide a quantitative measure of performance of the various diagnostic quantities. In this domain-selection stage of this analysis, we also test differing degrees of smoothing of the diagnostic time-series.

## 5.1 Defining and matching events

We define a single ECL event to occur irrespective of its duration in the ECL data base. Single impact events are defined for periods of contiguous “event days” as defined in Section 2 for heavy localised rainfall, heavy widespread rainfall, and strong wind events.

We define an “indicative event” if the maximum value of a particular diagnostic (i.e. based on either the geostrophic vorticity, IPV or “forcing term”) within a target area exceeds its 90<sup>th</sup> percentile value at any time on a given day. Thus an indicative event may also have a variable duration depending on the number of consecutive days on which the maximum value of the diagnostic exceeds the threshold value. The previously shown plots (Figs 6-11, as well as similar Figures in Appendix A and B) were used as a first-pass at selecting the geographic area to use for selecting the indicative events. This was then followed by a calculation of contingency table statistics (i.e. based on the number of hits, misses and false alarms) in relation to ECL event days, so as to fine-tune the latitudinal and longitudinal ranges used to define the diagnostic area. The resultant diagnostic box area (using the 1.5 degree grid resolution of the ERA-Interim dataset) was selected to be 15 degrees in longitude and 10.5 degrees of latitude.

Matching these variable length events was done as follows: if the diagnostic time series (with a 1-day running mean applied to the 6-hourly data) is above its threshold (selected here as its 90<sup>th</sup> percentile for the period 1989-2006) at any time within 1 day of an ECL event occurring, then a ‘hit’ is counted, otherwise a ‘miss’ is counted. A ‘false alarm’ is counted if an ECL event does not occur during the time period that the diagnostic time series is above its threshold. The number of times that an ECL event did not occur when the diagnostic was lower than its threshold (i.e. ‘correct negatives’) is not presented since this quantity is difficult to define for variable length events. Consequently, this analysis represents an events-based perspective, with ECLs that persist for multiple days being counted as single ECL events, and continuous periods where a diagnostic is above its threshold being counted as single indicative events. This method allows for the possibility that large-scale drivers of ECL occurrence may occur only at a particular time during a multi-day event, including the likelihood that they are precursors (by up to one day) of the start of an ECL event.

## 5.2 Domain selection for ECL events

Figure 12 shows values of the CSI calculated for different positions of the diagnostic box for each of the diagnostics and for each pressure level for the events in the ECL data base. The geostrophic vorticity at 400 and 500 hPa produce the highest indicative skill of the three diagnostics, with CSI values of 0.40 and 0.39, respectively. Isentropic potential vorticity, in contrast to the geostrophic vorticity, produces the highest CSI at 300 hPa, with a CSI value of 0.35. The forcing term does not show as high values of the CSI as the other 2 diagnostic quantities, with maximum CSI values in the range 0.28-0.31 for the 300, 400 and 500 hPa levels.

In general, based on all 9 plots shown in Fig. 12, the best position of the centre of the diagnostic box appears to be about 153°E and 30°S – that is, the box is centred close to the coastal border of NSW and Queensland.

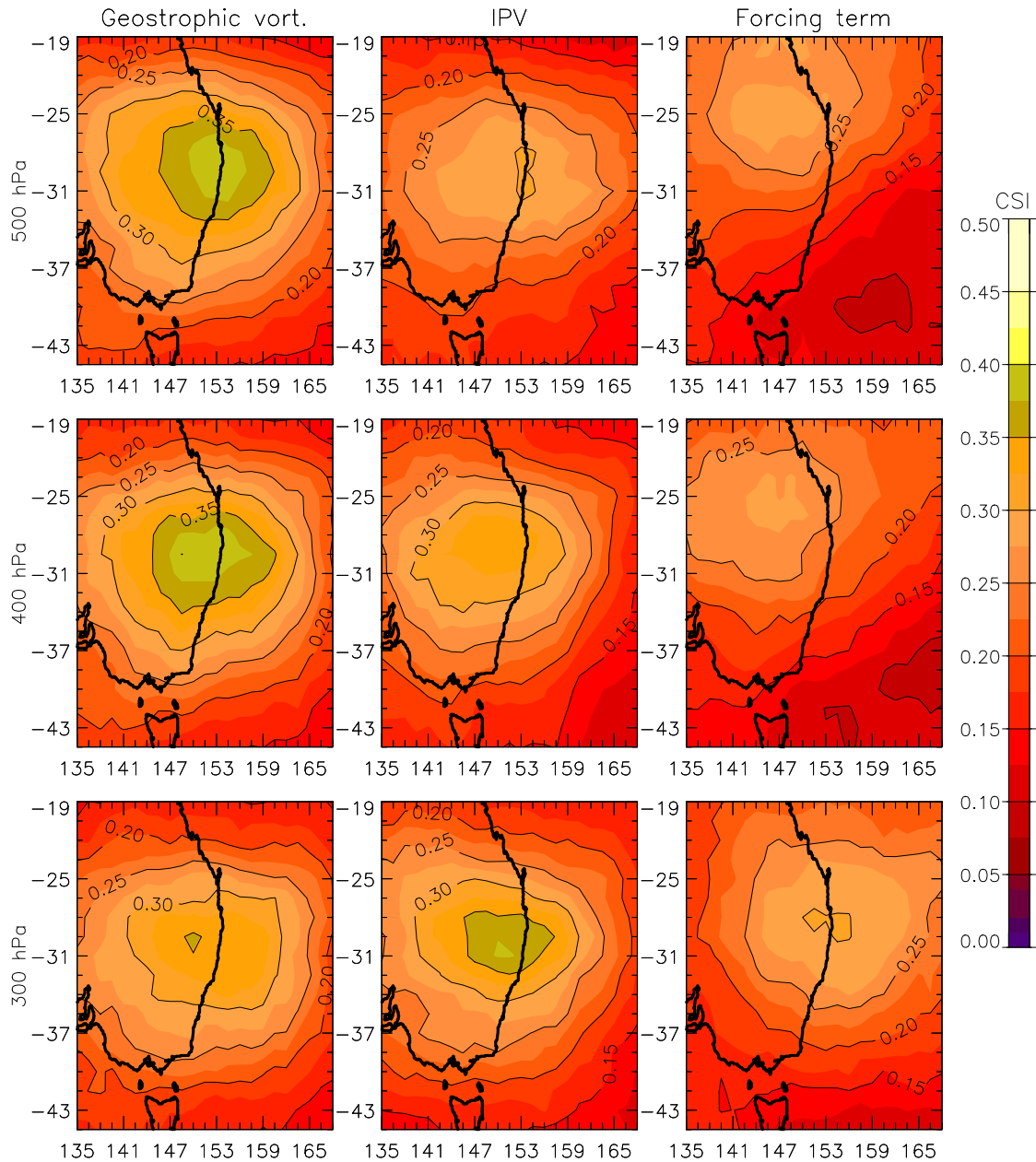


**Fig. 12** CSI for different diagnostic box positions, for ECL events, with a 1-day running mean applied to the diagnostic. The different panels correspond to geostrophic vorticity (left column), IPV (middle column) and the forcing term (right column) at 500 hPa (upper row), 400 hPa (middle row) and 300 hPa (lower row). The x and y axis represent the longitude and latitude, respectively, of the centre of the diagnostic box (which has geographic dimensions of 15 degrees in longitude and 10.5 degrees in latitude).

A 2-day smoothing applied to the diagnostic quantities produces broadly similar results (Fig. 13) as occurs for a 1-day smoothing for all three diagnostics at all three pressure levels. The peak CSI values occur once again for the 400 and 500 hPa geostrophic vorticity, with a value of 0.41 in both cases, and for the 300 hPa IPV, with a peak value of 0.39. These peak values are slightly higher than the case for 1-day smoothing (from Fig. 12). In contrast, the CSI values are slightly lower for the 400 hPa and 500 hPa forcing terms than is the case for a 1-day smoothing. The peak IPV value (0.39) occurs for the 300 hPa pressure level, similar to the case for the 1-

day smoothing. In general, increasing the degree of smoothing applied to the time series reduces the number of false alarms, while also reducing the number of hits. These two effects produce opposing effects on the CSI value, and so the optimal smoothing may vary depending on the diagnostic used and the observed event to which it is compared, as well as other factors such as the temporal and spatial resolutions of the datasets.

There is some indication that the location of the best diagnostic position is somewhat height dependent, with the optimal position tending to occur further south and east at higher altitudes. This is similar to the tilt in the vertical structure of the ECL associated with the ECL event during the 1998 Sydney to Hobart yacht race tragedy, associated with the advection of IPV on the southern side of the low (Mills, 2001).

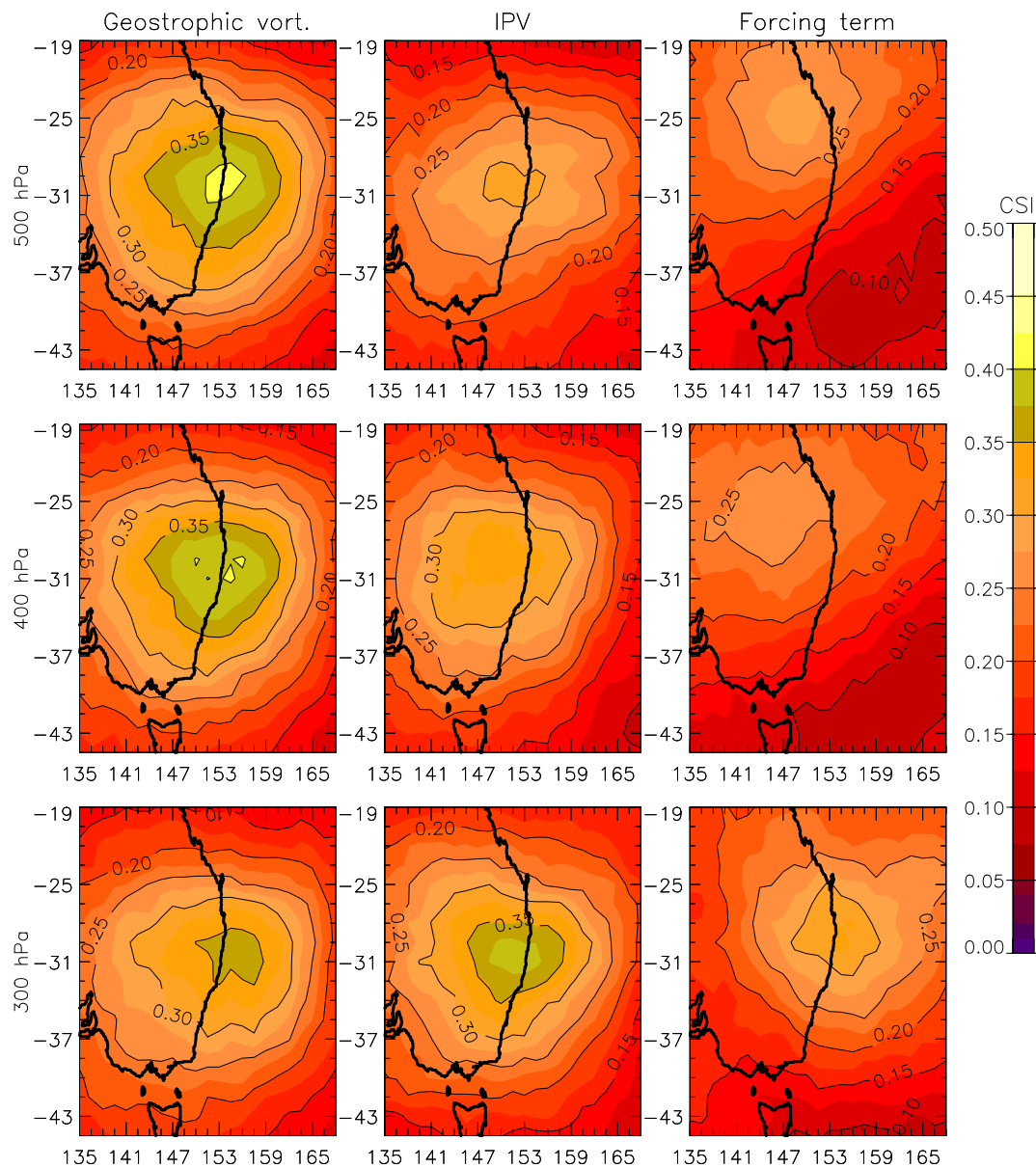


**Fig. 13** As for Fig. 12, but with a 2-day running mean applied to the diagnostic time series.

### 5.3 Domain selection for high impact events

Figures 14 and 15 are similar to Figs. 12 and 13, but for extreme wind speed events. Geostrophic vorticity at 500 hPa and IPV at 300 hPa produce the highest indicative skill of the three diagnostics, again the forcing term does not show as high values of CSI as the other two diagnostic quantities. The CSI values are lower by a significant amount than for ECL events, with maximum CSI values of about 0.25 instead of about 0.41 as was the case for the ECL events. In general, the best position of the centre of the diagnostic box appears to be some 4° equatorward and 3° westward of the optimal area for ECL events, with the optimal domain position centred over about 150°E and 26°S.

The optimal smoothing appears to be different for wind events than for ECL events: applying a 2-day running mean to the diagnostic time series produces remarkably better results than a 1-day running mean for all three diagnostics at all three levels. For example, geostrophic vorticity produces CSI values of the order 0.05 higher than when using a 1-day running mean, indicating that the wind event database benefits from a broader time resolution than the ECL event database.

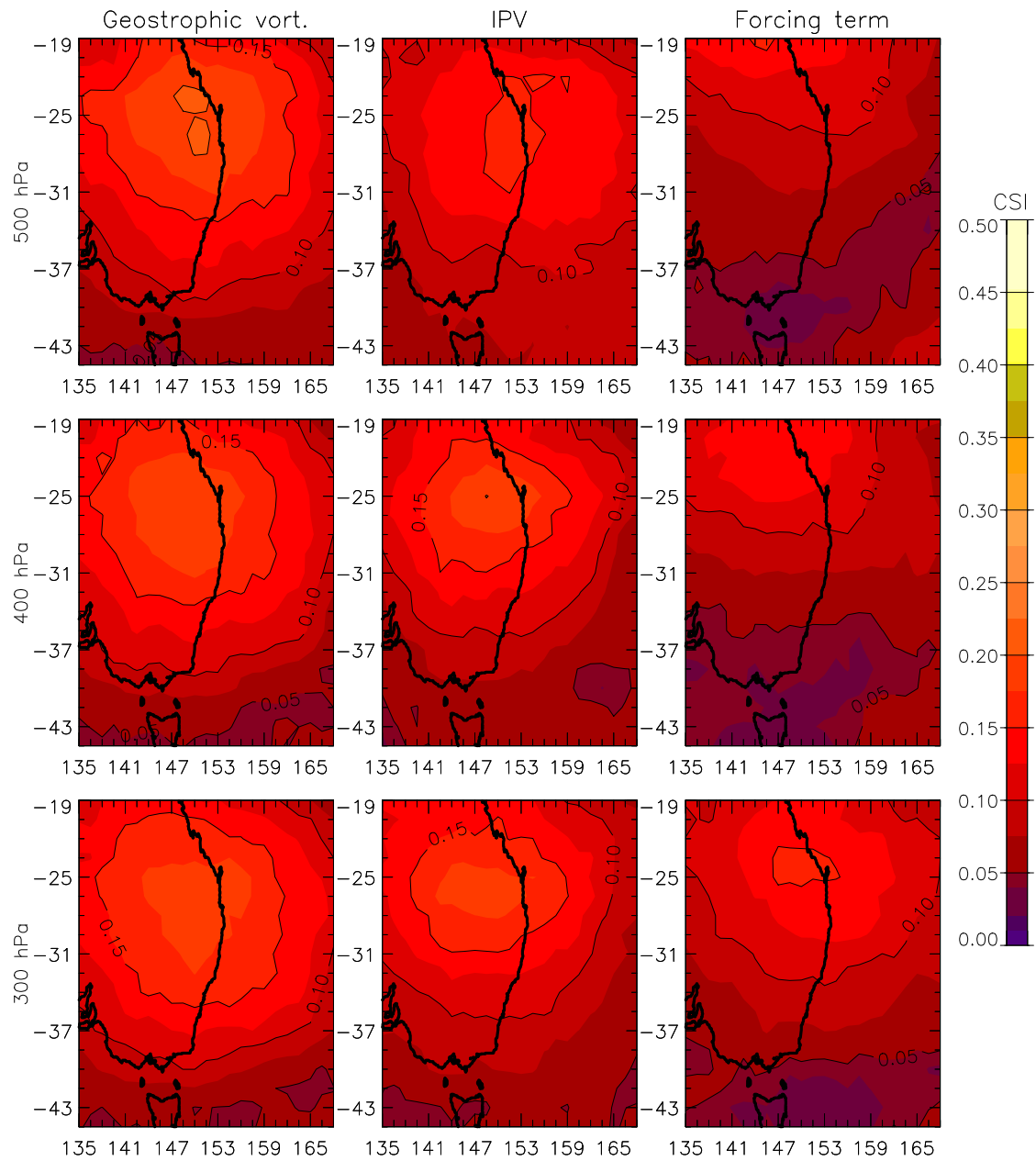


**Fig. 14** As for Fig. 12, but for strong wind event days, with a 1-day running mean applied to the diagnostic.

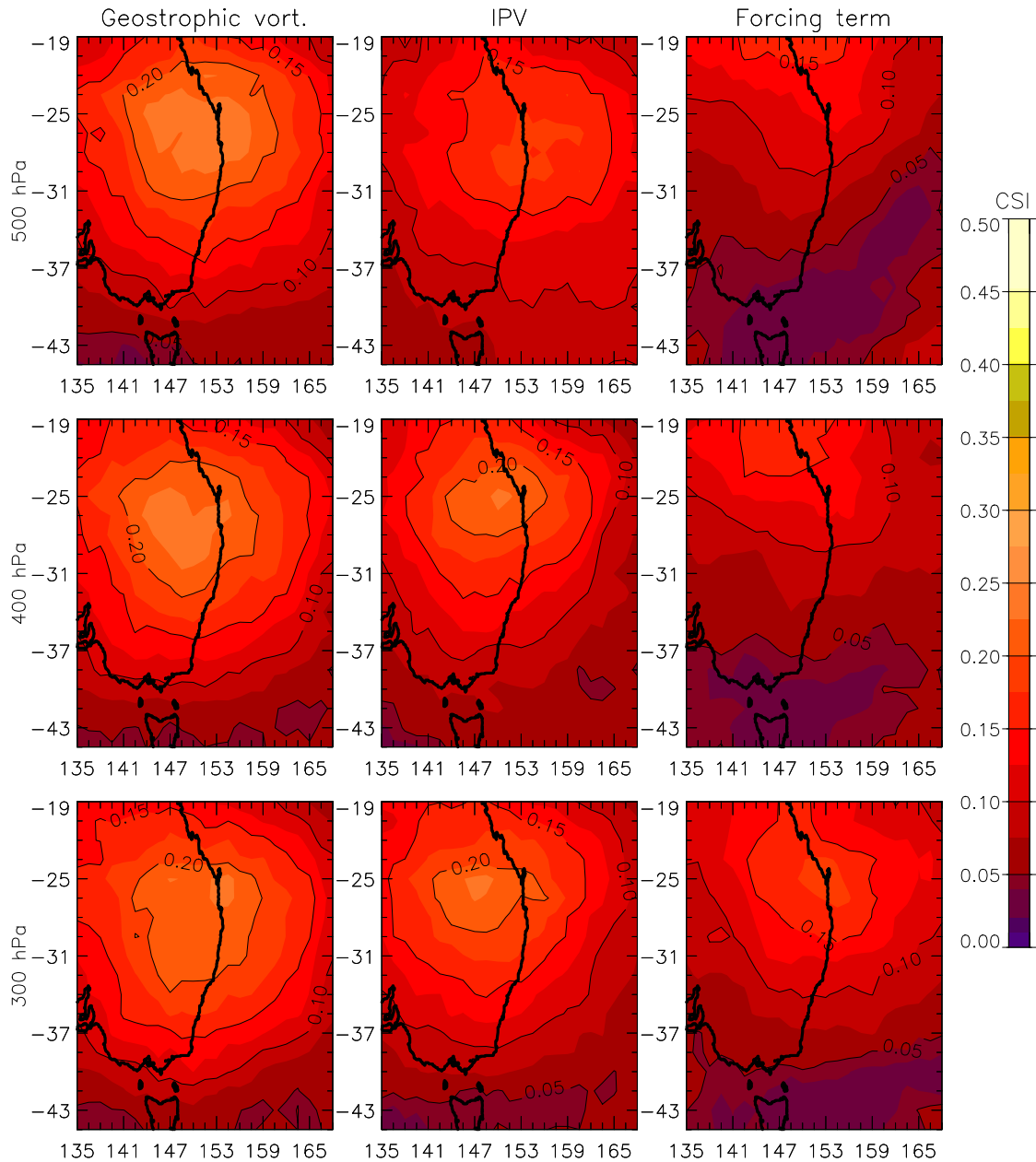


**Fig. 15** As for Fig. 12, but for strong wind event days with a 2-day running mean applied to the diagnostic.

Similar results to Figs 12-15 were obtained for extreme local rainfall events (defined as days on which the maximum rainfall in the Eastern Seaboard was above 50 mm) as shown in Figs 16 and 17, and for heavy widespread rainfall events (based on the integrated amount of rainfall throughout the entire eastern seaboard of NSW being above the chosen threshold value approximately equal to its 90<sup>th</sup> percentile) as shown in Figs 18 and 19. The CSI values for these two rainfall event definitions are larger than was the case for the strong wind events, being closer in magnitude to the case for the ECL events.

In the case of the extreme rainfall events, the geostrophic vorticity gives the highest CSI values, and the forcing term the lowest, but in these cases while the forcing term still has its highest CSI at the 300 hPa level, the highest CSI for the geostrophic vorticity is achieved using the 300 hPa

level. It is also notable that the centre of the diagnostic area that leads to the highest values of CSI for the extreme rainfall events is located further west than was seen for ECL events, with the optimal domain position centred over about 147°E and 29°S for extreme localised rainfall events and about 144°E and 29°S for extreme widespread rainfall events. For extreme local rainfall events, the highest CSI are gained using 1-day running averages rather than 2-day running averages for all three diagnostic quantities at all three levels. In contrast, for extreme widespread rainfall events, similar peak CSI values tend to occur for 2-day as for 1-day running averages.

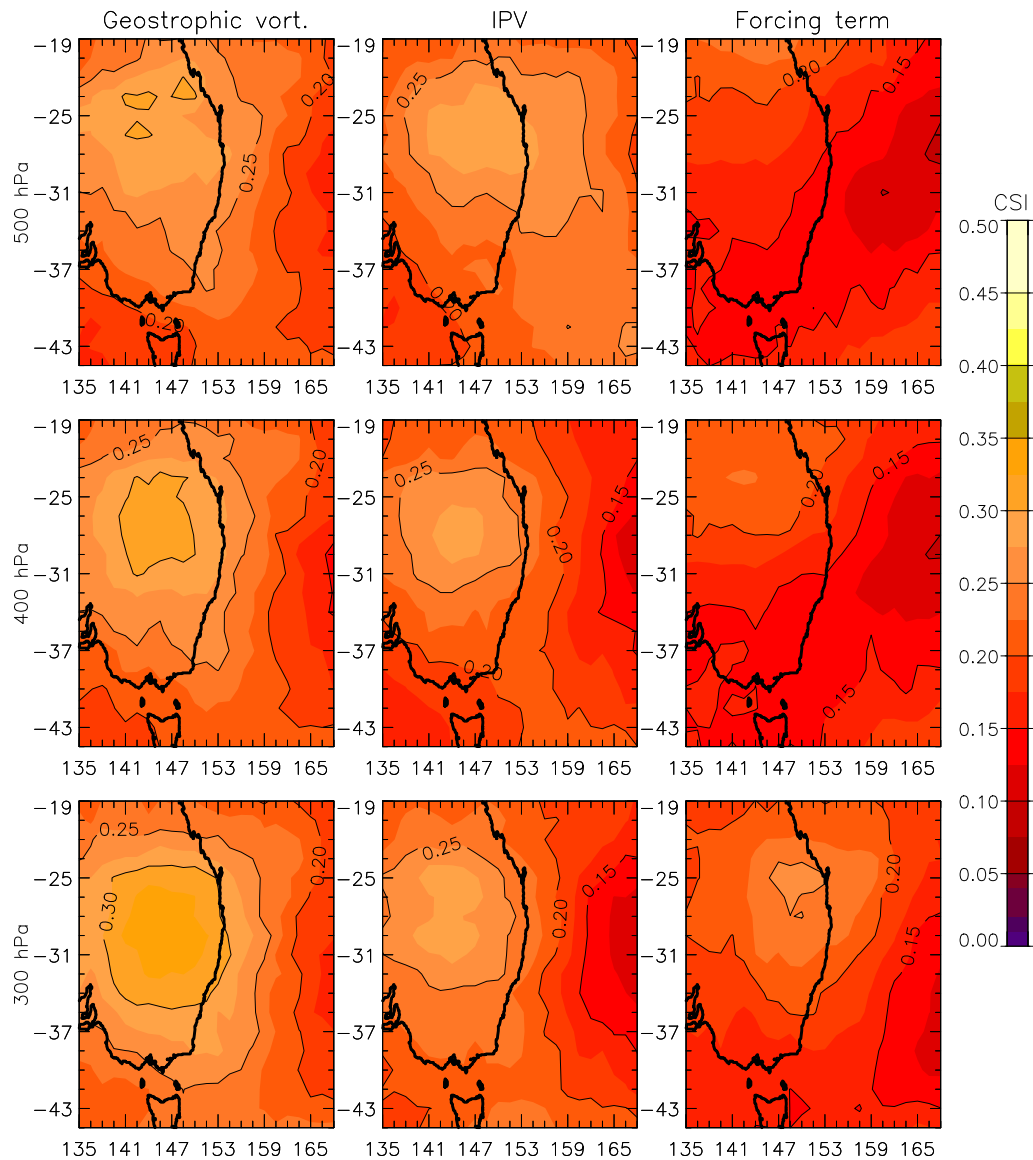


**Fig. 16** As for Fig. 12, but for days on which the maximum localised rainfall in the eastern seaboard was above 50 mm, with a 1-day running mean applied to the diagnostic.

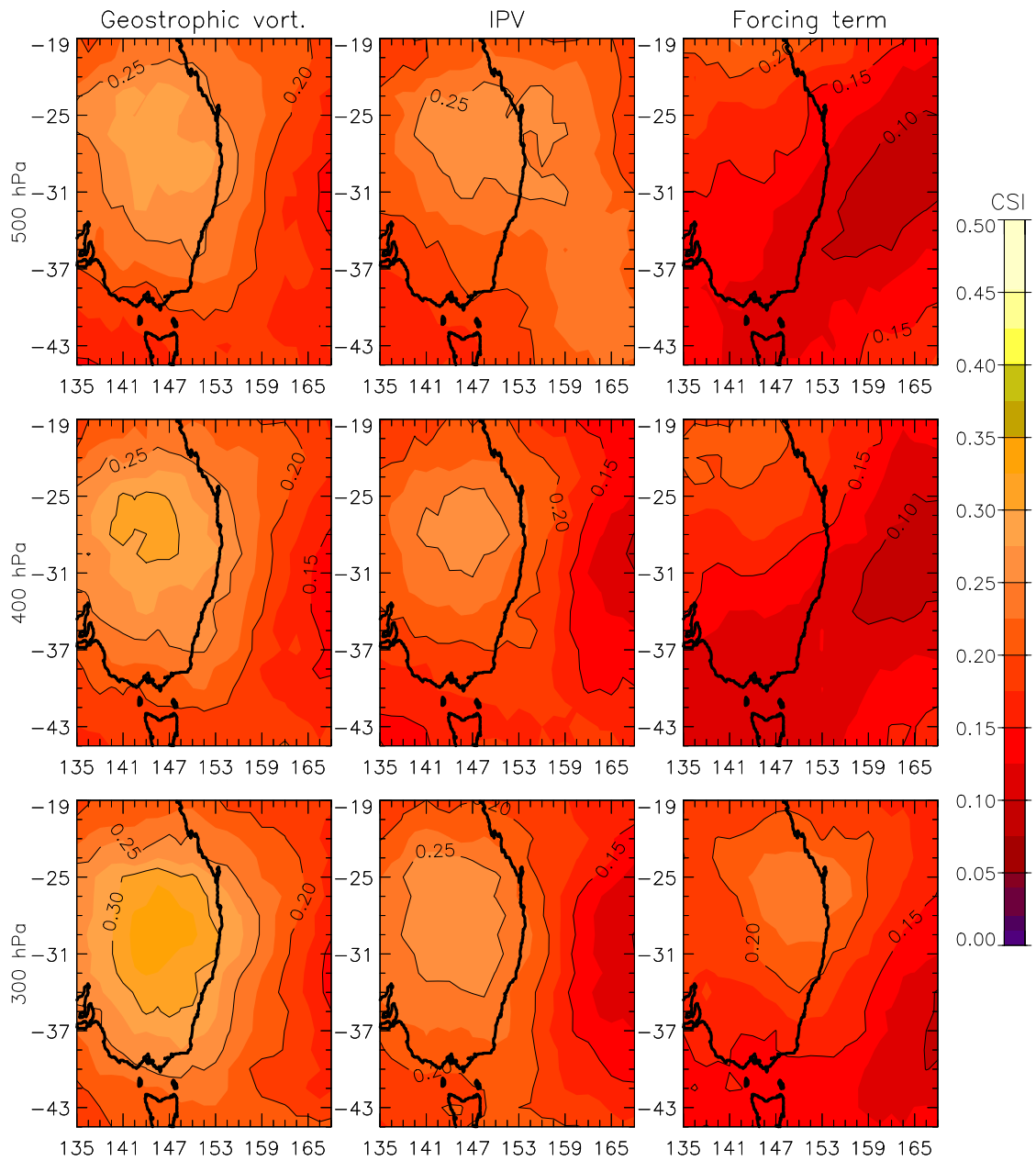


**Fig. 17** As for Fig. 12, but for days on which the maximum localised rainfall in the eastern seaboard was above 50 mm, with a 2-day running mean applied to the diagnostic.

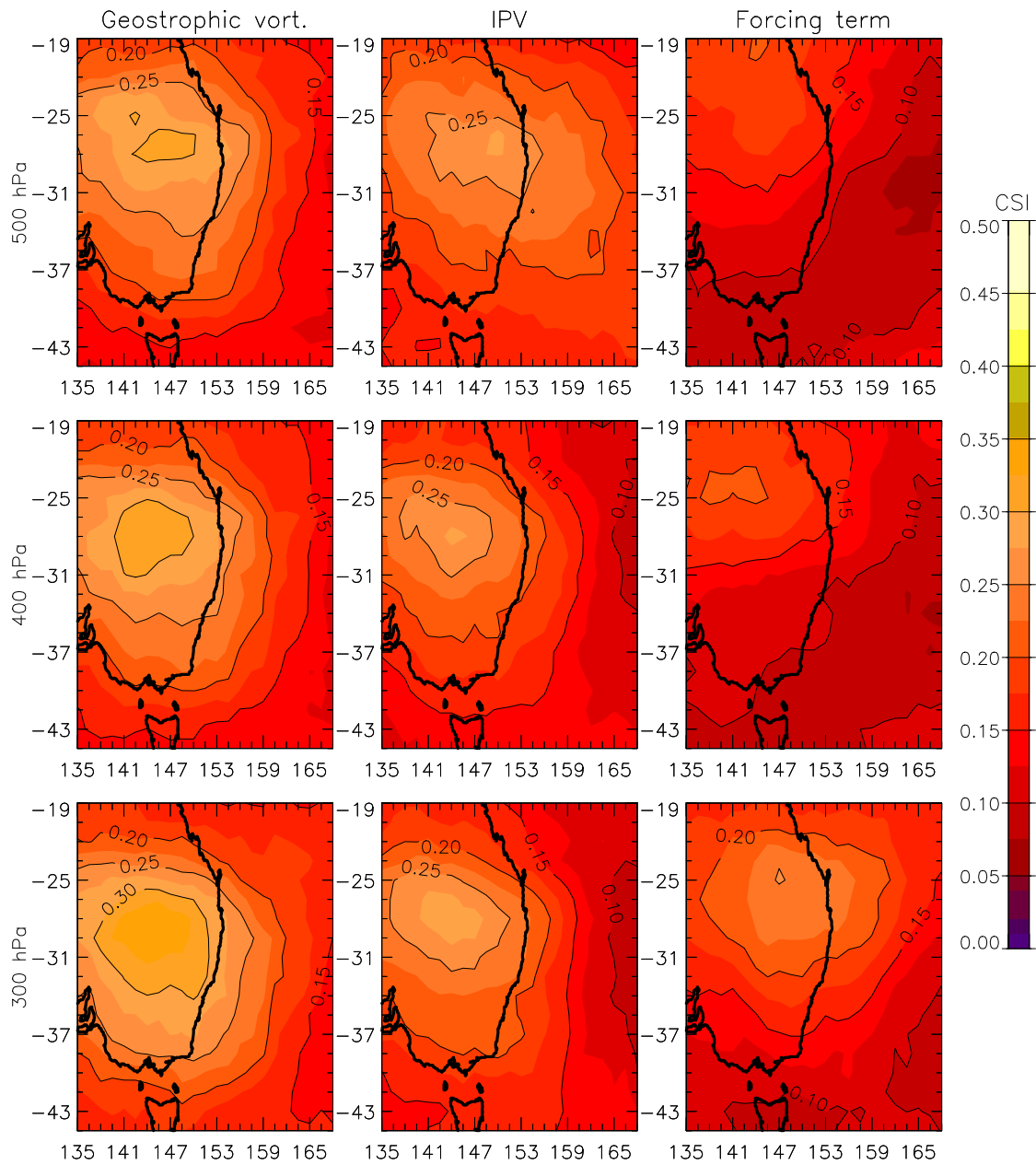


**Fig. 18** As for Fig. 12, but for days on which the total rainfall in the eastern seaboard was above its 90th percentile.

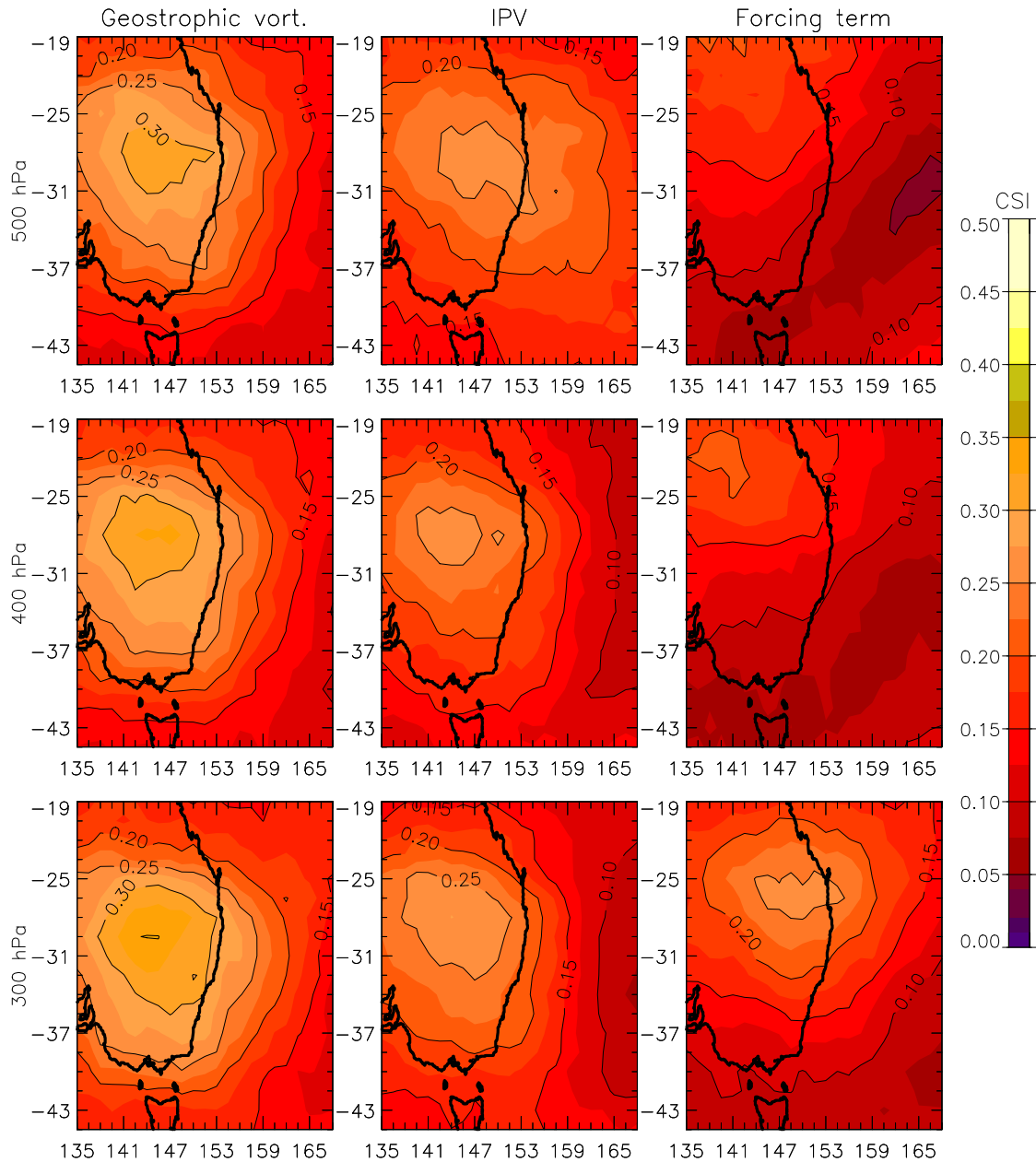


**Fig. 19** As for Fig. 12, but for days on which the total rainfall in the eastern seaboard was above its 90th percentile, with a 2-day running mean applied to the diagnostic.

## 5.4 Optimum performance statistics for ECL events

In this section we present CSI statistics for ECL events for all diagnostic quantities and levels using the optimal diagnostic areas as determined in the previous section. As well as the CSI, we list the centre of the optimal diagnostic box and the numbers of hits, misses, and false alarms for each diagnostic and event category. A 2-day running mean was applied to the diagnostic time series as this was shown above to generally produce the best results for indicating ECL events (from Figs 12 and 13).

Table 2 shows the verification statistics for ECL events for the best position of the diagnostic box (i.e. the maximum value shown in figures such as Fig. 12). The CSI is shown for all three diagnostics, as well as for all three pressure levels.

As described earlier, the geostrophic vorticity generally produces the highest CSI values, while the forcing term performs less well than the IPV term. The number of misses and false alarms are, subjectively, greater for these latter diagnostics, with the exception being the 300 hPa IPV which performs better than geostrophic vorticity at this pressure level only. For the forcing term, the fact that both the number of misses and the number of false alarms are greater indicates that the performance of this diagnostic is not simply a matter of threshold choice (the false alarms could undoubtedly be reduced by increasing the threshold above the 90<sup>th</sup> percentile). One avenue for further research would be to include a lower tropospheric response ingredient. For example, Bluestein (1992) (his Equation 5.8.15) shows that the lower tropospheric response is clearly a function of the static stability as well as the magnitude of the upper-level forcing.

Even for the 500 hPa geostrophic vorticity, the number of false alarms is 63 per cent of the number of hits, and the number of misses is 81 per cent of the number of hits. While some of these discrepancies can be argued away as being due to the difficulties of definition of an ECL event (see Chapter 3), more careful evaluation of this behaviour is clearly warranted.

**Table 2** Summary of diagnostic performance for ECL events, with a 2-day running mean applied to the diagnostic time series. The maximum CSI value is shown, with its corresponding number of hits, misses and false alarms. The latitude and longitude values shown represent the centre of the geographic box that produced the maximum CSI value for each diagnostic and pressure level.

Diagnostic	Pressure level (hPa)	Max. CSI	Hits	Misses	False alarms	Latitude (°S) of max. CSI	Longitude (°E) of max. CSI
Geostrophic vorticity	300	0.37	183	183	133	31.0	156.0
	400	0.41	201	165	130	29.0	156.0
	500	0.41	202	164	127	29.0	153.0
Isentropic potential vorticity	300	0.40	196	170	132	31.0	151.5
	400	0.35	171	195	129	28.0	147.0
	500	0.32	167	199	161	29.0	150.0
Forcing term	300	0.34	173	193	145	29.0	154.5
	400	0.28	146	220	164	26.0	147.0
	500	0.29	148	218	148	23.0	148.5

## 5.5 Optimum performance statistics for high impact events

Tables 3, 4 and 5 are similar to Table 2, but for strong wind events, heavy localised rain events and heavy widespread rain events, respectively. Looking at the results for the strong wind events (Table 3), we see that compared to the ECL events (Table 2) first, there are a much lower number of events than are contained in the ECL database, and, second, that there are a very large number of false alarms. Indeed, while the POD is around 66% for the 500 hPa geostrophic vorticity, against 55% in Table 2, the False Alarm Ratio (FAR) is 71% rather than 39%. Clearly there is the need for refinement of this impact criterion, or the diagnostic indicator of this impact criterion, if a large-scale diagnostic of strong wind events in this region is to be defined. Other alternatives include the possibility that large-scale upper tropospheric diagnostics do not provide a good indication of strong surface wind events, or the possibility that the strong wind event database derived from the ERA-Interim dataset is not suitable for this type of analysis.

The heavy rainfall criterion verifications are also different in character to both the ECL database criterion and to the strong wind criterion. For the heavy local rainfall events (Table 4), there are first many more events than in any of the ECL, the strong winds, or the extreme total rain event sets. One implication is that too many events of varying synoptic forcing, are captured by this criterion. While the number of false alarms is very low, particularly for the geostrophic vorticity diagnostic, the number of misses is very large. There also may need to be some further assessment of the diagnostic definitions in this case, if a large-scale diagnostic of heavy localised rainfall events in this region is to be defined and optimised. For example, it may be that the best definition of a heavy rainfall event is based on an area that is larger than a single 5 km by 5 km grid point as is done here for the heavy local rainfall events as defined in this report, but smaller than the entire area used for the heavy widespread rainfall events as defined in this report.

For the heavy widespread rainfall events (Table 5), the CSI are similar to the extreme maximum rainfalls, but the ratios of hits to misses is improved, particularly for the geostrophic vorticity term, but still much worse than desirable. The proportion of false alarms is also improved. Again more development should be applied to this definition in order for it to be applied to climatological investigations.

**Table 3** As for Table 2, but for extreme wind events.

Diagnostic	Pressure level (hPa)	Max. CSI	Hits	Misses	False alarms	Latitude (°S) of max. CSI	Longitude (°E) of max. CSI
Geostrophic vorticity	300	0.23	76	42	206	25.0	154.5
	400	0.24	79	39	207	28.0	150.0
	500	0.25	78	40	195	26.0	153.0
Isentropic potential vorticity	300	0.23	75	43	202	25.0	148.5
	400	0.23	74	44	204	25.0	150.0
	500	0.19	70	48	257	29.0	153.0
Forcing term	300	0.18	65	53	238	26.0	154.5
	400	0.17	60	58	228	22.0	148.5
	500	0.17	57	61	227	19.0	147.0

**Table 4** As for Table 2, but for extreme localised rainfall.

Diagnostic	Pressure level (hPa)	Max. CSI	Hits	Misses	False alarms	Latitude (°S) of max. CSI	Longitude (°E) of max. CSI
Geostrophic vorticity	300	0.34	215	312	108	29.0	144.0
	400	0.31	200	327	116	28.0	141.0
	500	0.29	186	341	110	23.0	147.0
Isentropic potential vorticity	300	0.27	179	348	125	26.0	145.5
	400	0.27	177	350	129	28.0	144.0
	500	0.27	184	343	157	28.0	144.0
Forcing term	300	0.25	167	360	153	26.0	153.0
	400	0.22	149	378	161	23.0	142.5
	500	0.23	152	375	140	19.0	142.5

**Table 5** As for Table 2, but for extreme widespread rainfall events.

Diagnostic	Pressure level (hPa)	Max. CSI	Hits	Misses	False alarms	Latitude (°S) of max. CSI	Longitude (°E) of max. CSI
Geostrophic vorticity	300	0.35	171	169	147	29.0	144.0
	400	0.33	159	181	136	28.0	147.0
	500	0.32	156	184	141	29.0	144.0
Isentropic potential vorticity	300	0.28	139	201	164	28.0	144.0
	400	0.27	138	202	165	28.0	141.0
	500	0.27	138	202	175	28.0	148.5
Forcing term	300	0.27	136	204	172	26.0	148.5
	400	0.27	107	233	169	20.0	139.5
	500	0.21	108	232	177	19.0	138.0

## 6 SEASONAL VARIATION

Given that there is a well-known seasonal cycle in the latitudes of the subtropical ridge (Drosowsky 2005) and the subtropical jet stream (Nakamura and Shimpo 2004), it is pertinent to test the sensitivity of the results presented in the previous section to seasonal influences. This section examines the seasonal variation of the diagnostic performance.

Figures 20 and 21 are similar to Fig. 9, but for summer (defined for this report as November-April) and winter (defined for this report as May-October), respectively. The seasonal results are qualitatively similar to the all-year results (Fig. 6), but with lower amplitudes and greater noise for the summer period, and with the centres in summer a little further south.

CSI values for Figs. 22 and 23 are similar to Fig. 13 but for summer and winter, respectively. The CSI values for winter (Fig. 23) are generally higher than for data from all times throughout the year (Fig. 13), with a maximum CSI value of 0.46 for the 400 hPa and 500 hPa geostrophic vorticity. In contrast, the maximum CSI value based on data throughout the entire year (from Fig. 13) was 0.41 for the 400 and 500 hPa geostrophic vorticity. Similar plots to these, but for extreme wind and rain events during summer and winter, are included in Appendix C for all three diagnostic quantities.

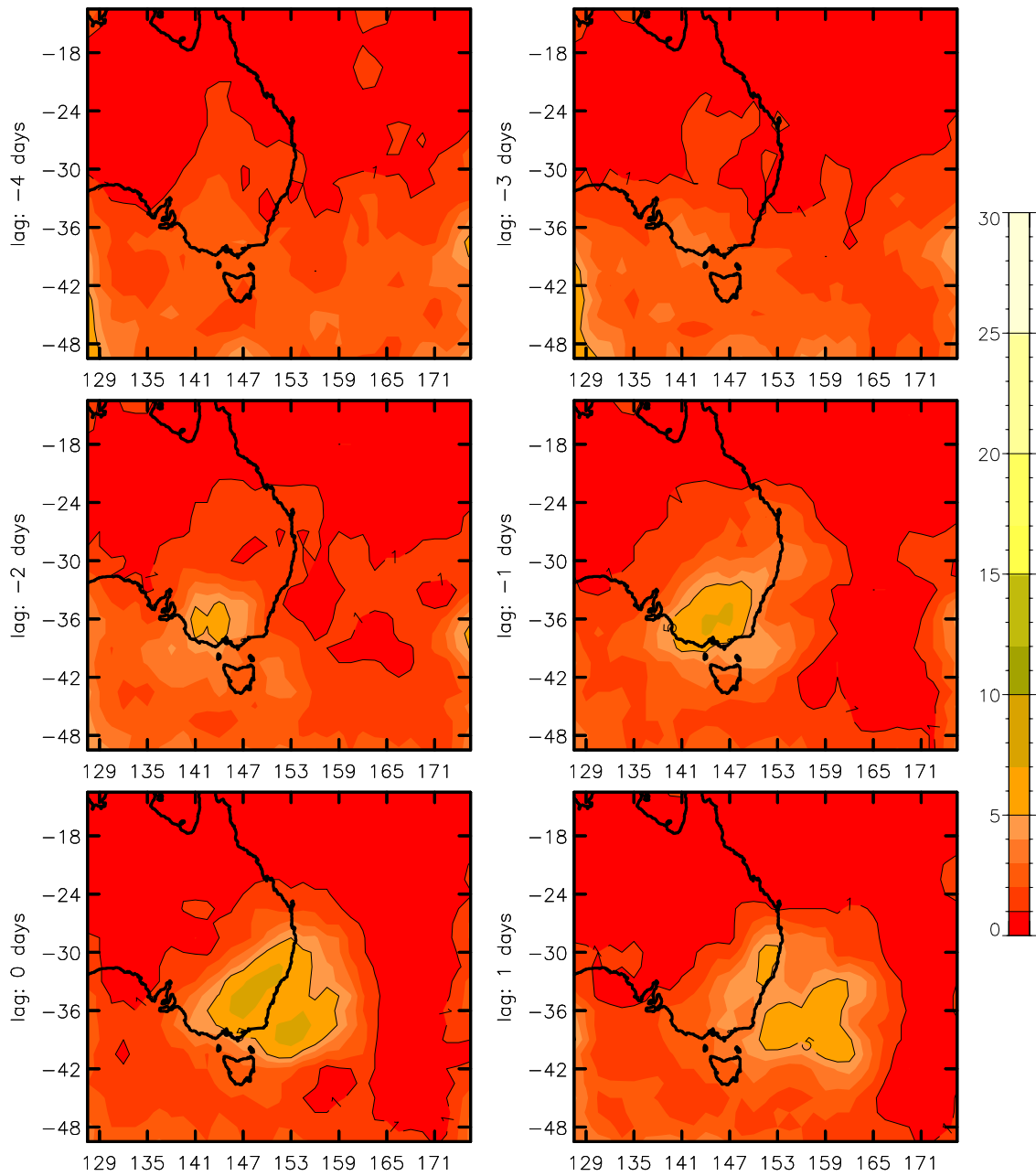


**Fig. 20** Number of times that the minimum value of the 400 hPa geostrophic vorticity in the area displayed occurred at a particular location, using all ECL event days that occurred during summer (November-April), at six different time lags (from -4 days to +1 day) with respect to the ECL event day. X and Y axes show latitude and longitude, respectively.

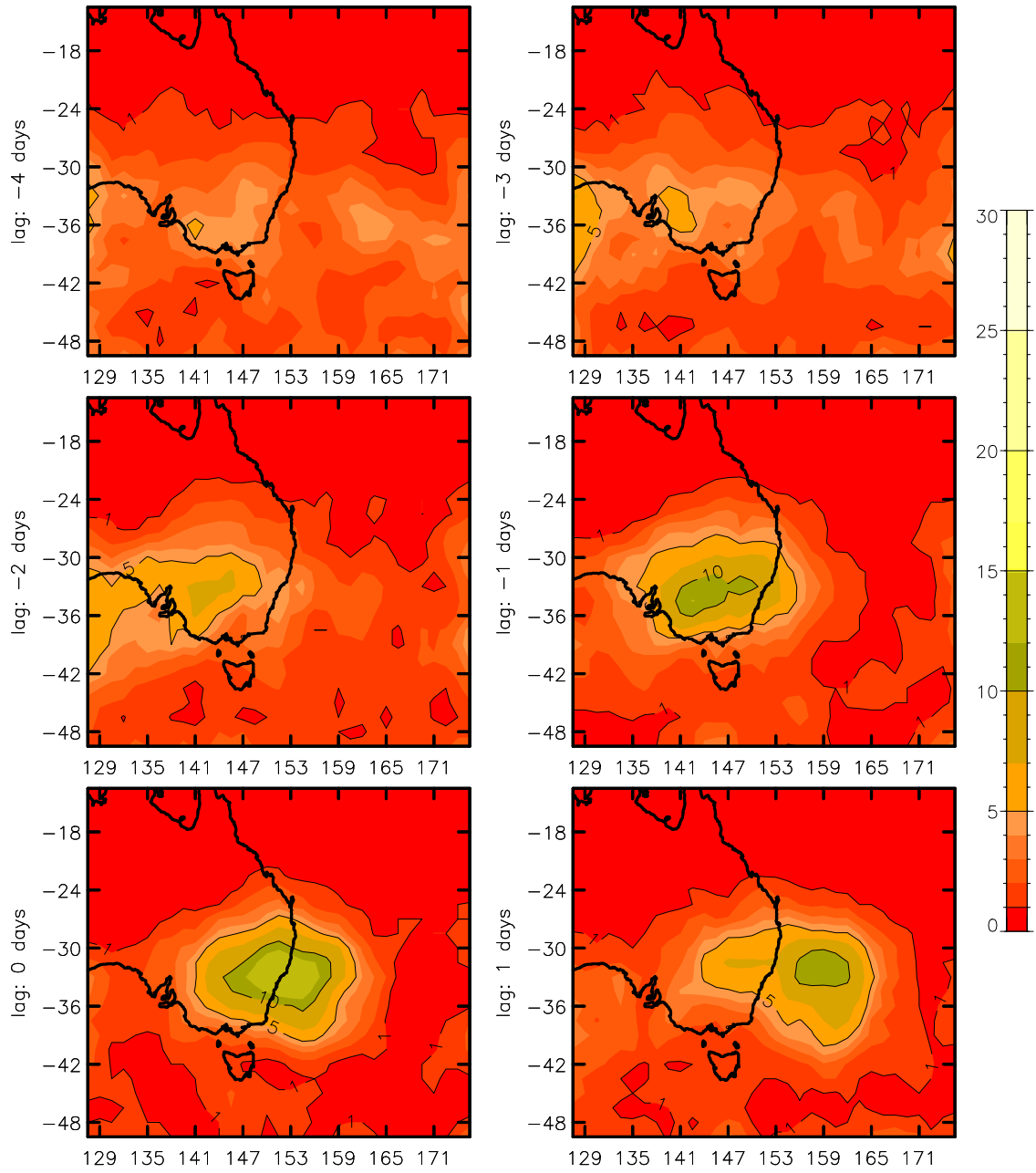


**Fig. 21** As for Fig. 20, but only using data for winter (May-October).

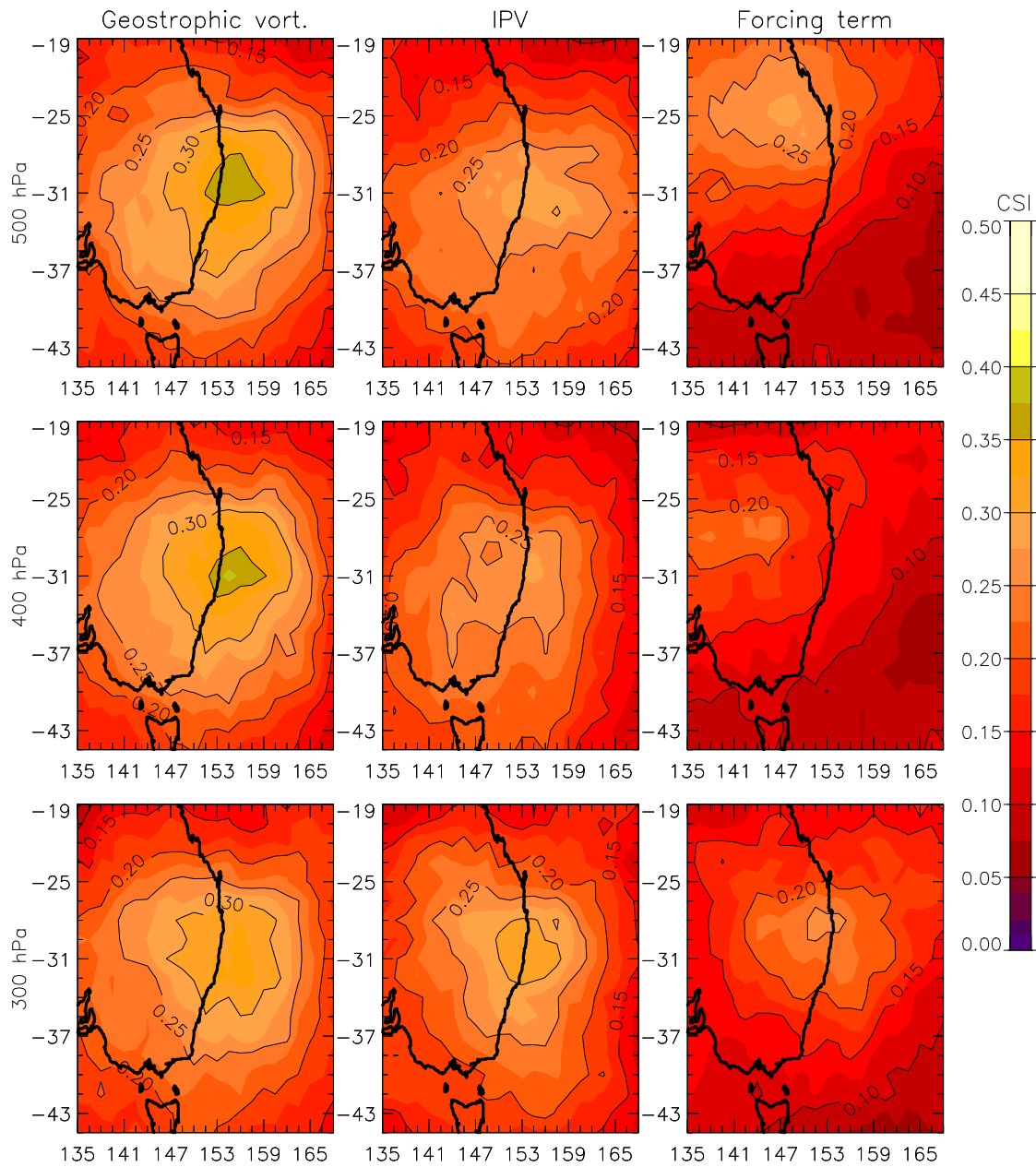


**Fig. 22** As for Fig. 13, but only using data for summer (November-April).

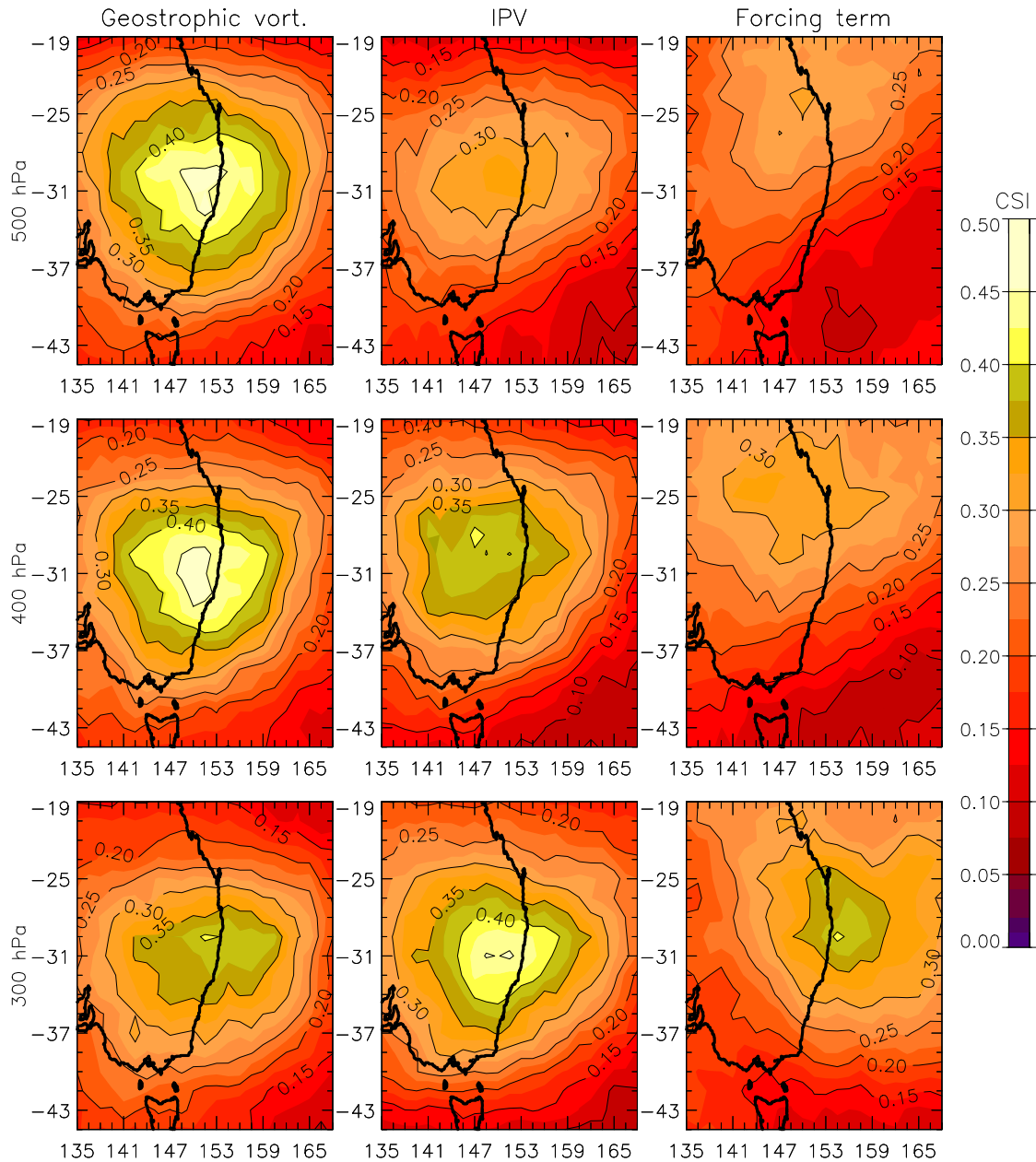


**Fig. 23** As for Fig. 13, but only using data for winter (May-October).

Tables 6 and 7 show, first, that there are slightly more ECL events in the winter than the summer period (190 vs 180), but also that the diagnostic approach being tested in this study performs markedly better during the winter period. For all three diagnostics, at all three pressure levels, the CSI values for winter (Table 7) are higher than for summer (Table 6) and also for all times throughout the year (Table 2). In particular, the ratio of hits to the sum of hits and misses (the Probability of Detection, POD) is dramatically improved during winter for the forcing term. This behaviour is also worth further study, as many of the classic ECL events described in Mills et al. (2010) occurred during the winter period. One aspect to be tested would be to test whether different thresholds need to be used in winter versus summer, but also from a climate variability and change perspective, are there different levels of impact for summer versus winter ECLs?

**Table 6** As for Table 2, but only using data only for winter.

Diagnostic	Pressure level (hPa)	Max. CSI	Hits	Misses	False alarms	Latitude (°S) of max. CSI	Longitude (°E) of max. CSI
Geostrophic vorticity	300	0.41	104	86	66	29.0	151.5
	400	0.46	119	71	66	29.0	151.5
	500	0.46	119	71	69	32.0	151.5
Isentropic potential vorticity	300	0.46	124	66	82	31.0	151.5
	400	0.42	115	75	87	28.0	147.0
	500	0.35	98	92	92	29.0	150.0
Forcing term	300	0.41	119	71	101	29.0	154.5
	400	0.34	104	86	117	25.0	145.5
	500	0.31	85	105	86	23.0	150.0

**Table 7** As for Table 2, but only using data only for summer.

Diagnostic	Pressure level (hPa)	Max. CSI	Hits	Misses	False alarms	Latitude (°S) of max. CSI	Longitude (°E) of max. CSI
Geostrophic vorticity	300	0.33	82	98	65	29.0	156.0
	400	0.39	92	88	58	31.0	154.5
	500	0.37	86	94	52	29.0	156.0
Isentropic potential vorticity	300	0.32	76	104	54	31.0	154.5
	400	0.29	68	112	58	31.0	154.5
	500	0.31	85	95	97	32.0	157.5
Forcing term	300	0.26	59	121	47	28.0	153.0
	400	0.23	57	123	65	28.0	138.0
	500	0.29	71	109	69	25.0	147.0

Tables similar to Tables 3-5, but calculated separately for summer and winter, are included for reference in Appendix D. These tables show similar results to that seen for ECL events in that there is less skill during summer than during winter, with the winter CSI values often being slightly higher than the values based on the entire year.

## 7 CONCLUSION AND FUTURE DIRECTIONS

This study discusses the methodology for and presents initial results of a project examining the feasibility of using large-scale upper-tropospheric diagnostics to indicate ECL occurrence. Early results are encouraging: two of the three diagnostics tested (based on geostrophic vorticity and isentropic potential vorticity) are found to be useful indicators of east-coast cyclogenesis in that they correctly indicate a high number of the observed ECL events without producing a high number of false alarms or missed ECL events. A third diagnostic, based on the forcing term of the pseudo-potential vorticity form of the quasi-geostrophic height tendency equation, referred to more simply here as the ‘forcing term’, does not perform as well as the other two diagnostic quantities.

Some seasonality in the results is apparent, with all three diagnostics producing better results during winter than during summer. Climatologies of the diagnostics (from 6-hourly values throughout the period 1989 to 2006) clearly identify the East Coast as a preferred region for extreme values of the diagnostics to occur. Understanding the reason for this provides scope for future work, including investigating a number of potentially influential factors such as orography (cold continent relative to the ocean, Great Diving Range, etc.) and Rossby wave activity.

With a view to future impact-based studies, the diagnostics are also compared with severe weather events such as extreme rainfall and wind speeds. As is the case for ECL events, geostrophic vorticity and isentropic potential vorticity are better than the forcing term at indicating the occurrence of heavy rainfall or strong wind events, as measured using the Critical Success Index (CSI). Heavy rainfall events are well represented by the diagnostics, with CSI values similar in magnitude to those for ECL events. Strong wind events are not as well indicated by the diagnostics as heavy rainfall or ECL events, possibly due to the limitations of reanalysis surface wind data. This could be investigated further in future studies using coastal wave data from the network of buoys located along the East Coast.

Following on from the results presented in this study, the next step is to improve the reliability of the diagnostics by examining the role of thresholds, geographic area, time periods and pressure levels used. It is also expected that further improvement in diagnostic performance can be obtained by combining diagnostics and analysing the seasonal dependence of the diagnostic performance. For example, summer ECLs during 2006 (Fig. 2) are well represented by isentropic potential vorticity, but not by the other three diagnostics including the best performing diagnostic (i.e. the geostrophic vorticity). Additional enhancements to the optimal diagnostic definition is also expected to be obtained through the application of the methodology developed in this report to other reanalysis data sets to investigate factors such as the influence of the spatial grid resolution of the diagnostic data. Another potential refinement could be to include a lower tropospheric response ingredient such as static stability or Eady Growth Rate (Hoskins and Valdez 1990).

Some studies have described a variety of different synoptic types of ECLs (e.g. Holland et al. 1987, Speer et al. 2009) and it may be that the optimal diagnostic determined for one ECL type may not necessarily be the optimal diagnostic for another ECL type. The best geographic position of the diagnostic area for strong wind events was further equatorward than for ECL events, and the best geographic position of the diagnostic for heavy rainfall events was further west than for ECL events. This suggests the possibility that there may be different subcategories of ECLs that might be identified by different upper-tropospheric large-scale characteristics.

Although ECLs are reasonably well represented by Numerical Weather Prediction models (Leslie and Speer 1998), the fine spatial and temporal resolutions required to resolve the

structure and intensity of these cyclones means that they are poorly represented by current global climate models (GCMs). Existing future climate projections are therefore unlikely to well capture the possible changes to ECLs, resulting in great uncertainty about rainfall projections for the eastern seaboard of Australia where ECLs are such an important feature. The results of this study show sufficient promise that the next stage of this project will apply these diagnostic techniques to other assimilated data sets with longer records but coarser resolution such as NCEP/NCAR reanalysis (Kalnay et al. 1996) to verify diagnostic performance in relation to the influence of model resolution, and to evaluate the effects of climate variability on the risk of ECL formation. If found suitable, the diagnostic will then be applied to current and future simulations of the climate by GCMs to infer the influence of climate change on ECL occurrence.

While it was argued that the definitions of ECL contain some ambiguity, blurring the verification statistics (as described in Section 3), the impact definitions proposed clearly are simplistic in terms of the large-scale diagnostic approach being tested. The results presented in Tables 1-5 do suggest several refinements to the heavy rainfall criteria used that are potentially much better than those proposed, while “combined” criteria such as “wind and precipitation”, or “ECL, wind and precipitation” may provide improvements to the statistical performance measures achieved in this report. In addition, further development of the diagnostic quantities is worth investigating – particularly the inclusion of some form of lower tropospheric response component, as all measures tested so far only represent (qualitatively) the upper-tropospheric forcing component of extra-tropical cyclogenesis.

## ACKNOWLEDGMENTS

This research was undertaken as part of the Australian Climate Change Science Program, with support from the New South Wales Department of Environment, Climate Change and Water. We would also like to acknowledge advice used for this paper provided by Clinton Rakich and Agata Imielska from the NSW Climate Services Centre of the Bureau of Meteorology, Perry Wiles from the National Climate Centre of the Bureau of Meteorology and Milton Speer from the University of NSW, as well as Mike Pook and Debbie Abbs from CSIRO as part of the Centre for Australian Weather and Climate Research for their comments on earlier drafts of this study

## REFERENCES

- Bluestein, H.B. 1992. Synoptic-Dynamic Meteorology in Midlatitudes. Volume 1. Oxford University Press, 431.
- Bridgeman, H.A. 1986. The Sygna storm at Newcastle-12 years later. *Meteorol. Aust.*, **3**(5), 10-16.
- CSIRO and Bureau of Meteorology. 2007. Climate Change in Australia, Technical report, Department of Climate Change, 148 (available at: <http://www.climatechangeinaustralia.gov.au>).
- Donaldson, R.J. Jr., Dyer, R.M. and Kraus, M.J. 1975. An objective evaluator of techniques for predicting severe weather events. 9th Conference on Severe Local Storms, Norman, OK, 321-326.

- Drosowsky, W. 2005. The latitude of the subtropical ridge over eastern Australia: the L index revisited. *Int J of Clim*, **25**, 1291-1299.
- Fuenzalida, H.A., Sanchez, R. and Garreaud, R.D. 2005. A climatology of cut-off lows in the Southern Hemisphere. *J. Geophys. Res.* **110**, D18101, doi:10.1029/2005JD005394.
- Holland, G.J., Lynch, A.H. and Leslie, L.M. 1987. Australian east-coast cyclones. Part I: synoptic overview and case study. *Mon. Wea. Rev.* **115**, 3024-3036.
- Hopkins, L.C. and Holland, G.J. 1997. Australian heavy-rain days and associated east coast cyclones 1958-92. *J. Climate* **10** 621-35.
- Hoskins, B.J., McIntyre, M.E. and Robertson, A.W. 1985. On the use and significance of isentropic potential vorticity maps. *Quart. J. Roy. Meteor. Soc.* **111**, 877-946.
- Hoskins, B.J. and Valdes, P.J. 1990. On the existence of Storm-Tracks. *J. Atmos. Sci.* **47**, 1854-1864.
- Jones, D.A., Wang, W. and Fawcett, R. 2009. High-quality spatial climate data sets for Australia. *Aust. Met. Oceanogr. J.* **58**, 233-48.
- Kuwano-Yoshida, A. and Asuma, Y. 2008. Numerical Study of Explosively Developing Extratropical Cyclones in the Northwestern Pacific Region. *Mon. Wea. Rev.*, **136**, 712-74.
- Kalnay, E. and co-authors. 1996. The NCEP/NCAR 40-year reanalysis project. *Bull. Am. Met. Soc.*, **77**, 437-471.
- Karoly, D.J. and Vincent, D.G. 1998. The meteorology of the Southern Hemisphere. American Meteorological Society, Boston, Mass, 410pp.
- Keable, M., Simmons, I. and Keay, K. 2002. Distribution and temporal variability of 500 hPa cyclone characteristics in the Southern Hemisphere. *Int. J. Climatol.* **22**, 131-150.
- Leslie, L.M. and Speer, M.S. 1998. Weather and Forecasting 13 822-32.
- Mills, G.A. 2001. Mesoscale cyclogenesis in reversed shear – the 1998 Sydney-Hobart yacht race storm. *Aust. Meteor. Mag.* **50**, 29-52.
- Mills, G.A., Webb, R., Davidson, N.E., Kepert, J., Seed, A. and Abbs, D. 2010. The Pasha Bulker east coast low of 8 June 2007. CAWCR Technical Report 23, 62pp.
- Nakamura, H. and Simpo, A. 2004. Seasonal variations in the southern hemisphere storm tracks and jet streams as revealed in a reanalysis dataset, *Journal of Climate*, **17**, 1828-1844.
- Ndarana, T. and Waugh, D.W. 2010. The link between cut-off lows and Rossby wave breaking in the Southern Hemisphere. *Quart. J. Roy. Meteor. Soc.*, **136**, 869-885.
- Nieto, R., Gimeno, L., de la Torre, L., Ribera, P., Gallego, D., Garcia-Herrera, R., Garcia, J.A., Nunez, M., Redano, A. and Lorente, J. 2005. Climatological features of cutoff low systems in the Northern Hemisphere. *J. Climate* **18**, 3085-3103.
- Otkin, J.A. and Martin, J.E. 2004. A synoptic climatology of the subtropical Kona storm. *Mon. Wea. Rev.* **132**, 1502-1517.

Pook, M.J., McIntosh, P.C. and Meyers, G.A. 2006. The synoptic decomposition of cool-season rainfall in the southeastern Australian cropping region. *J. Appl. Met. and Climatol.* **45**, 1156-1170.

Pepler, A.S. and Rakich, C.S. 2010. Proceedings of 17<sup>th</sup> National Conference of the Australian Meteorological and Oceanographic Society. IOP Conf. Series: Earth and Environmental Science **11** (2010) 012010, doi:10.1088/1755-1315/11/1/012010.

Qi, L., Leslie, L.M. and Speer, M.S. 2006. Cut-off low pressure systems over southern Australia: climatology and case study. *Meteorol. Atmos. Phys.*, **91**, 201–209.

Risbey, J.S., Pook, M.J., McIntosh, P.C., Ummenhofer, C.C. and Meyers, G. 2009. Characteristics and variability of synoptic features associated with cool season rainfall in southeastern Australia. *Int. J. Climatology*, **29**, 1595-1613.

Simpson, R.H. 1952. Evolution of the Kona storm a subtropical cyclone. *J. Atmos. Sci.*, **9**, 24-35.

Sinclair, M.R., Renwick, J.A. and Kidson, J.W. 1997. Low-Frequency Variability of Southern Hemisphere Sea Level Pressure and Weather System Activity. *Monthly Weather Review*, **125**, 2351-2543.

Speer, M.S., Wiles, P. and Pepler, A. 2009. Low pressure systems off the New South Wales coast and associated hazardous weather: establishment of a database. *Aust. Met. Oceanogr. J.*, **58**, 29-39.

Timbal, B. 2010. The climate of the Eastern Seaboard of Australia: a challenging entity now and for future projections. 2010 IOP Conf. Ser.: Earth Environ. Sci., 11 012013, doi: 10.1088/1755-1315/11/1/012013.

Uppala, S.P. and coauthors. 2005. The era-40 re-analysis, *Quart J Roy Meteor Soc*, **131**, 2961–3012.

Uppala, S., Dee, D., Kobayashi, S., Berrisford, P. and Simmons, A. 2008. Towards a climate data assimilation system: status update of ERA-Interim. ECMWF Newsletter, No. 115, ECMWF, Reading, United Kingdom, 12–18.

## Appendix A - Preferred positions of extreme values of the diagnostics

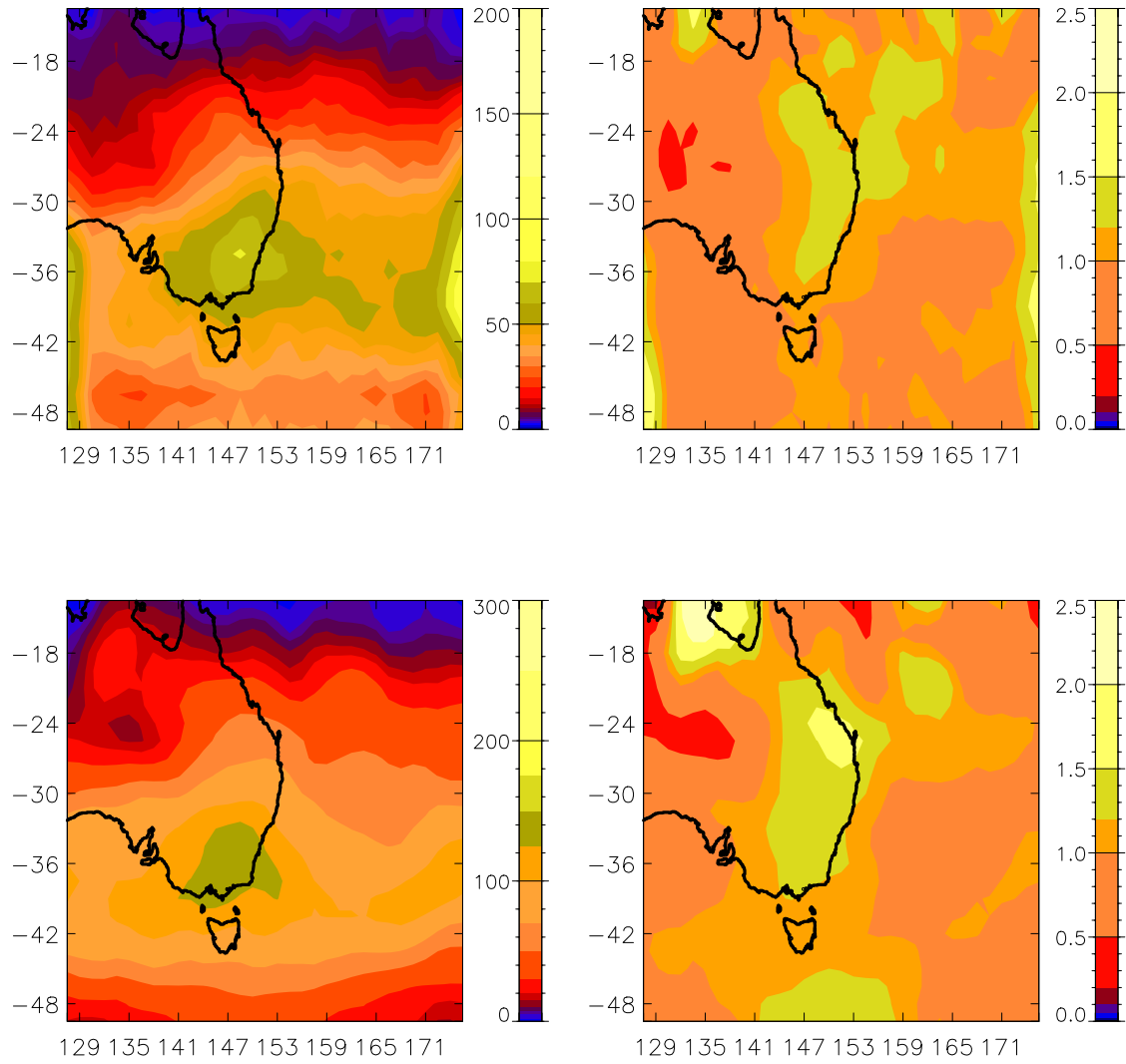


**Fig. A1** As for Fig. 6, but for the 300 hPa geostrophic vorticity.

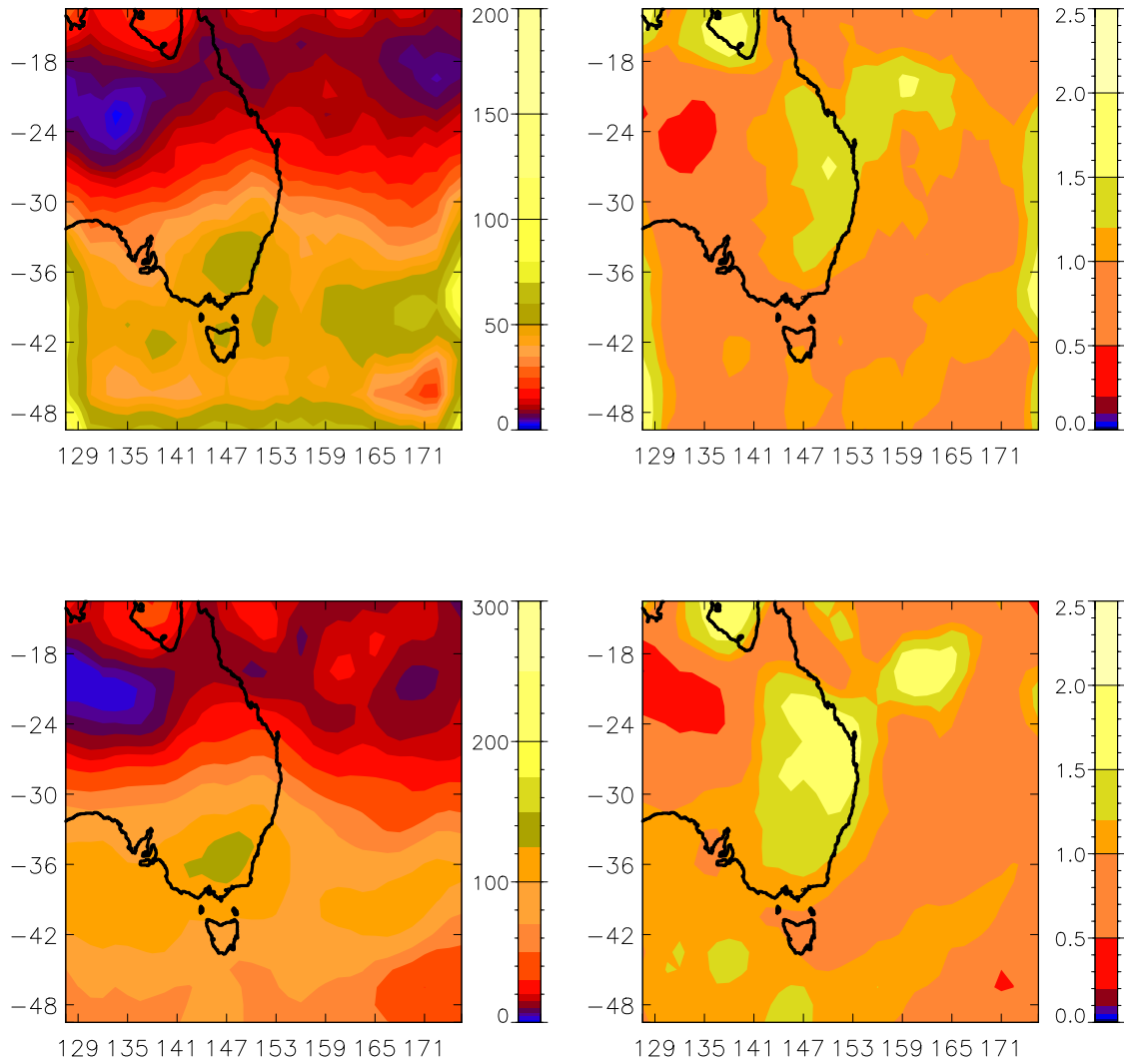


**Fig. A2** As for Fig. 6, but for the 500 hPa geostrophic vorticity.

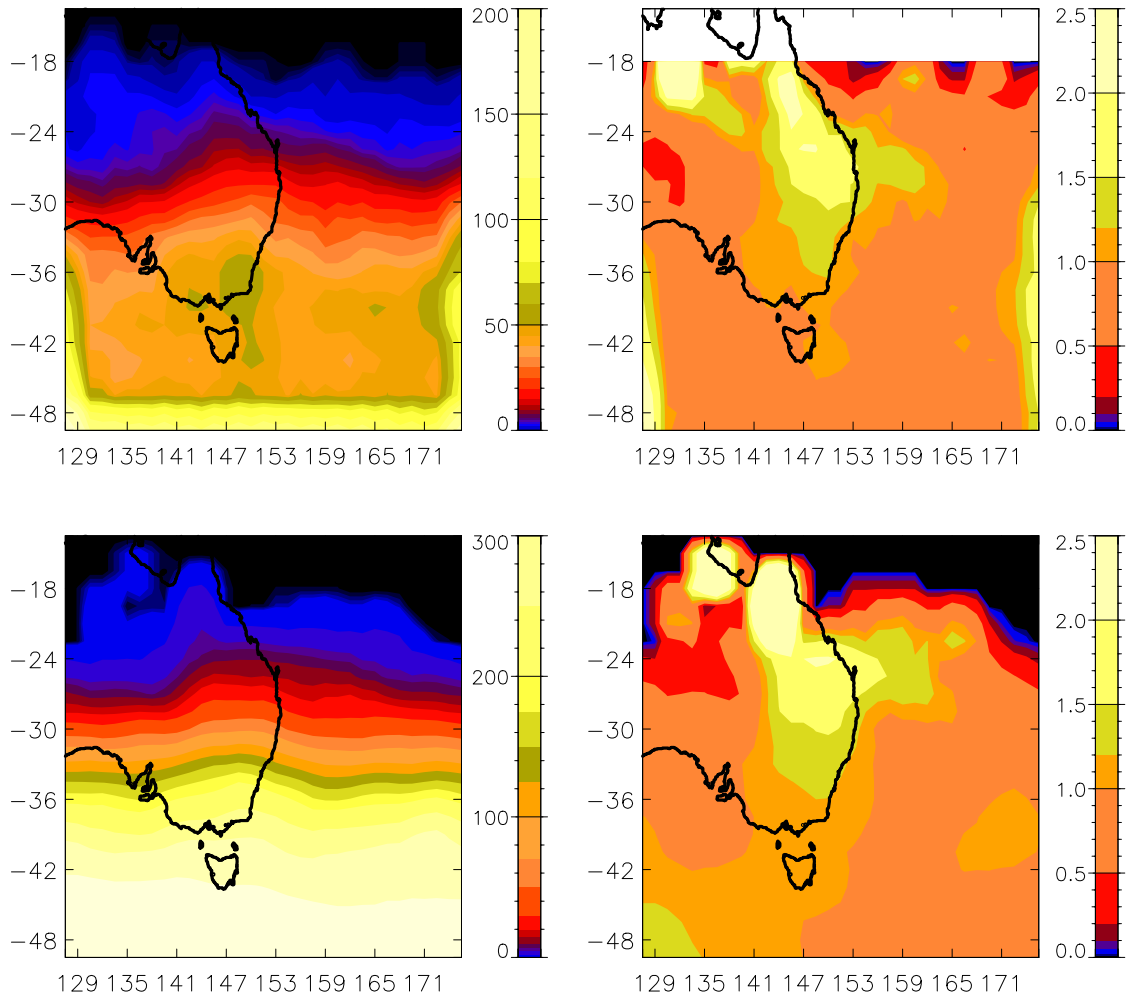


**Fig. A3** As for Fig. 6, but for the 300 hPa IPV.

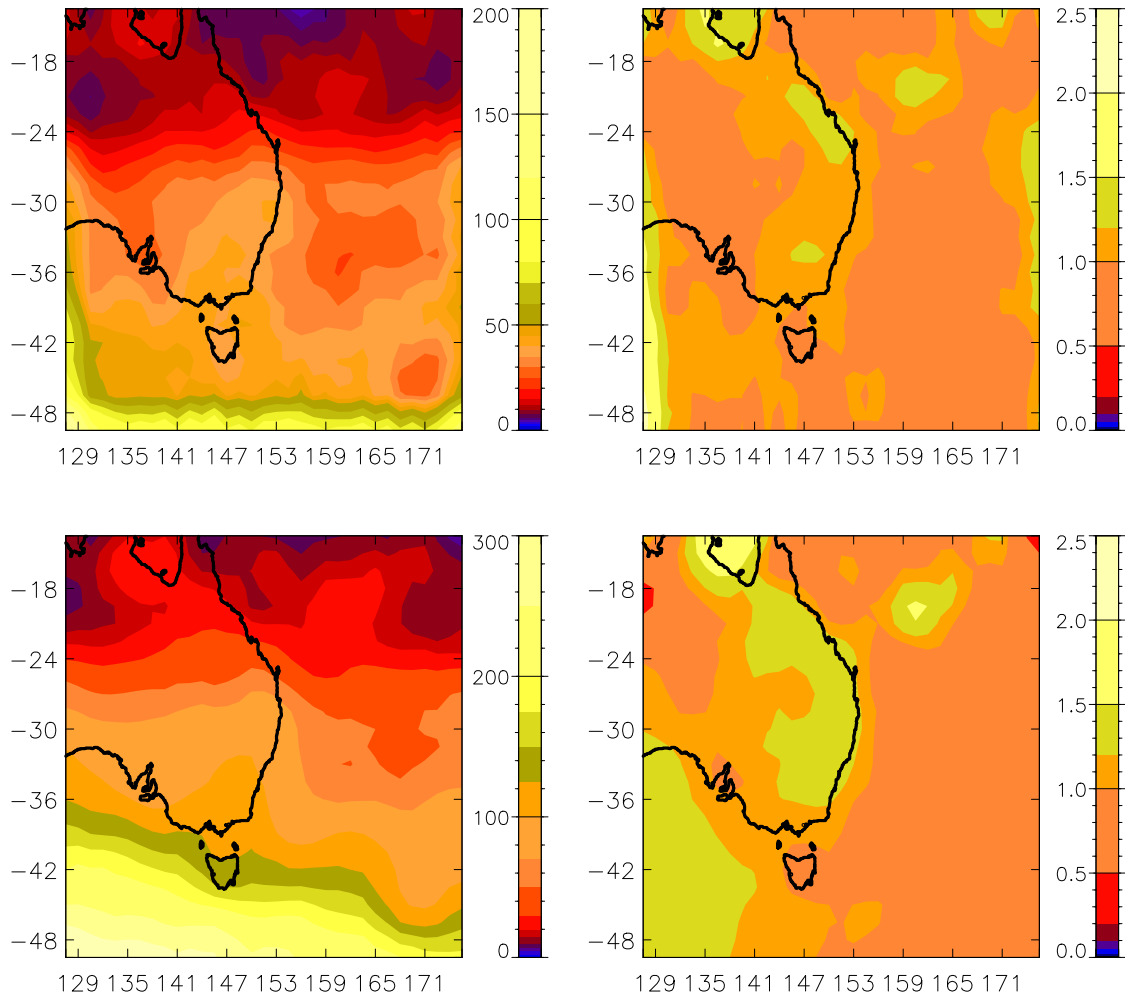


**Fig. A4** As for Fig. 6, but for the 500 hPa IPV.

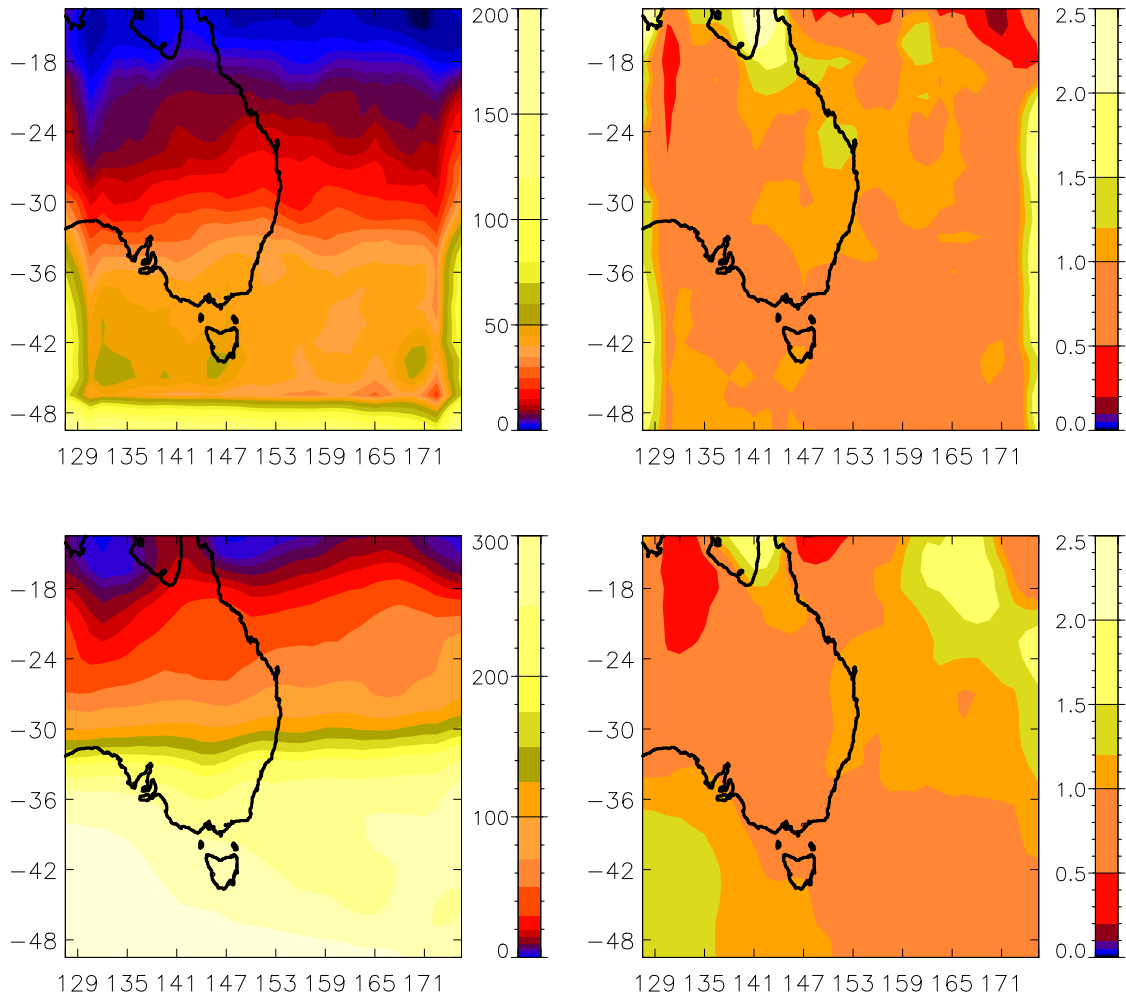


**Fig. A5** As for Fig. 6, but for the 300 hPa forcing term.

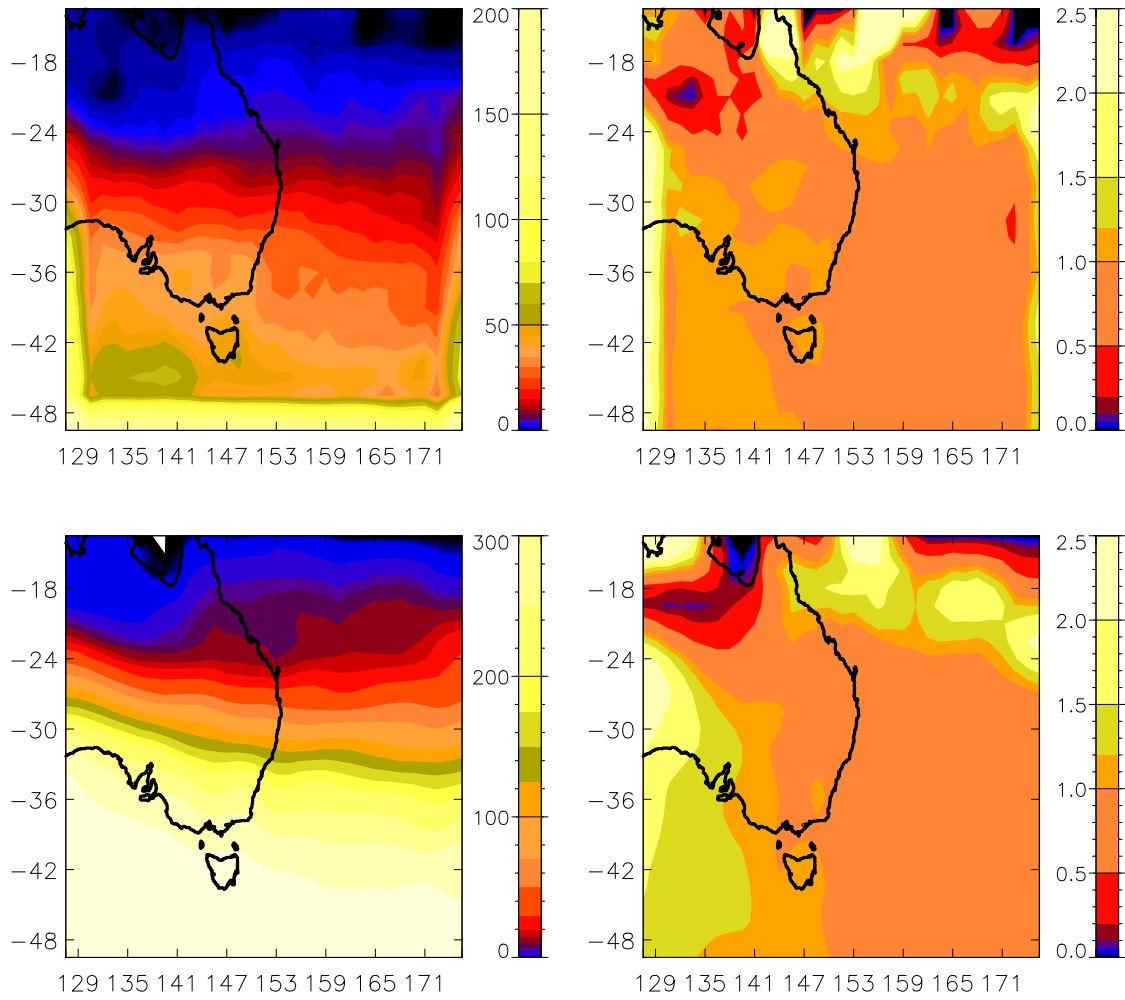


**Fig. A6** As for Fig. 6, but for the 500 hPa forcing term.

## APPENDIX B - EXTREME VALUES OF THE DIAGNOSTICS

### B.1 Extreme values of the diagnostics for days on which ECLs occurred

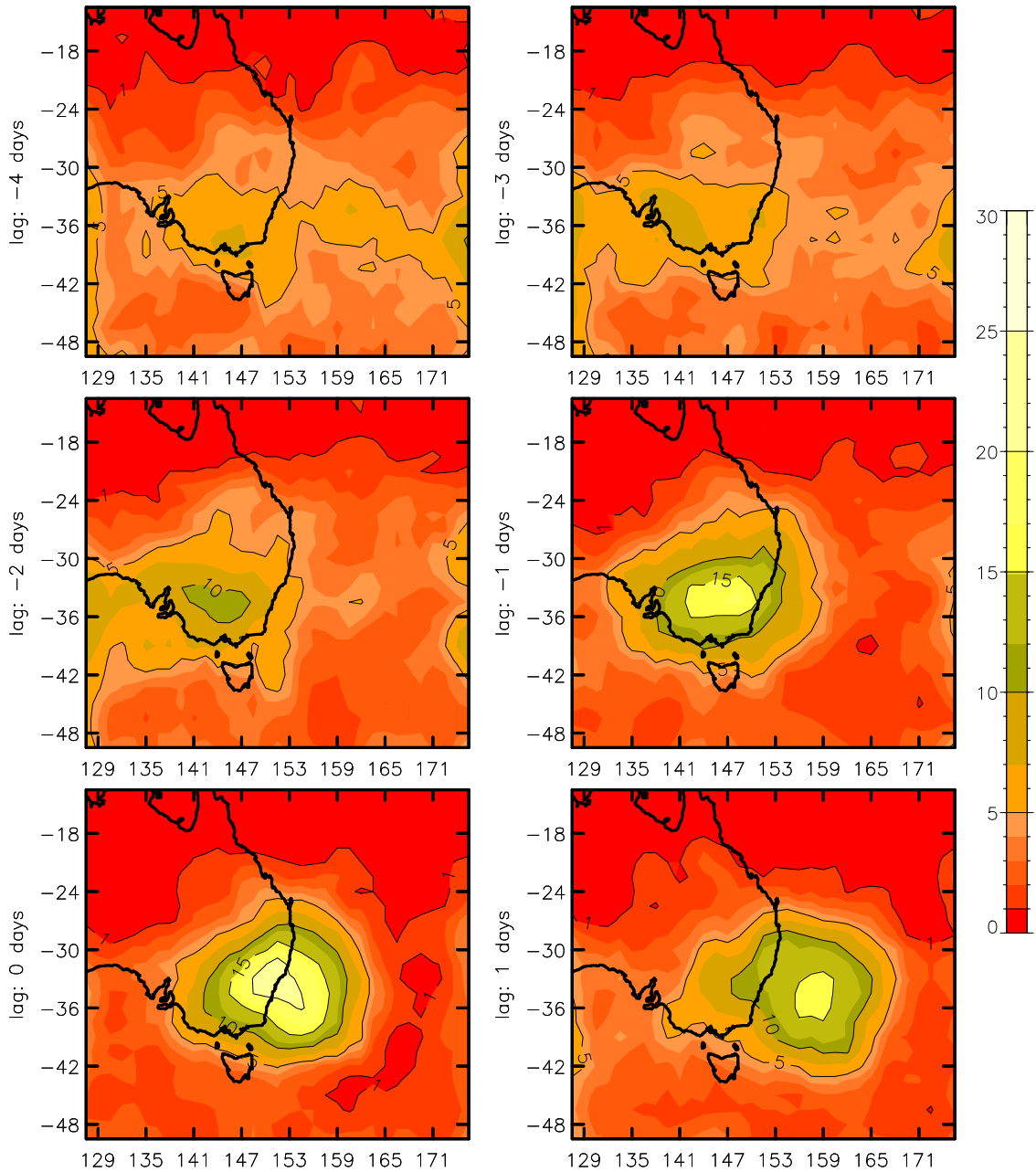


**Fig. B1** As for Fig. 9, but for the 300 hPa geostrophic vorticity.

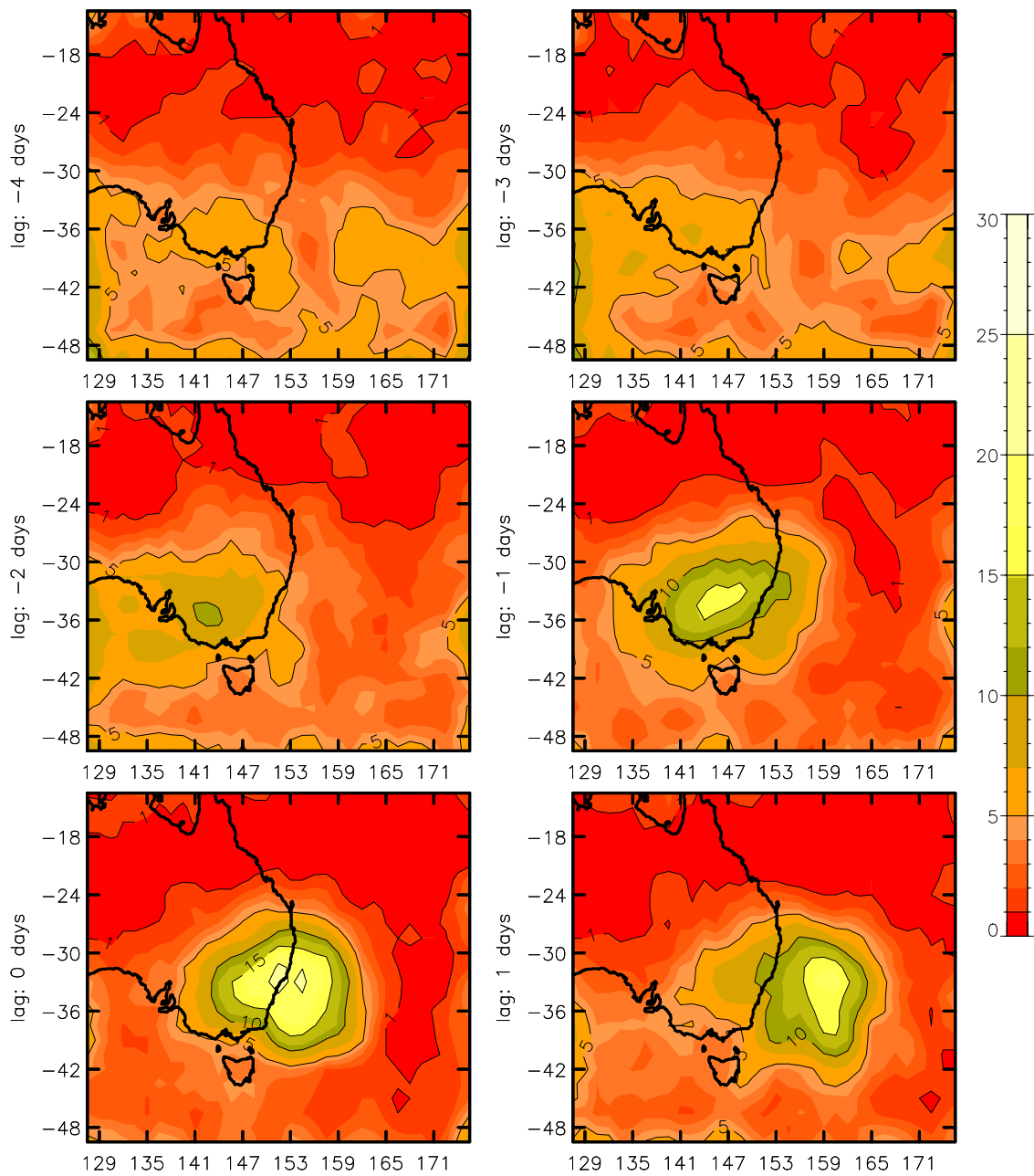


**Fig. B2** As for Fig. 9, but for the 500 hPa geostrophic vorticity.

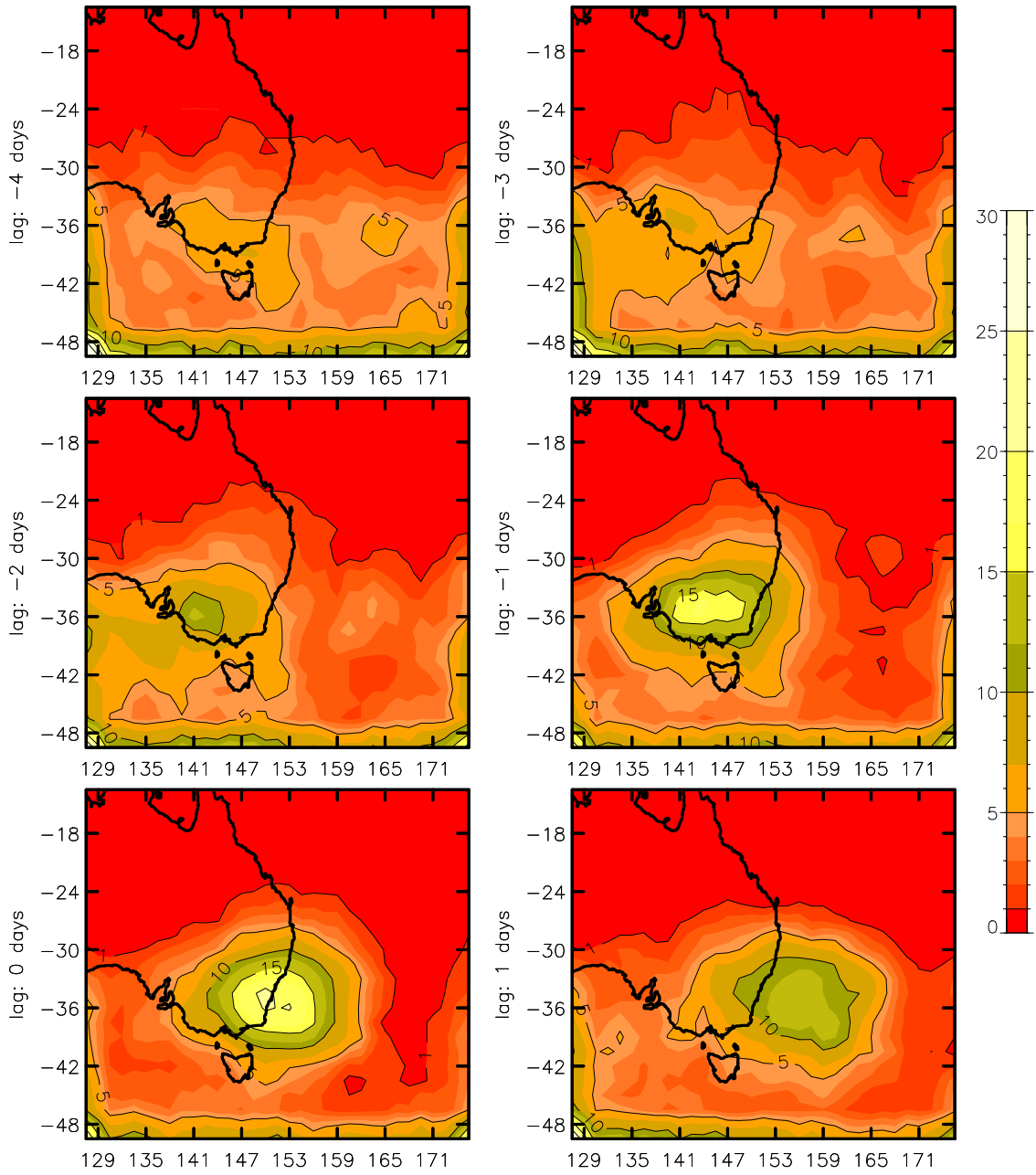


**Fig. B3** As for Fig. 9, but for the 300 hPa IPV.

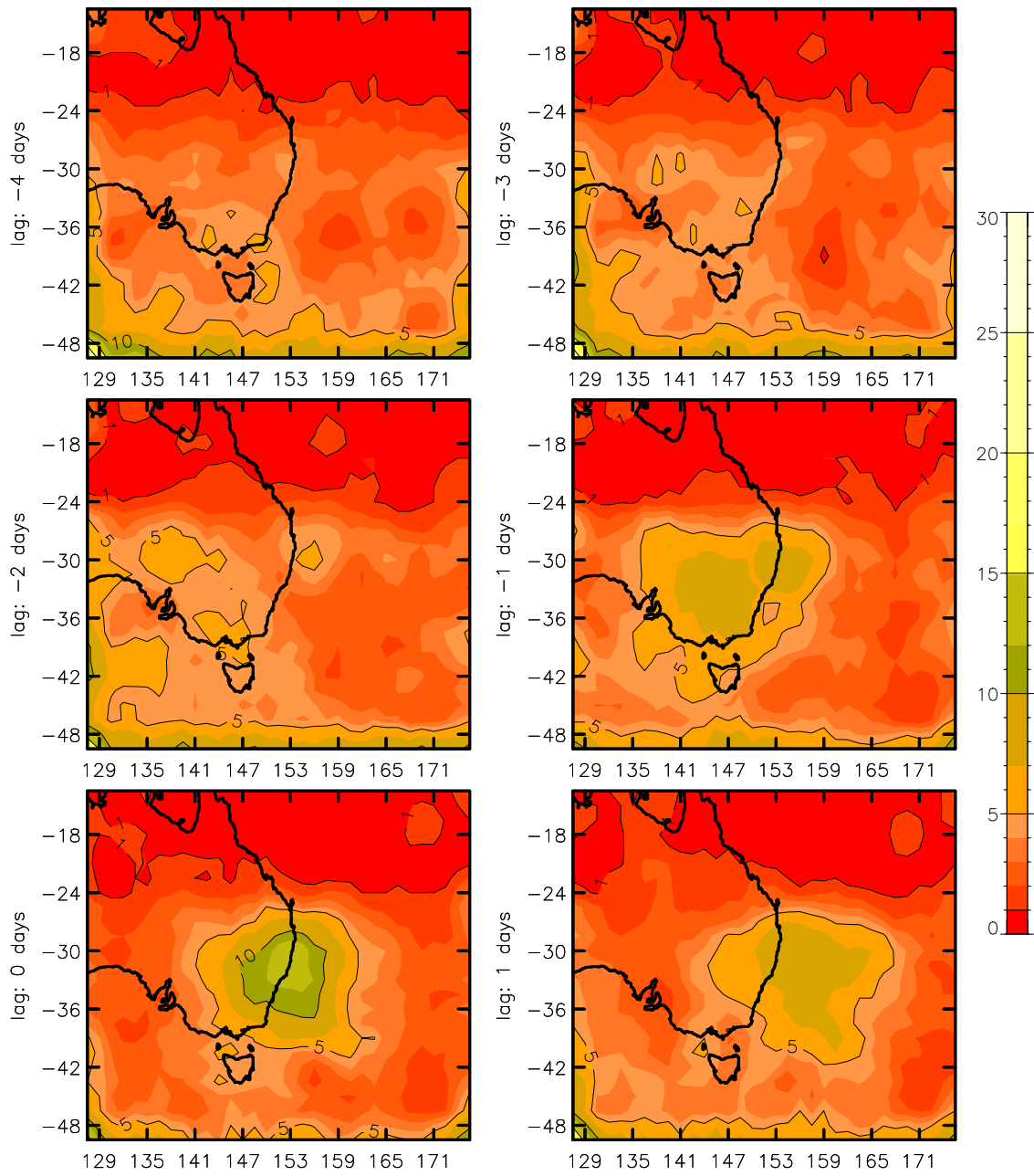


**Fig. B4** As for Fig. 9, but for the 500 hPa IPV.

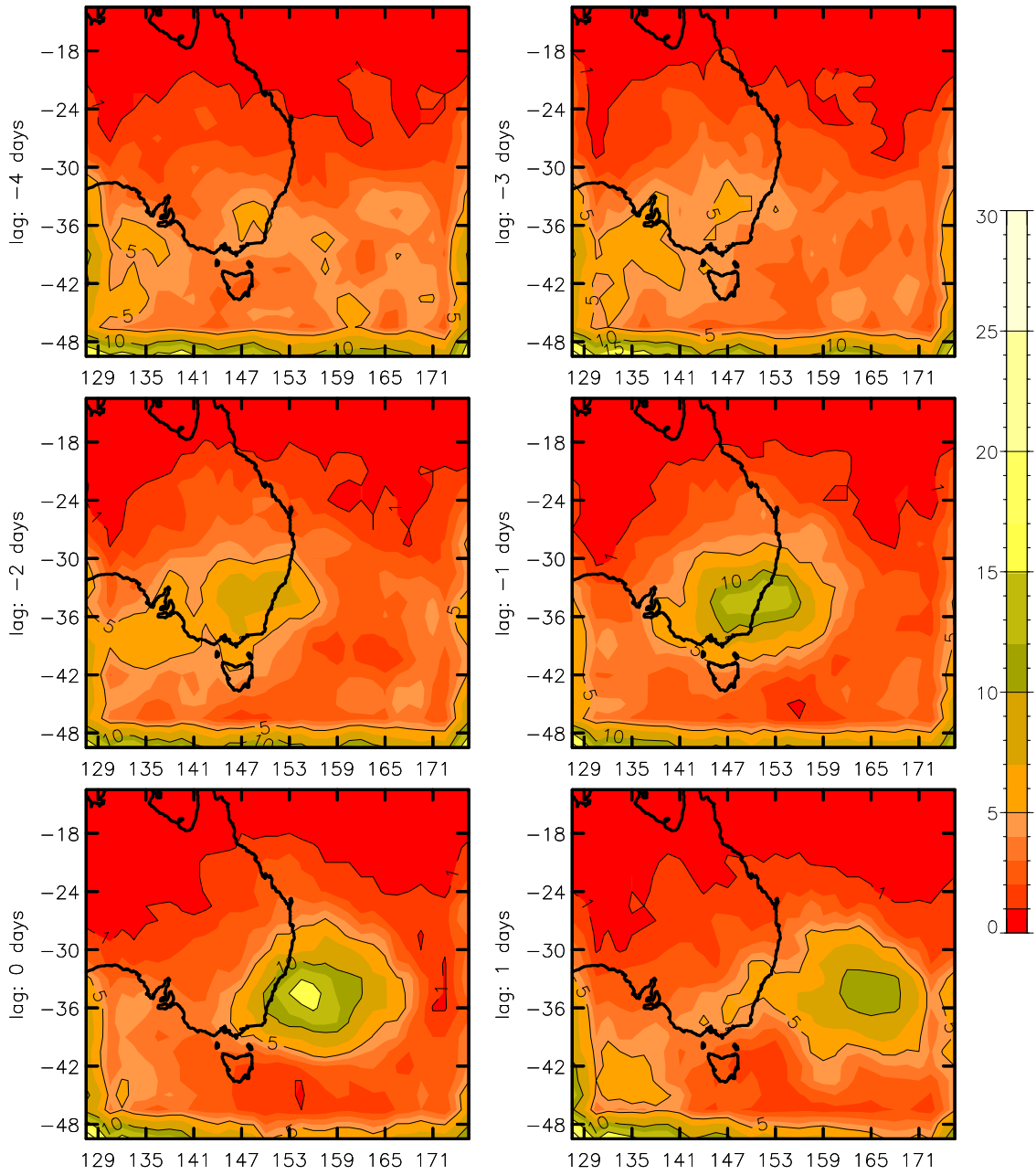


**Fig. B5** As for Fig. 9, but for the 300 hPa forcing term.

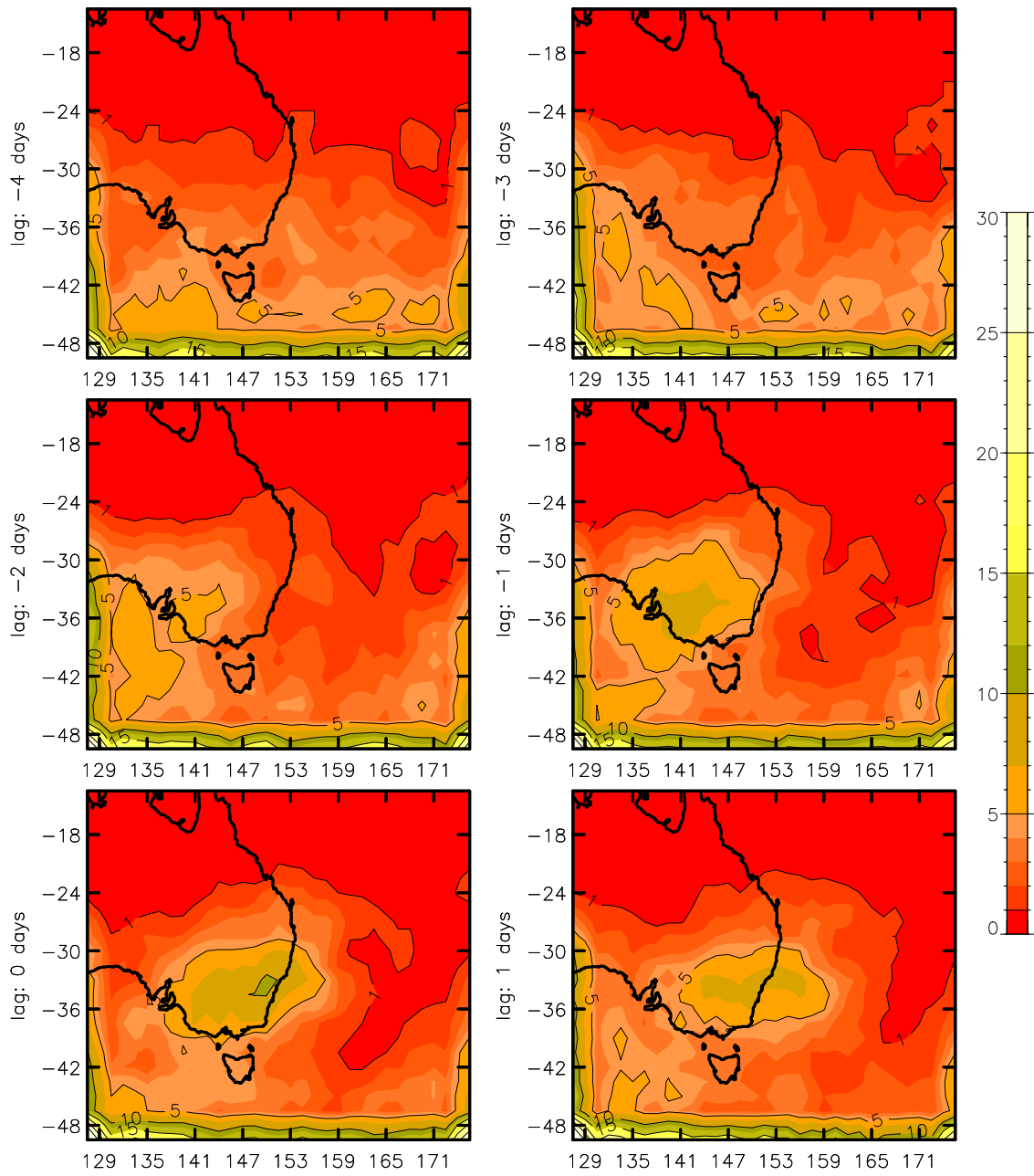


**Fig. B6** As for Fig. 9, but for the 500 hPa forcing term.

## B.2 Extreme values of the diagnostics for days on which strong wind events occurred

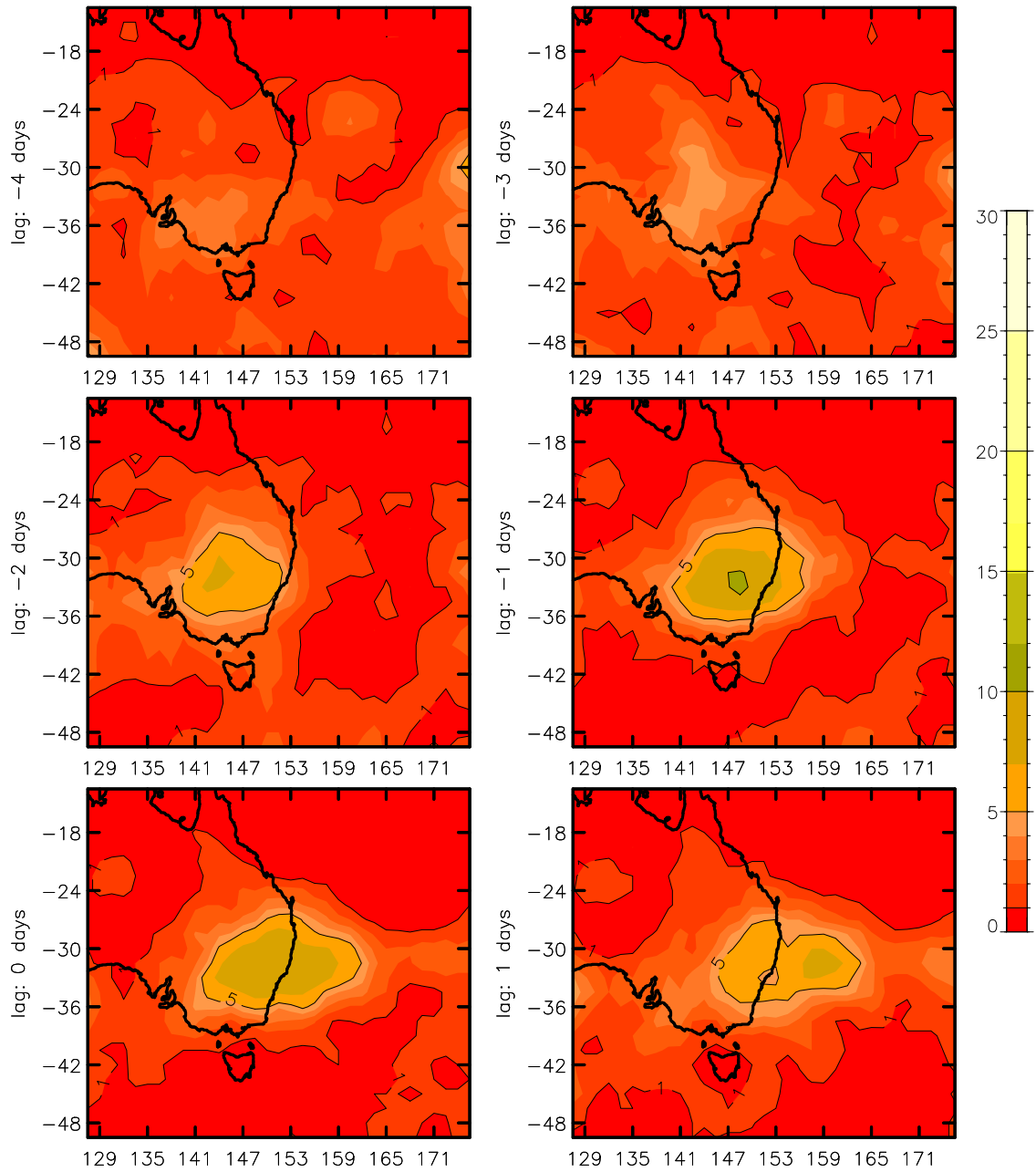


**Fig. B7** As for Fig. 9, but for the 300 hPa geostrophic vorticity as an indicator of strong wind events.

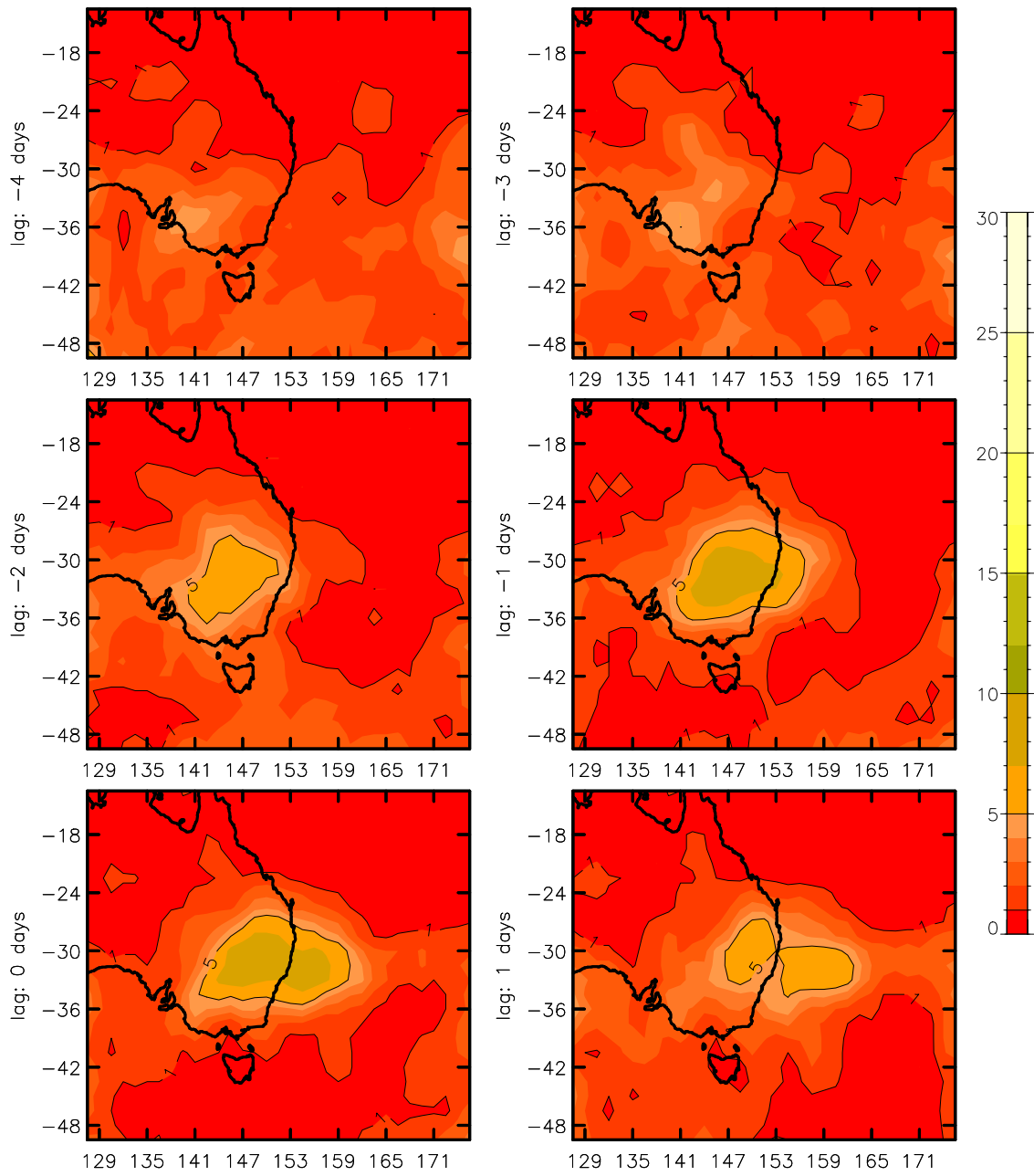


**Fig. B8** As for Fig. 9, but for the 400 hPa geostrophic vorticity as an indicator of strong wind events.

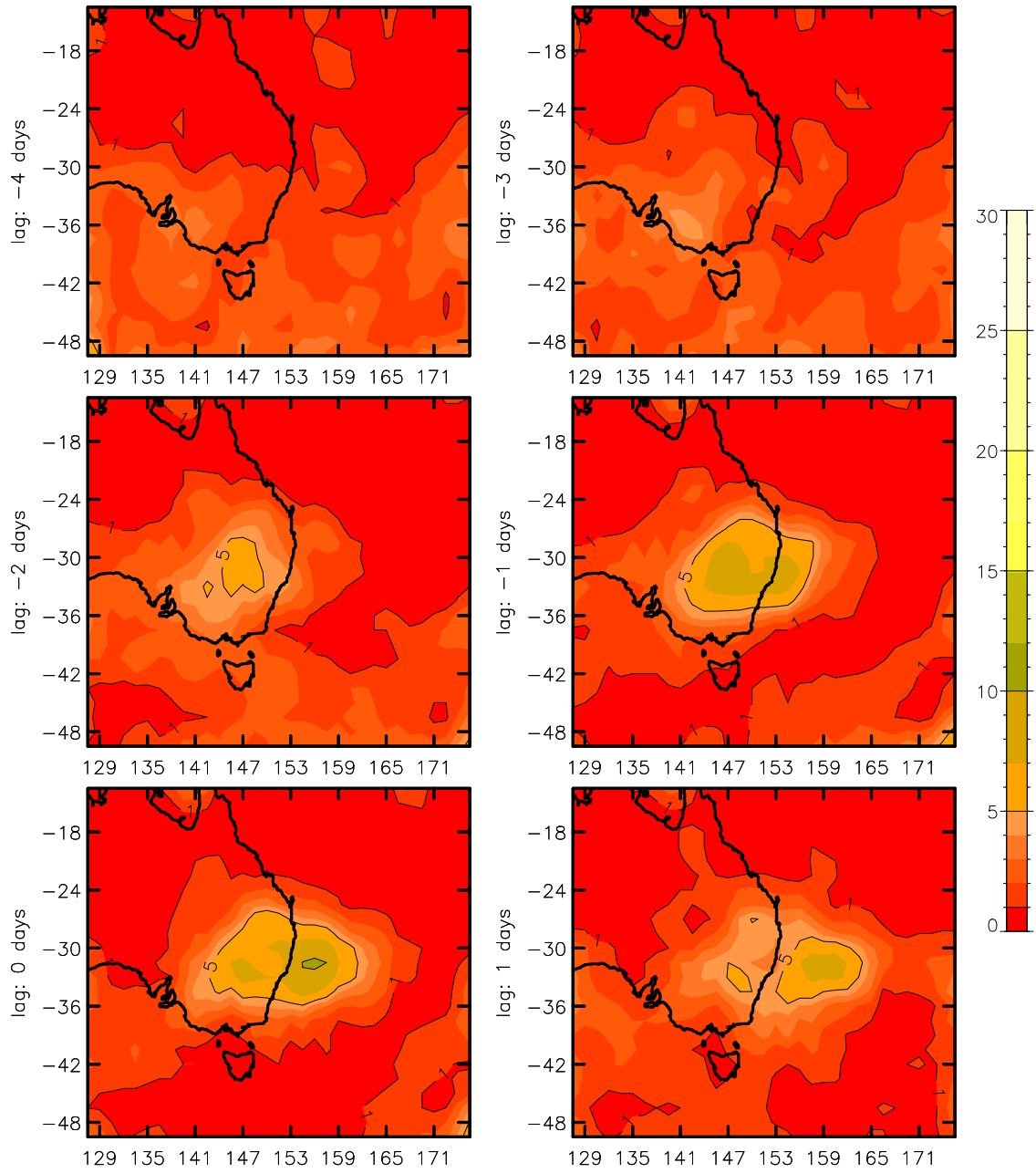


**Fig. B9** As for Fig. 9, but for the 500 hPa geostrophic vorticity as an indicator of strong wind events.

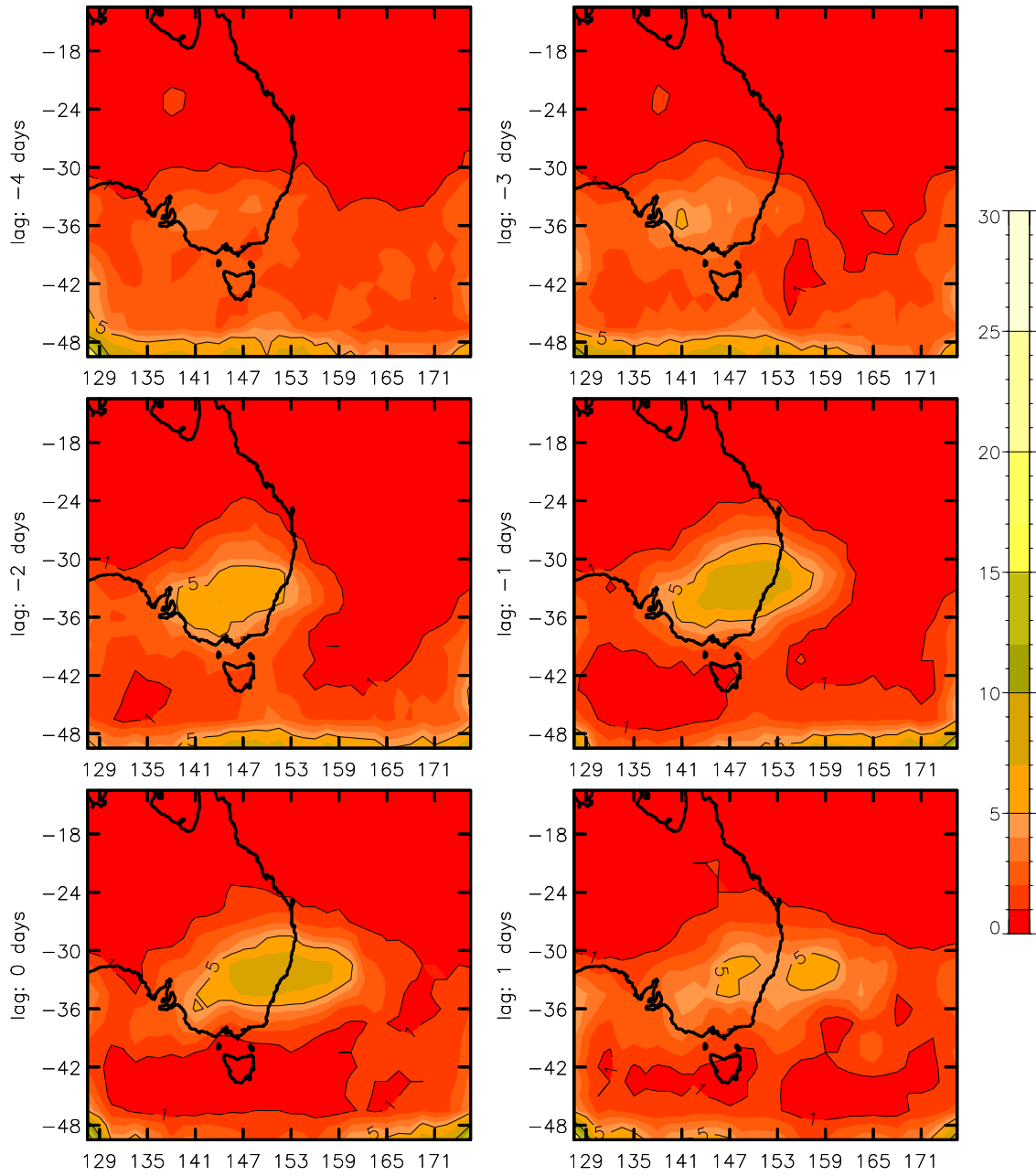


**Fig. B10As** for Fig. 9, but for the 300 hPa IPV as an indicator of strong wind events.

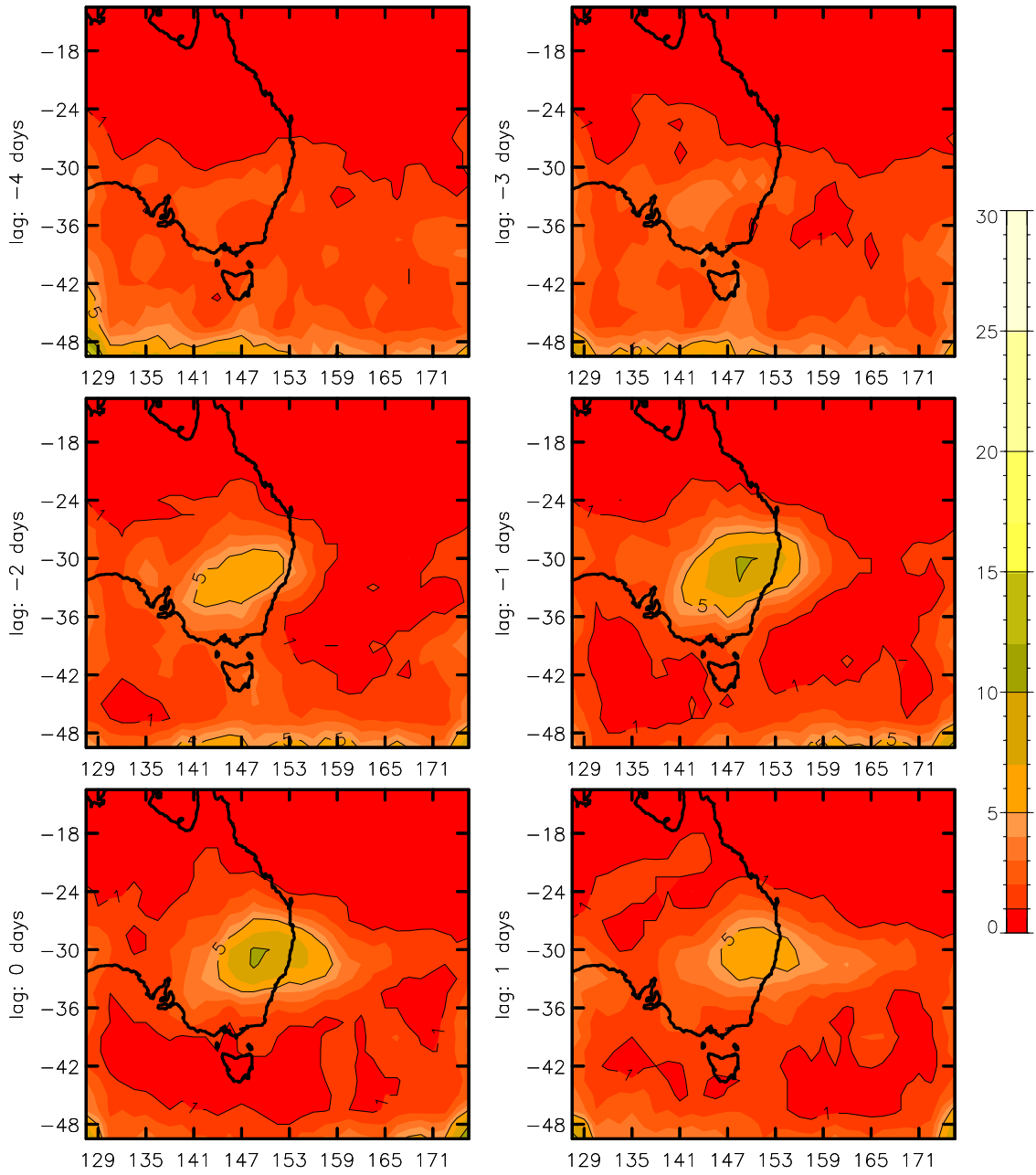


**Fig. B11** As for Fig. 9, but for the 400 hPa IPV as an indicator of strong wind events.

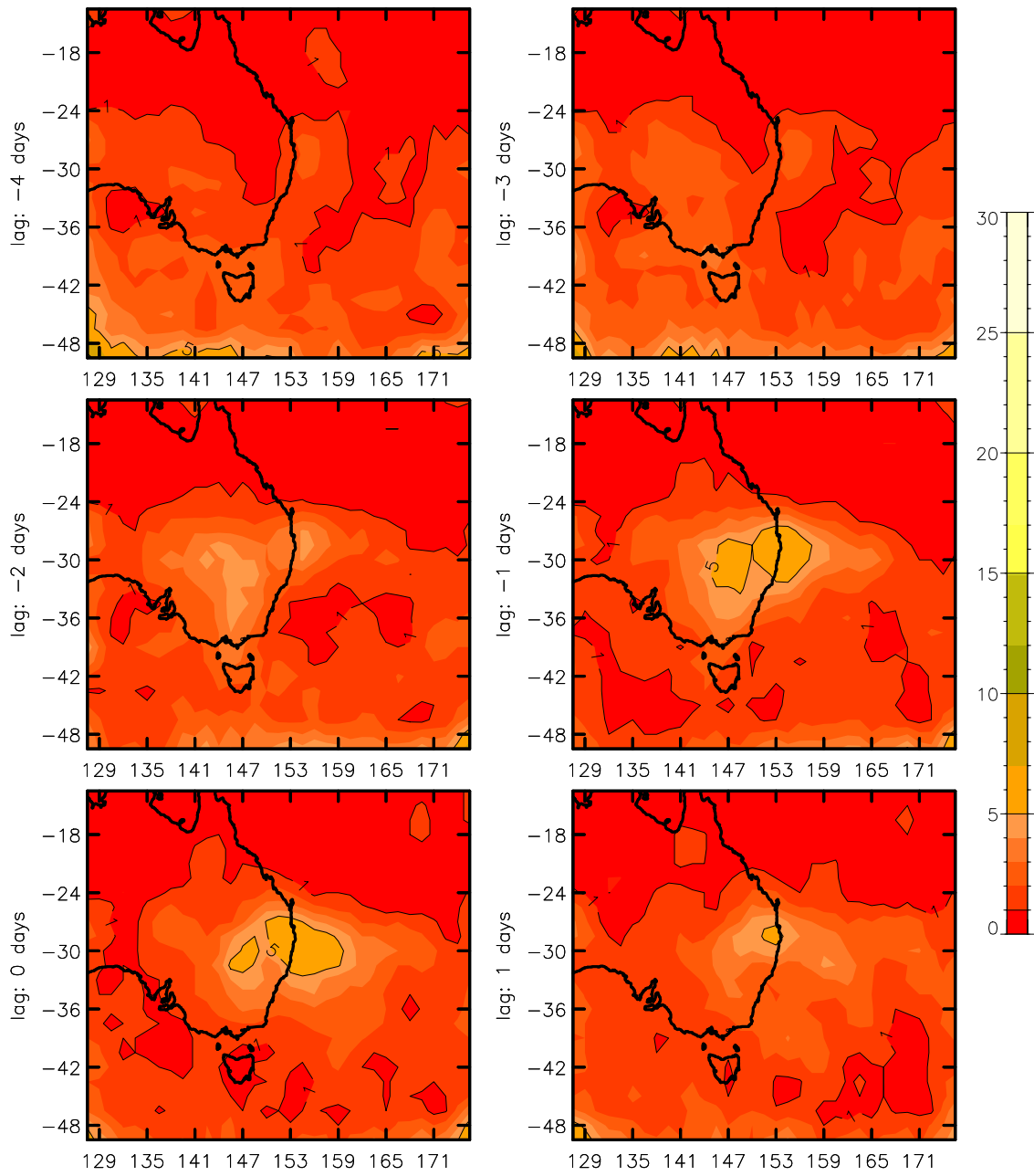


**Fig. B12As** for Fig. 9, but for the 500 hPa IPV as an indicator of strong wind events.

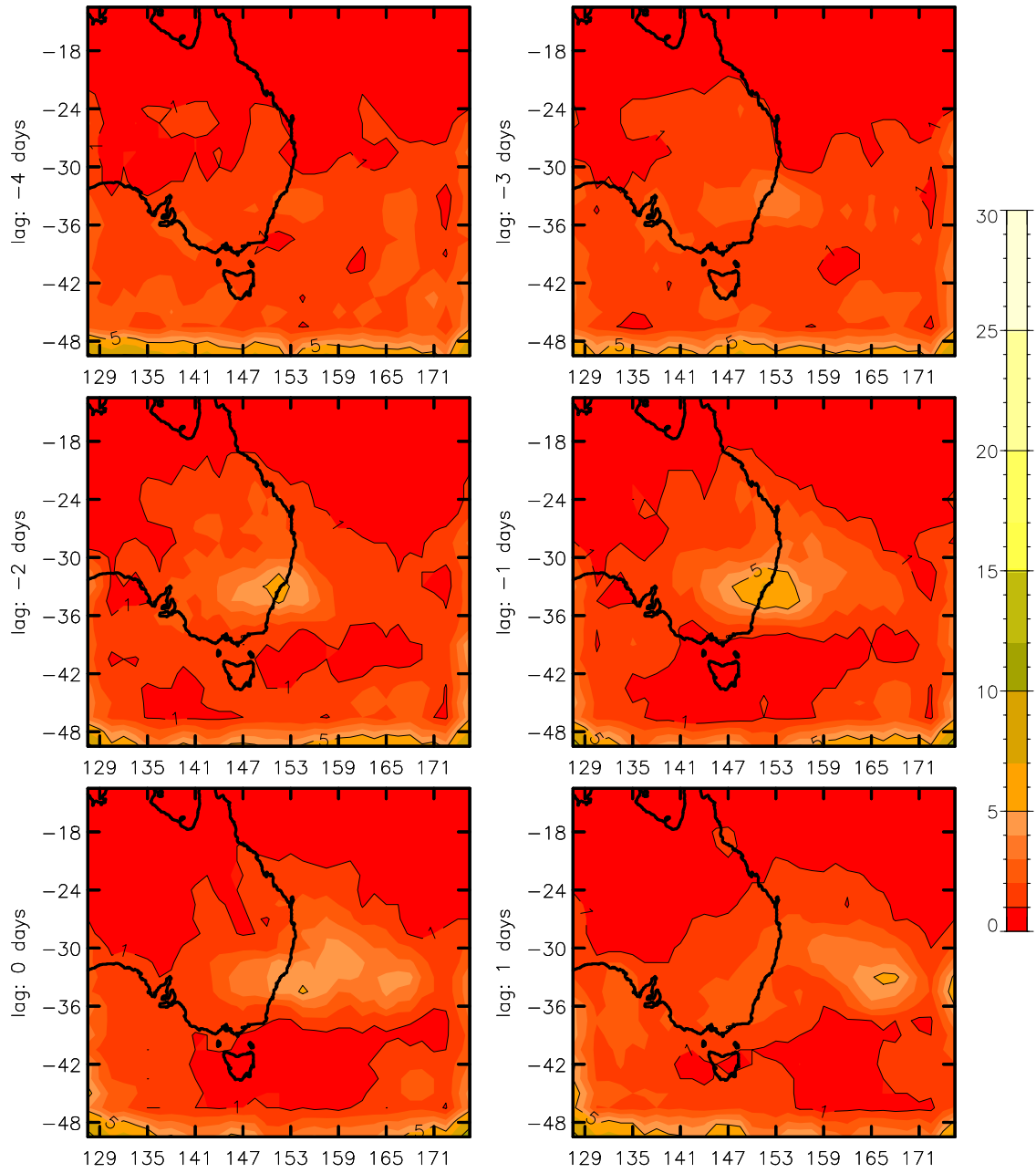


**Fig. B13As** for Fig. 9, but for the 300 hPa forcing term as an indicator of strong wind events.

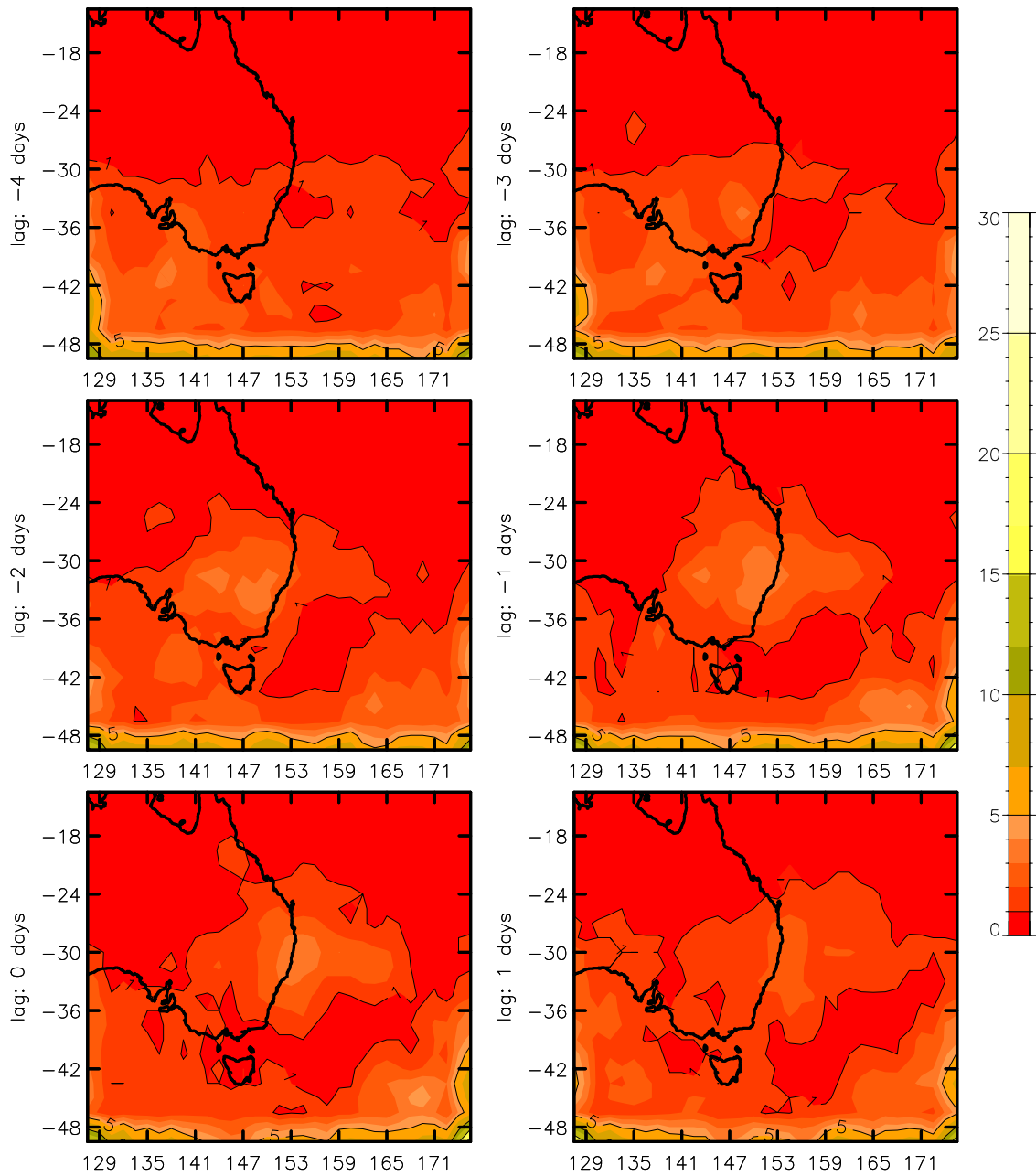


**Fig. B14As** for Fig. 9, but for the 400 hPa forcing term as an indicator of strong wind events.

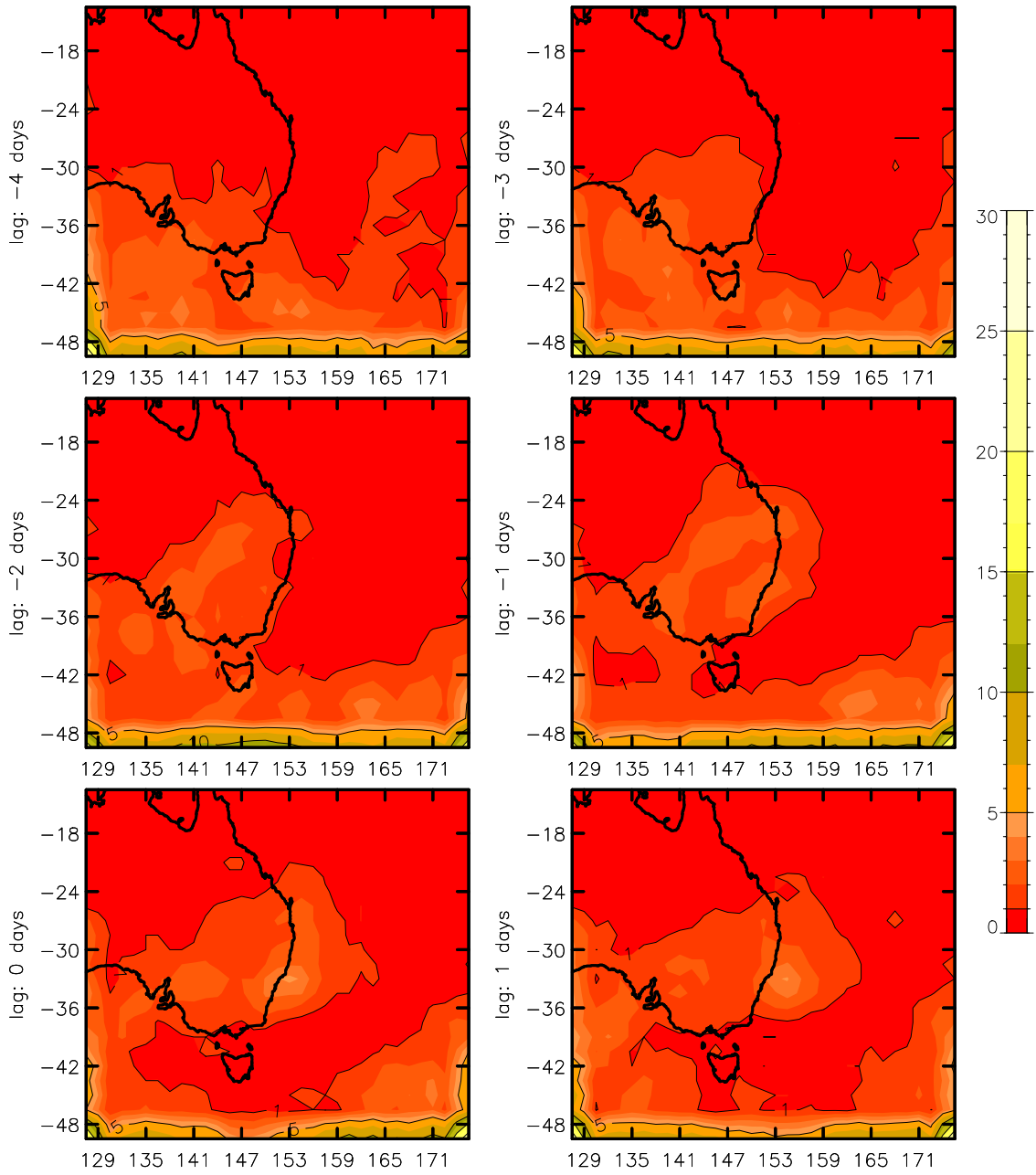


**Fig. B15As** for Fig. 9, but for the 500 hPa forcing term as an indicator of strong wind events.

### B.3 Extreme values of the diagnostics for days on which heavy localised rainfall events occurred

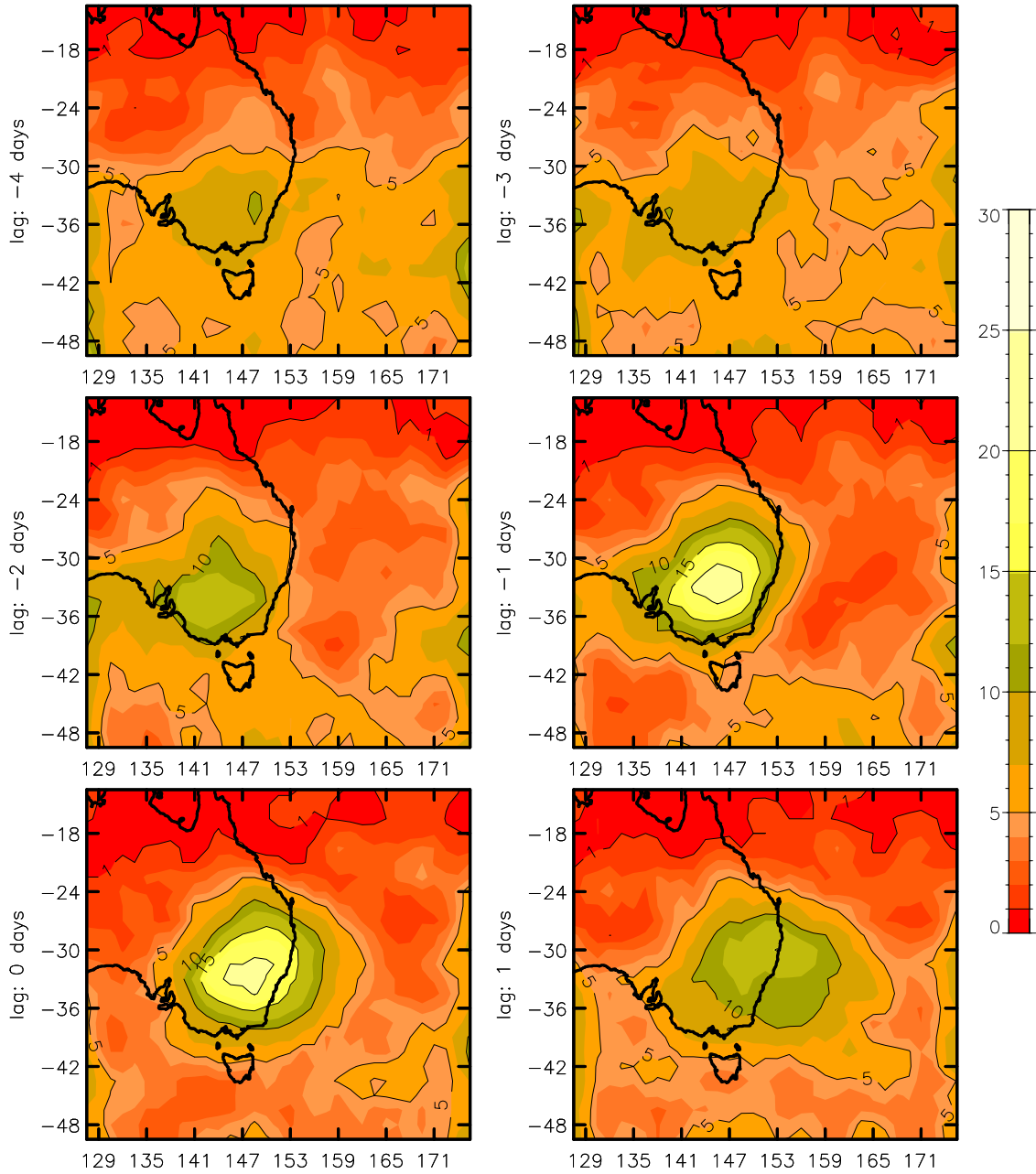


**Fig. B16As** for Fig. 9, but for the 300 hPa geostrophic vorticity as an indicator of heavy localised rain events.

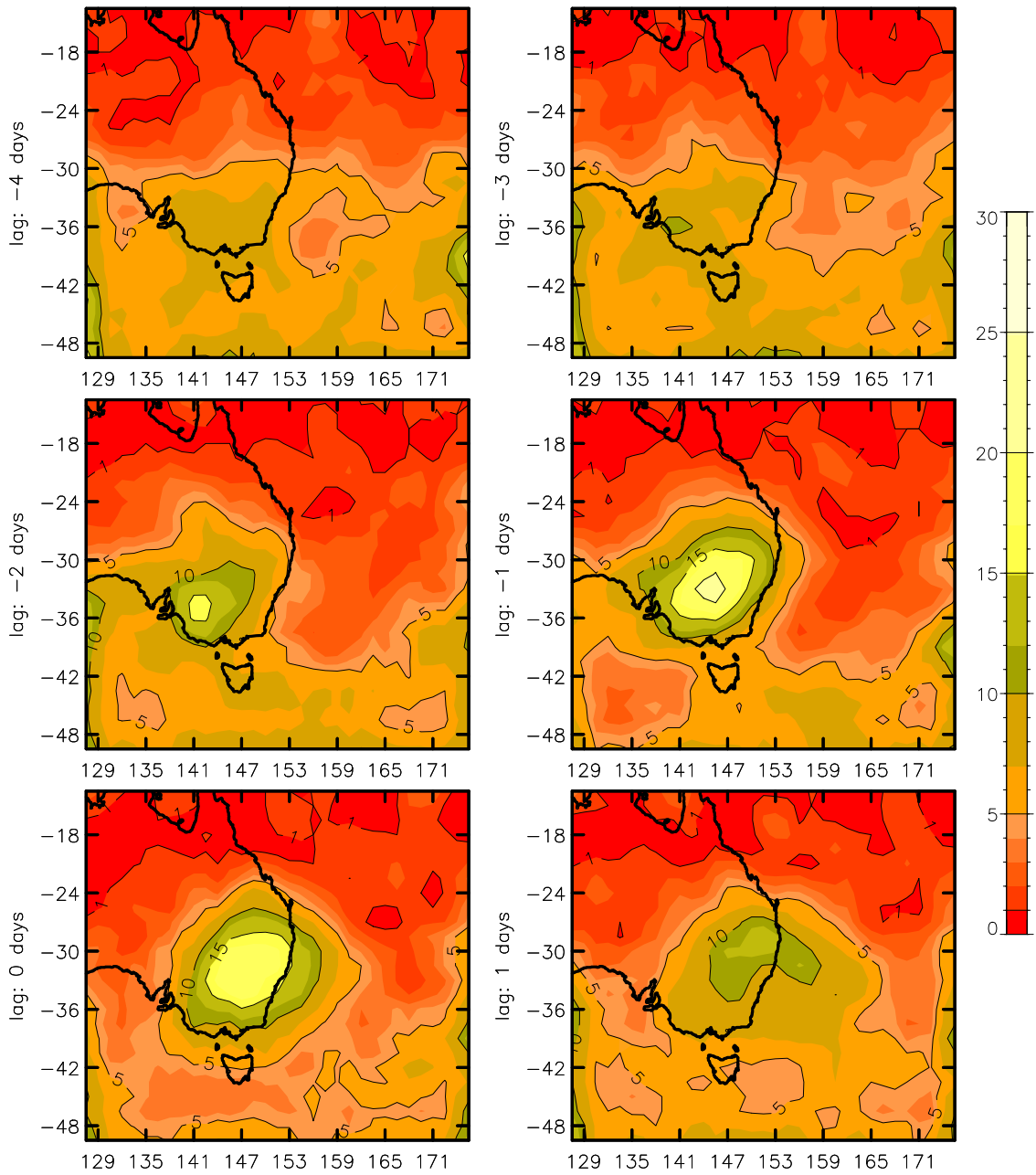


**Fig. B17As** for Fig. 9, but for the 400 hPa geostrophic vorticity as an indicator of heavy localised rain events.

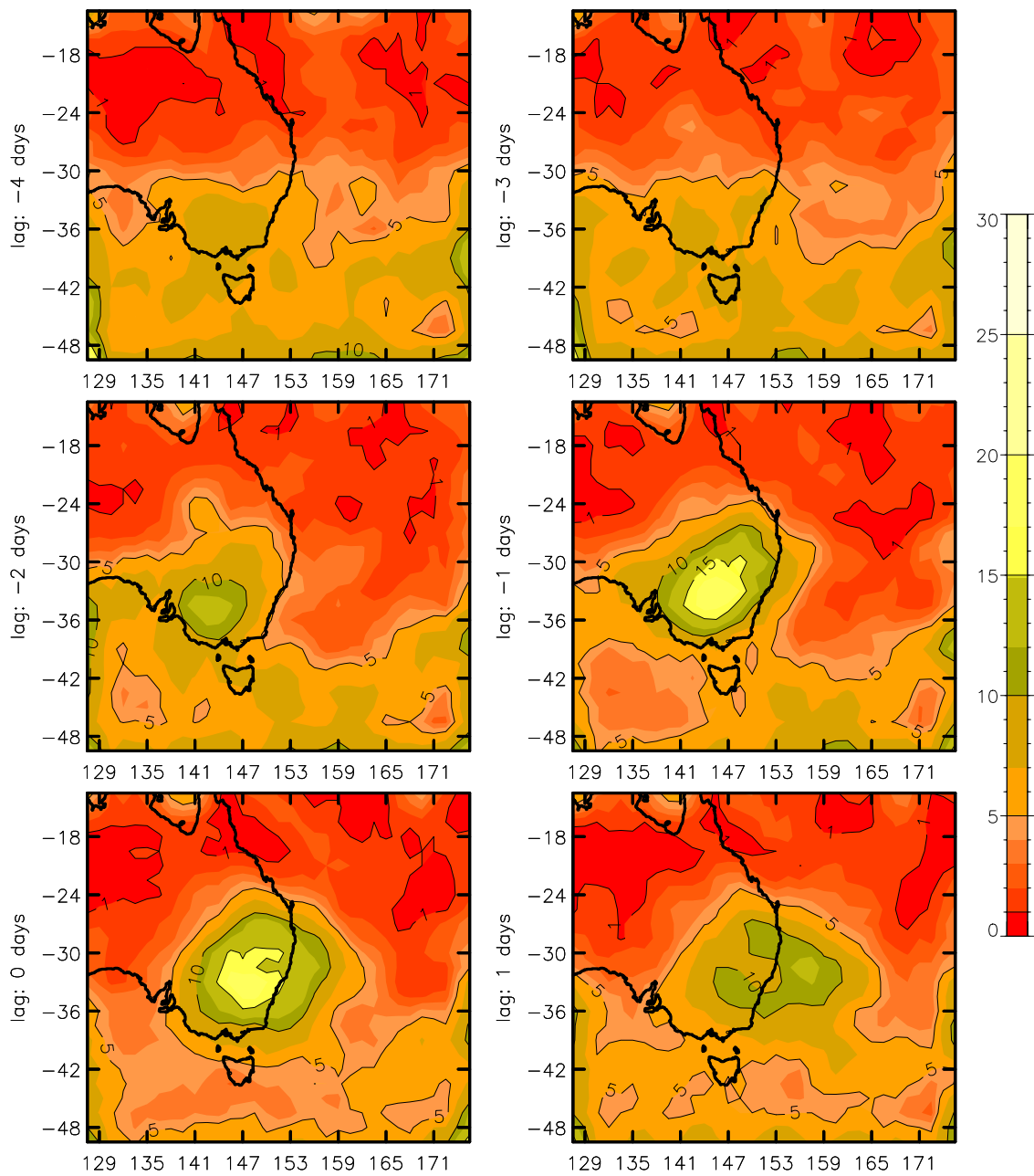


**Fig. B18As** for Fig. 9, but for the 500 hPa geostrophic vorticity as an indicator of heavy localised rain events.

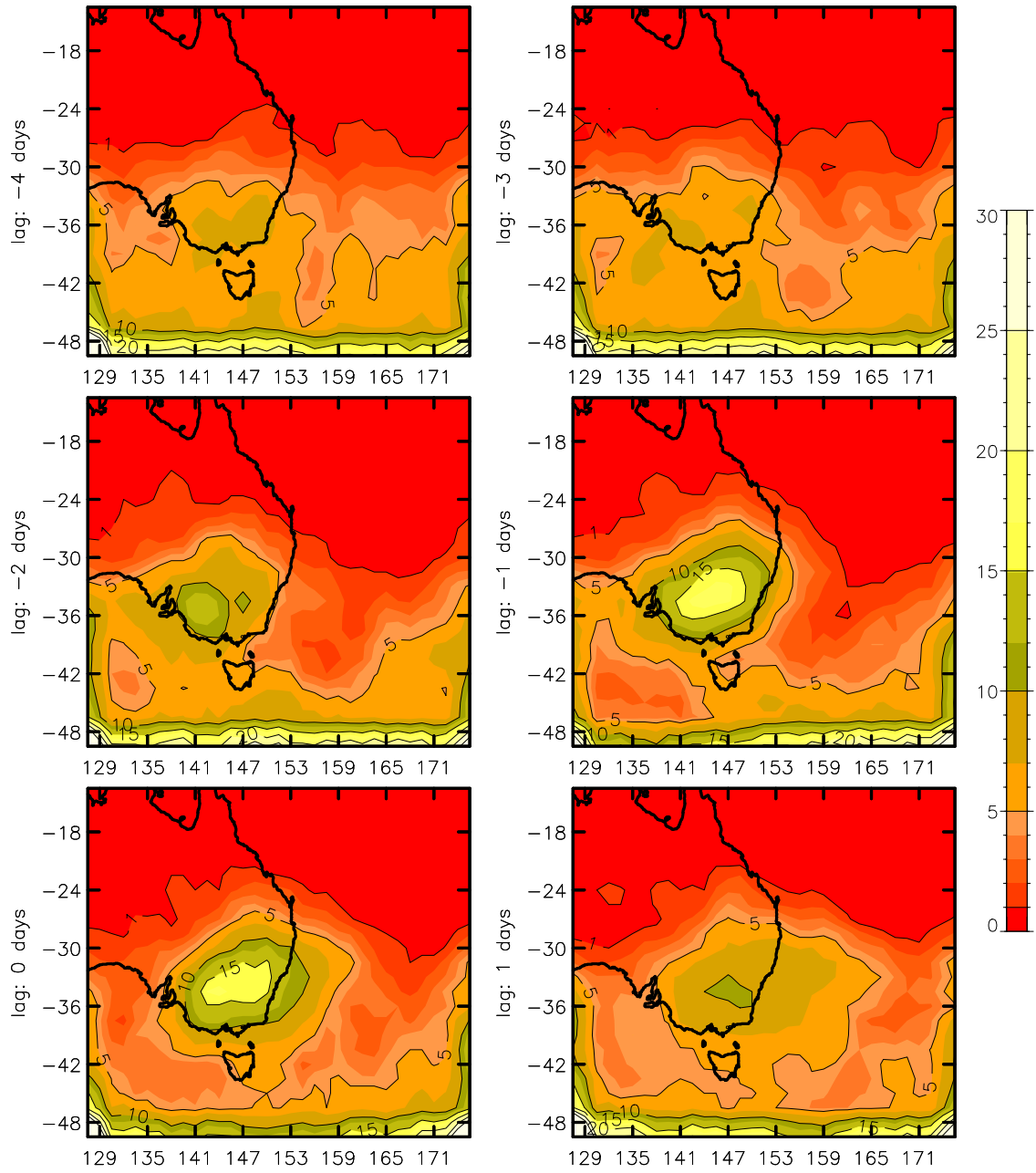


**Fig. B19As** for Fig. 9, but for the 300 hPa IPV as an indicator of heavy localised rain events.

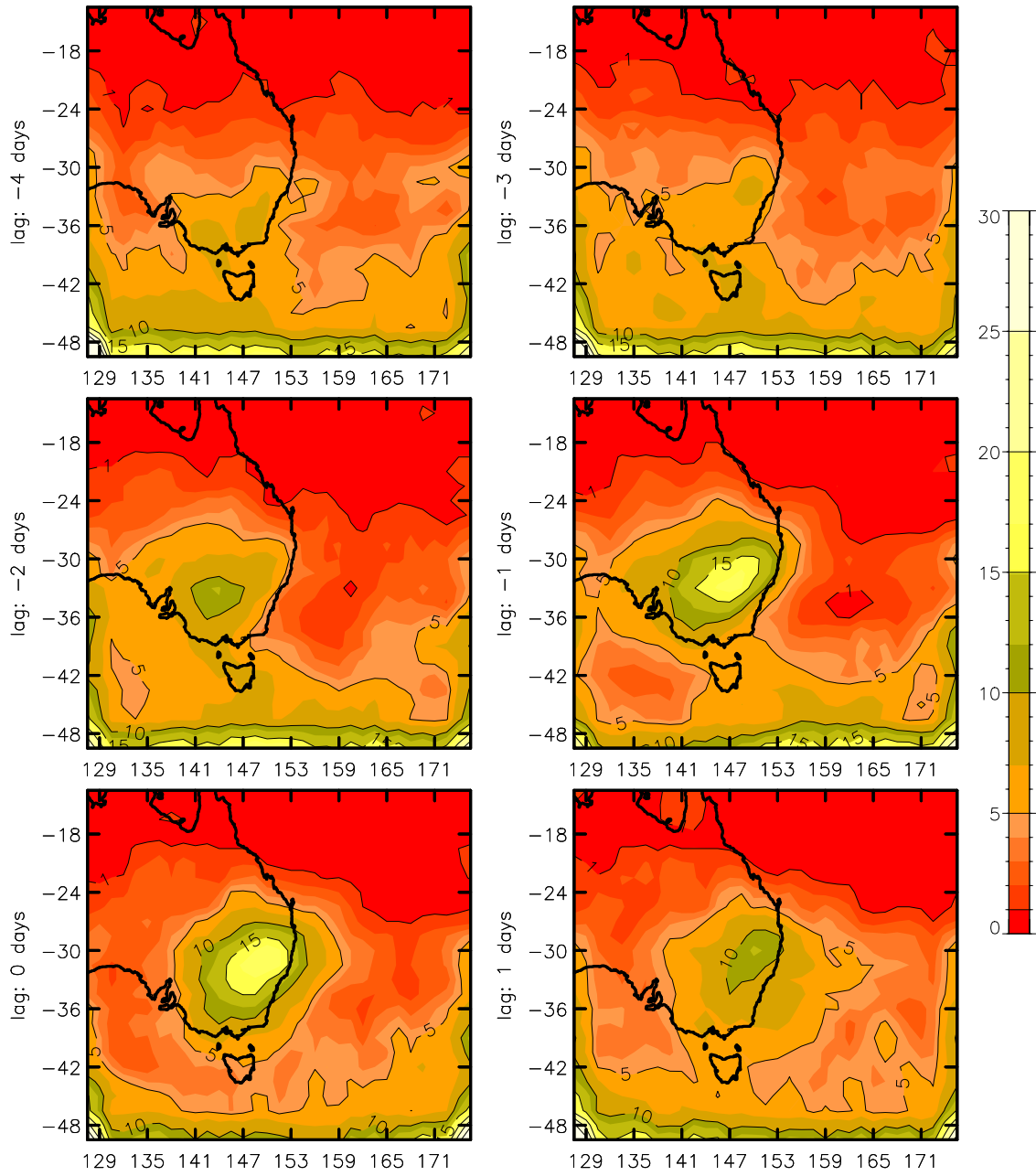


**Fig. B20As** for Fig. 9, but for the 400 hPa IPV as an indicator of heavy localised rain events.

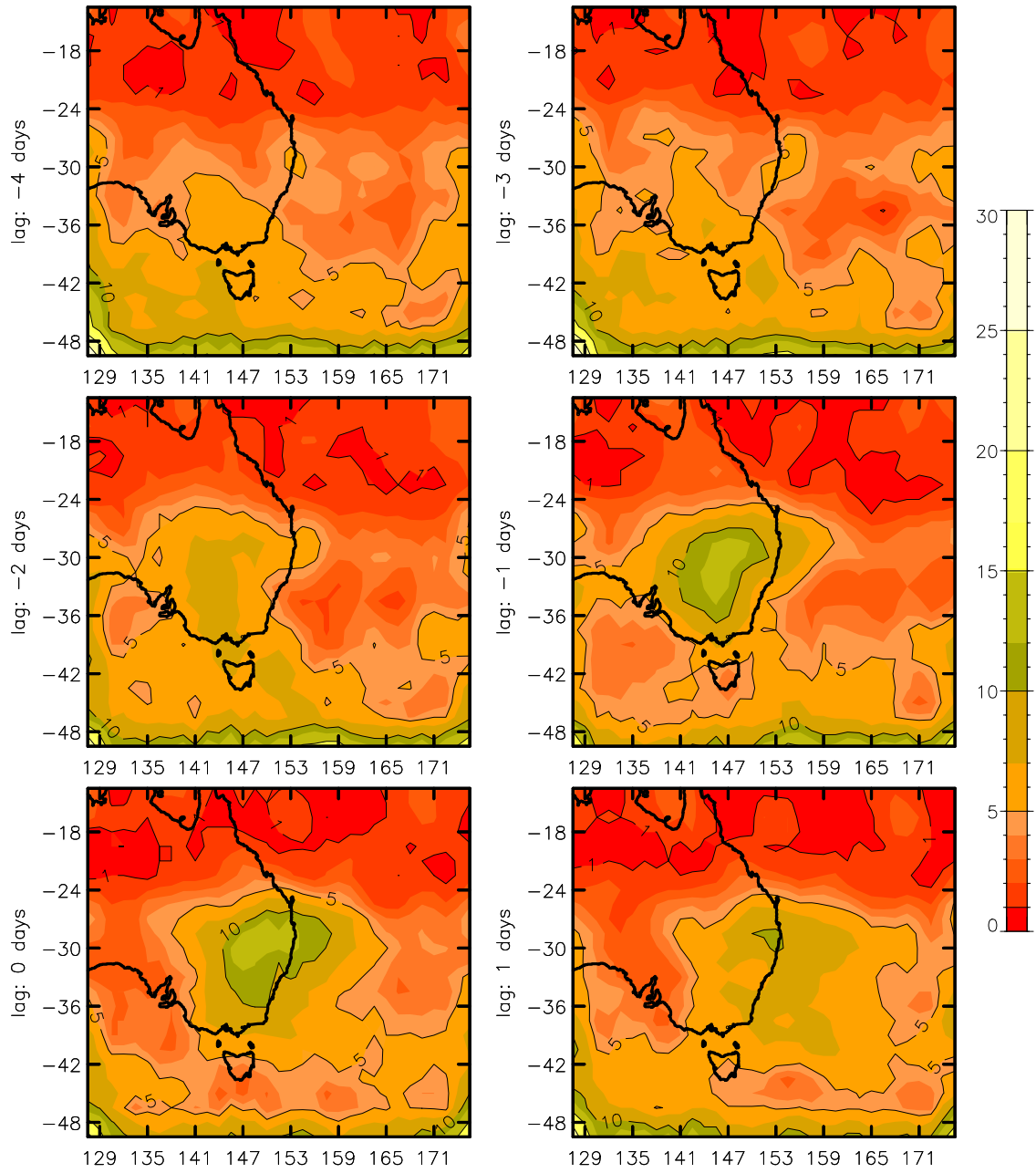


**Fig. B21** As for Fig. 9, but for the 500 hPa IPV as an indicator of heavy localised rain events.

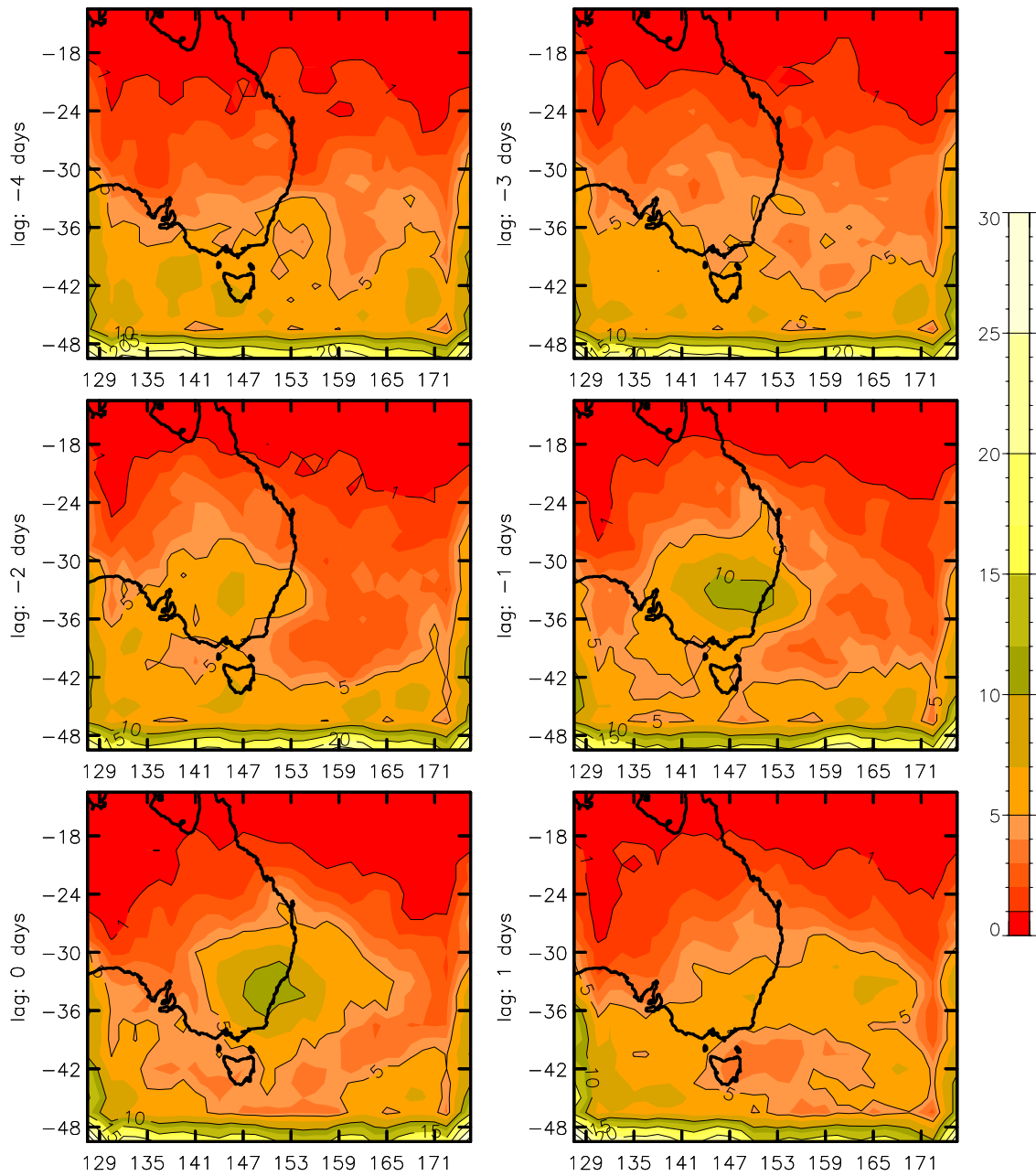


**Fig. B22As** for Fig. 9, but for the 300 hPa forcing term as an indicator of heavy localised rain events.

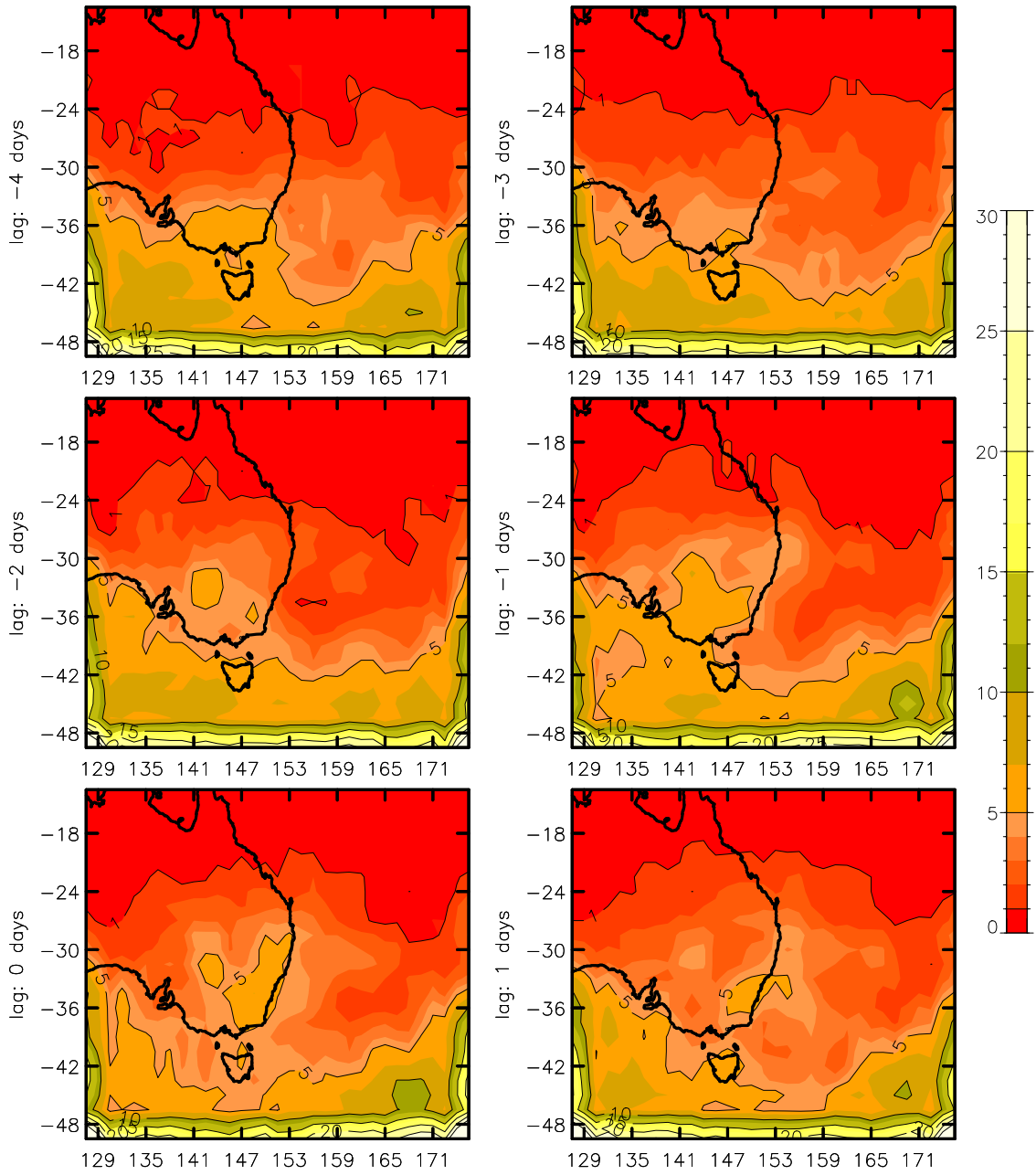


**Fig. B23As** for Fig. 9, but for the 400 hPa forcing term as an indicator of heavy localised rain events.

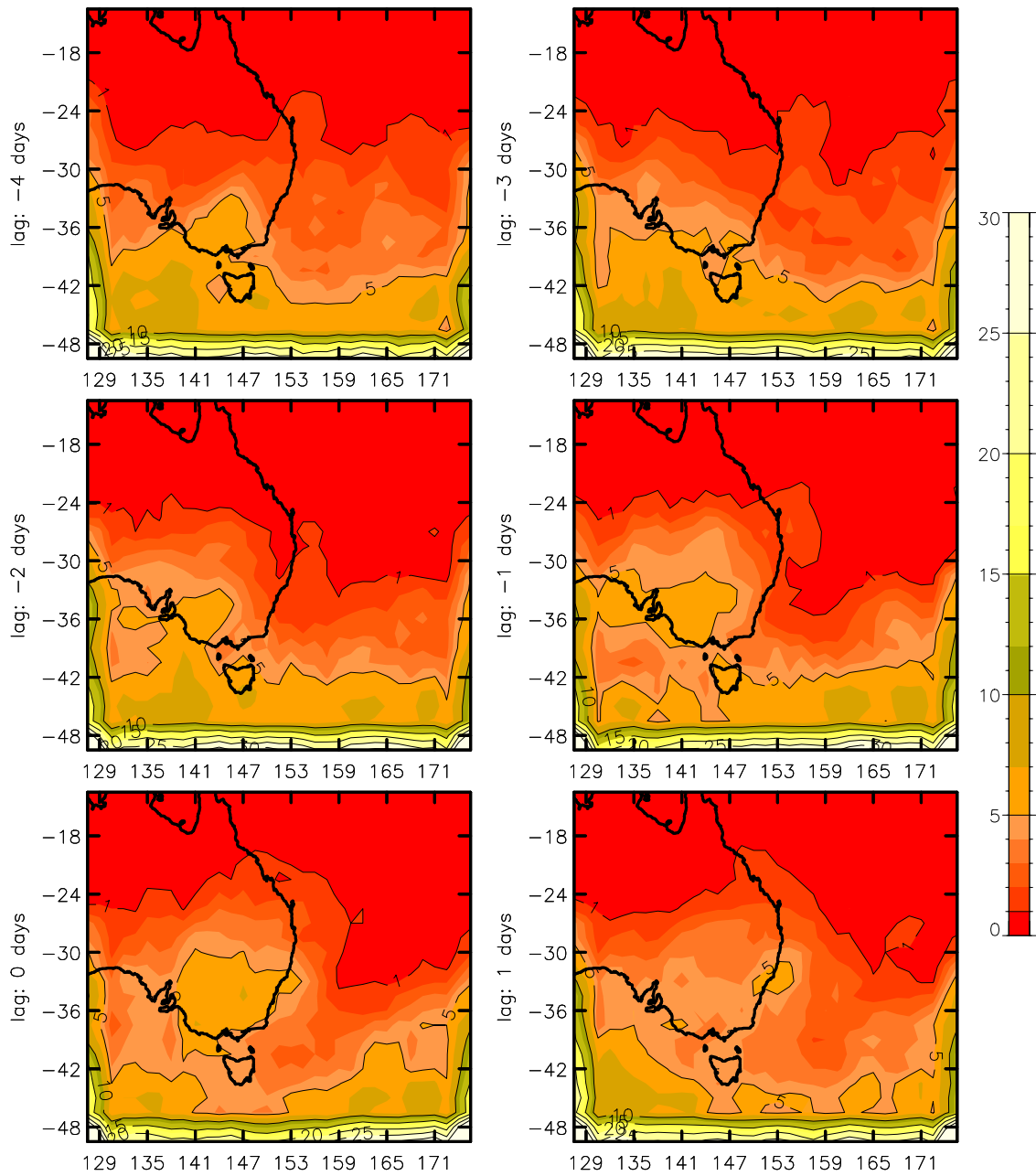


**Fig. B24As** for Fig. 9, but for the 500 hPa forcing term as an indicator of heavy localized rain events.

## B.4 Extreme values of the diagnostics for days on which heavy widespread rainfall events occurred

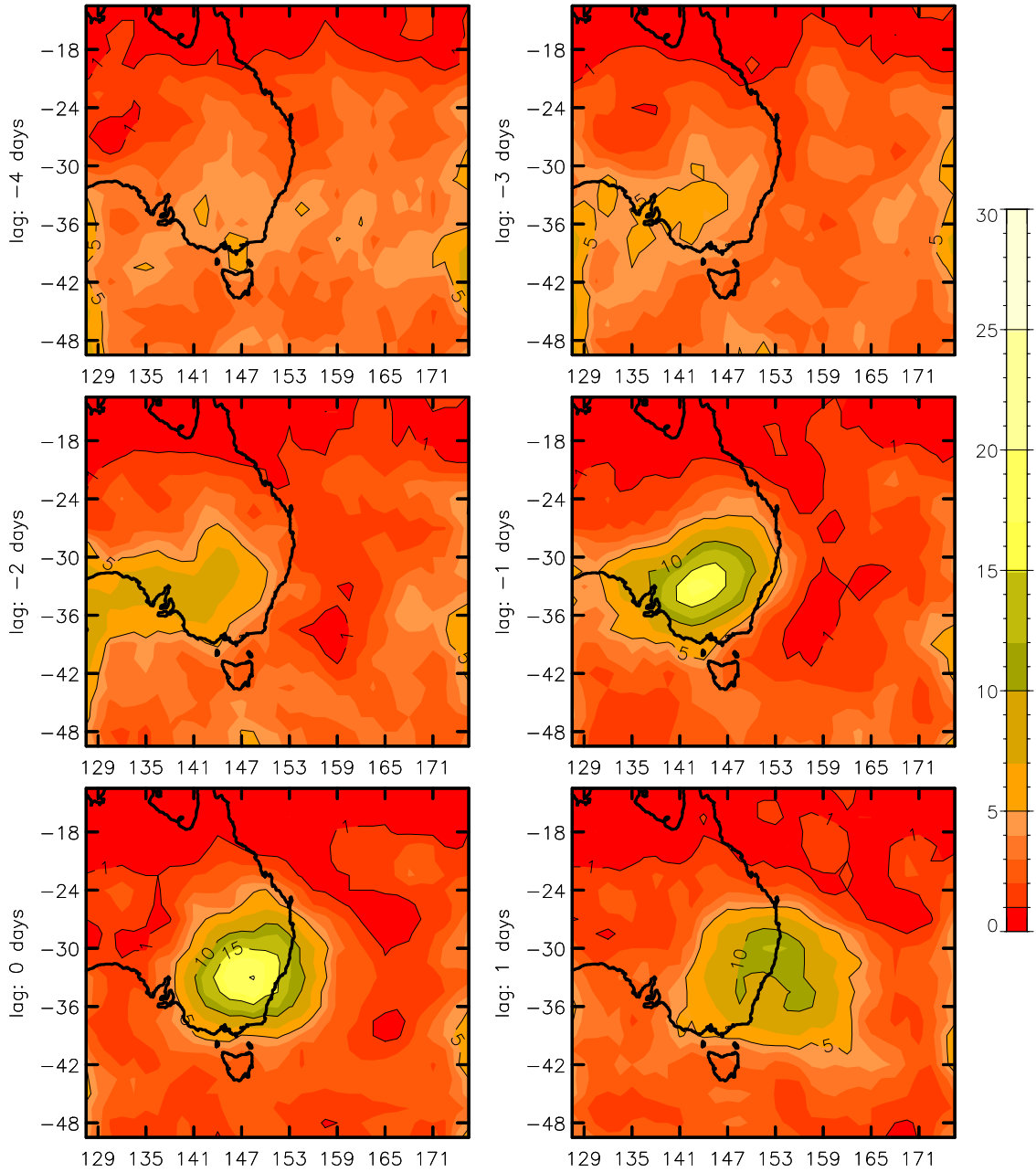


**Fig. B25** As for Fig. 9, but for the 300 hPa geostrophic vorticity as an indicator of heavy widespread rain events.

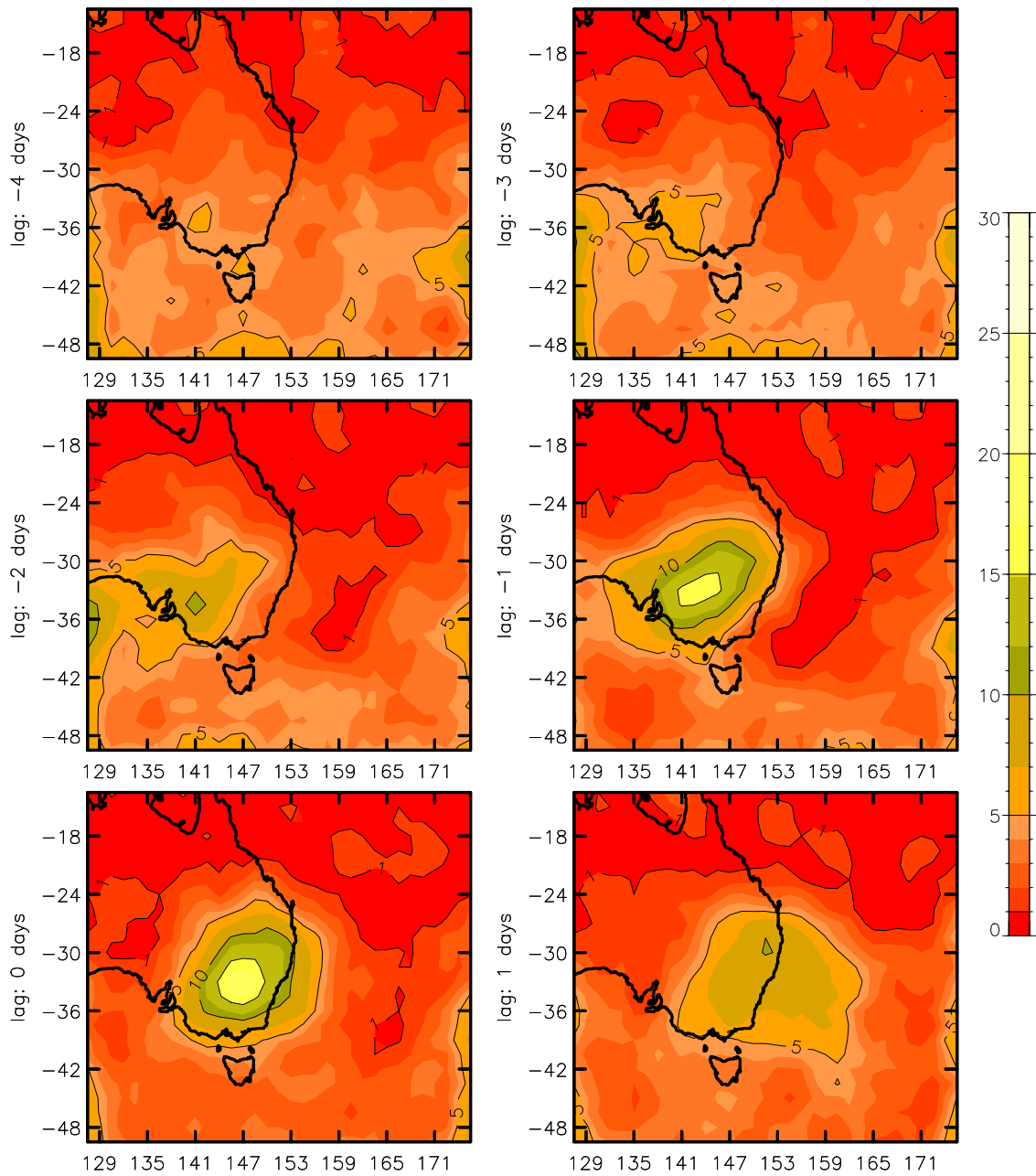


**Fig. B26As** for Fig. 9, but for the 400 hPa geostrophic vorticity as an indicator of heavy widespread rain events.

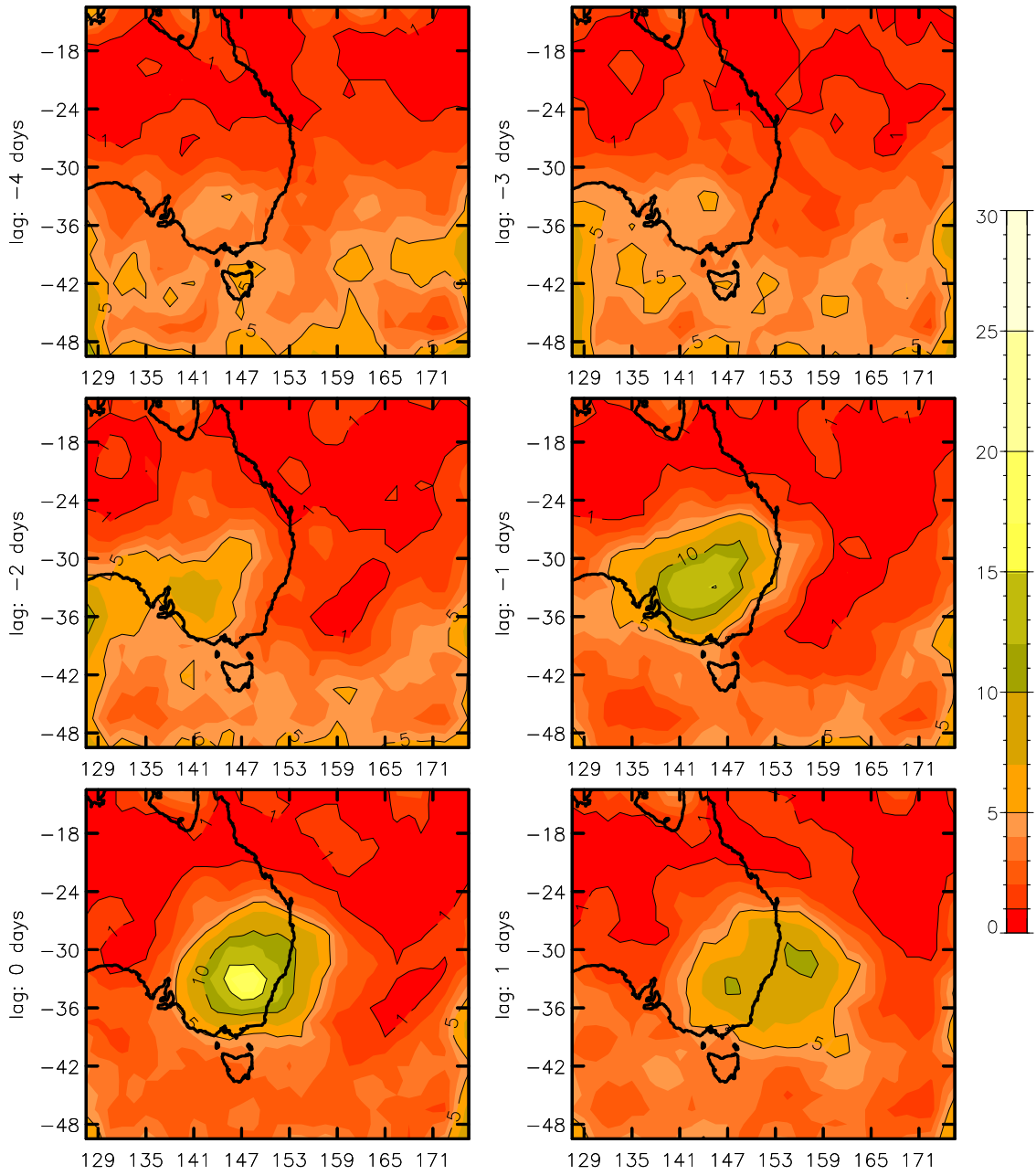


**Fig. B27** As for Fig. 9, but for the 500 hPa geostrophic vorticity as an indicator of heavy widespread rain events.

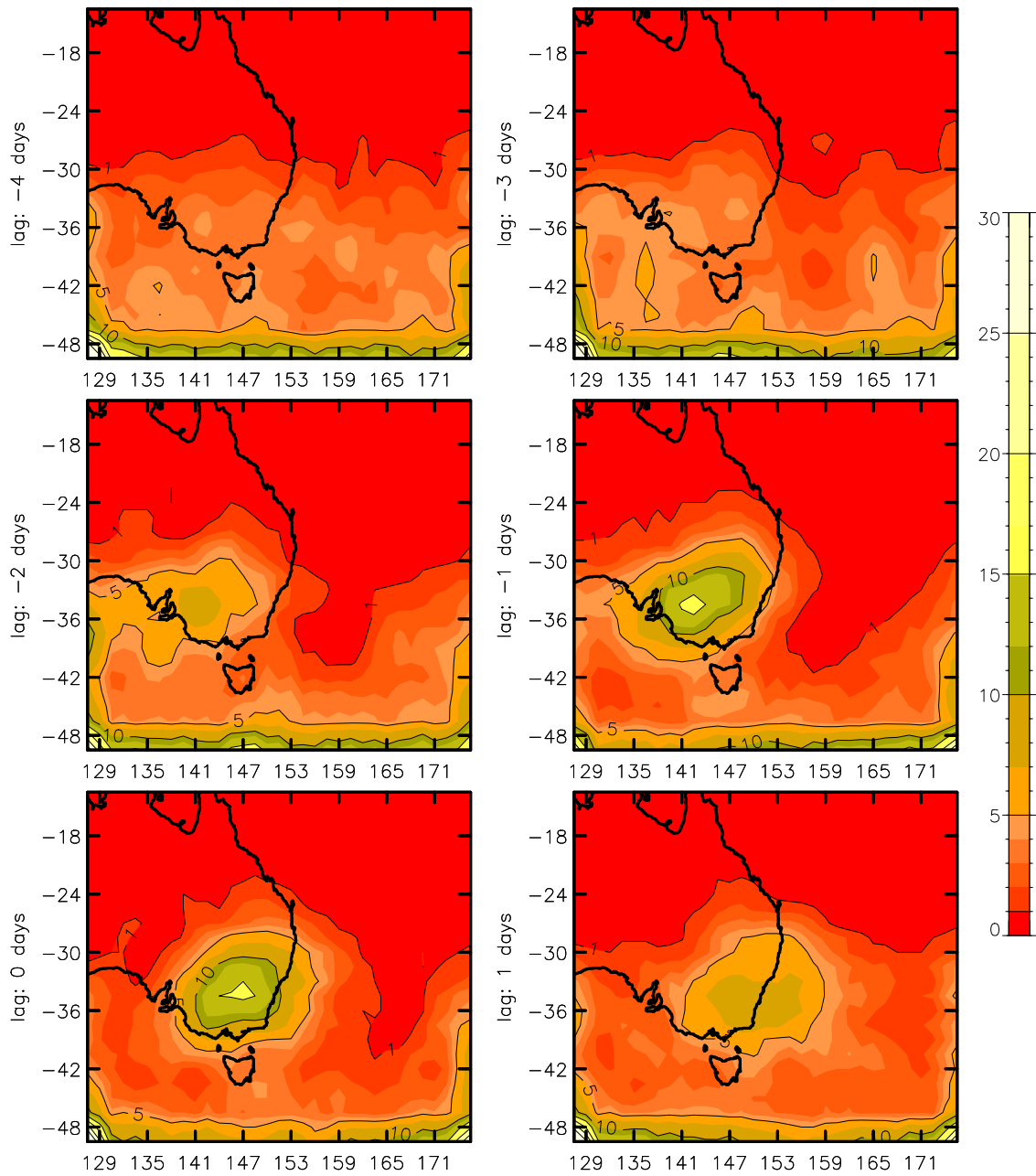


**Fig. B28As** for Fig. 9, but for the 300 hPa IPV as an indicator of heavy widespread rain events.

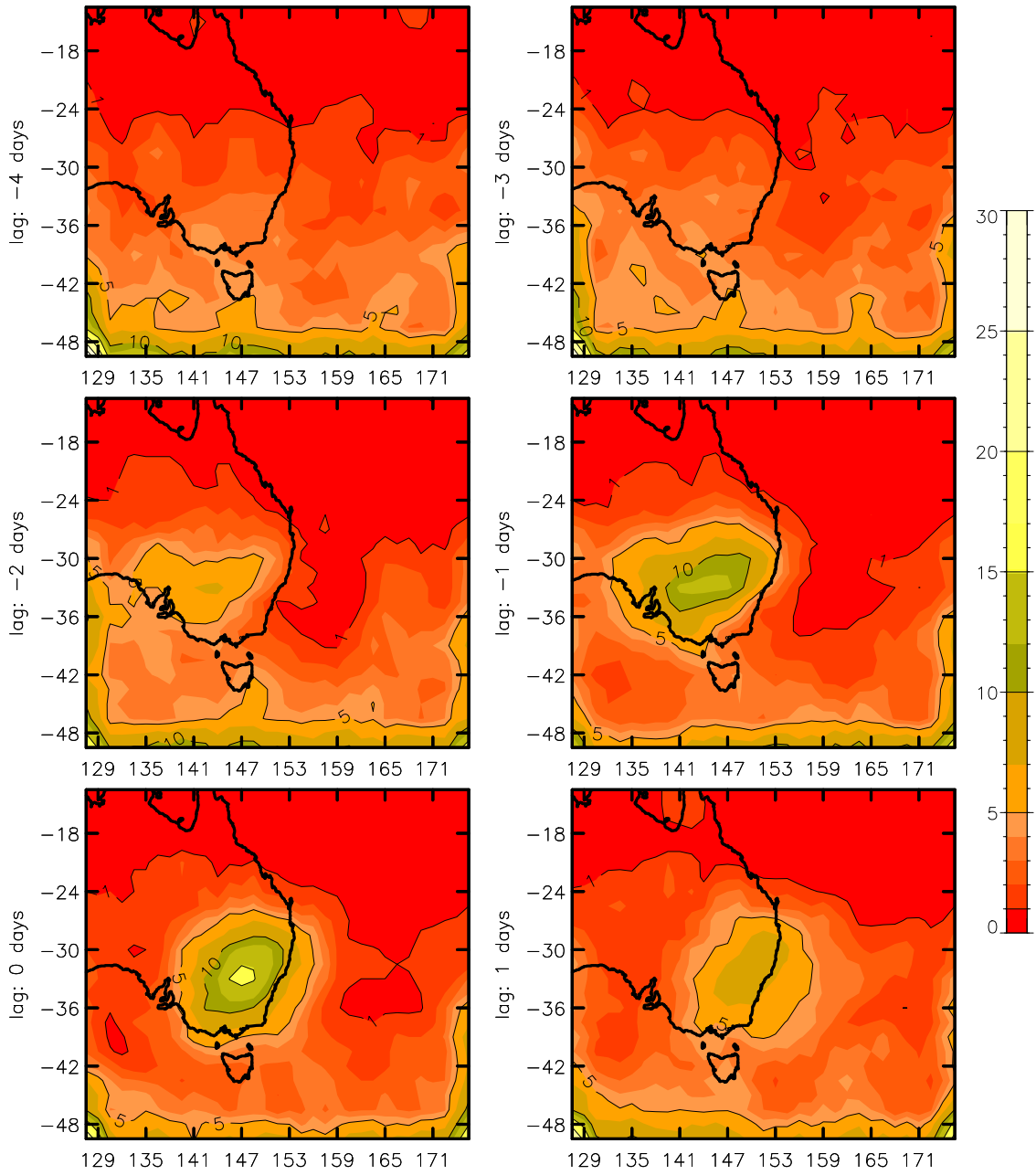


**Fig. B29**As for Fig. 9, but for the 400 hPa IPV as an indicator of heavy widespread rain events.

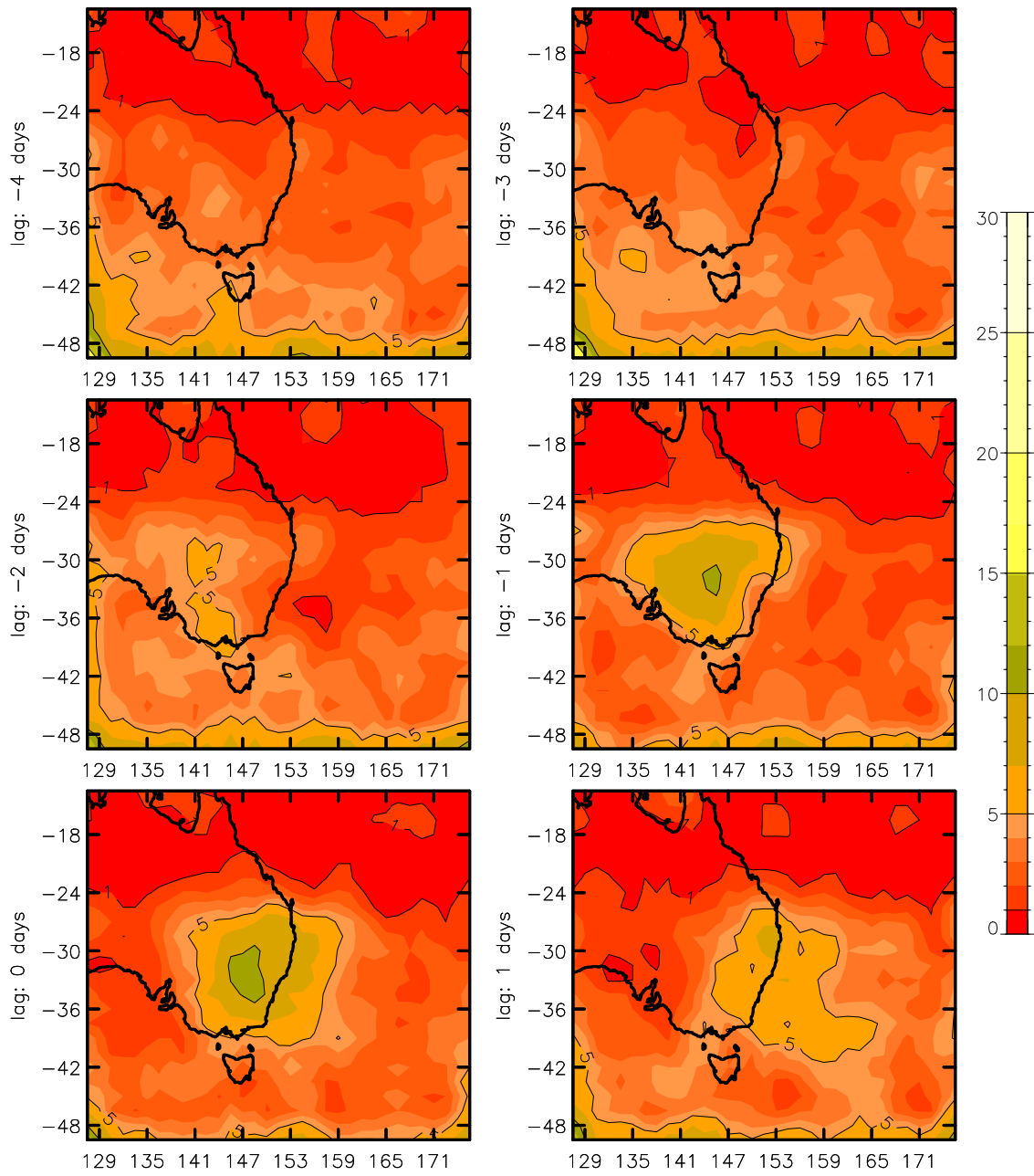


**Fig. B30As** for Fig. 9, but for the 500 hPa IPV as an indicator of heavy widespread rain events.

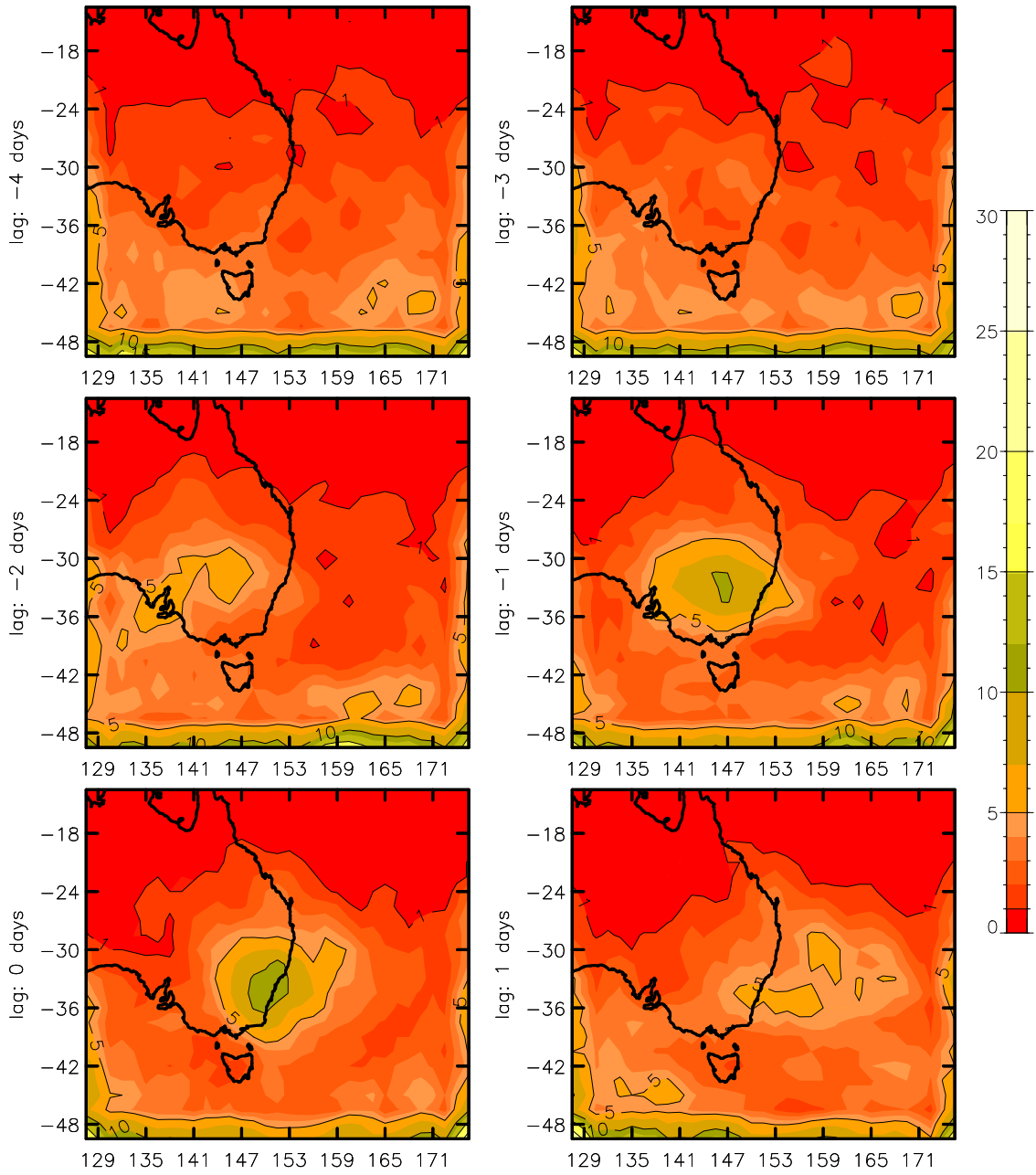


**Fig. B31** As for Fig. 9, but for the 300 hPa forcing term as an indicator of heavy widespread rain events.

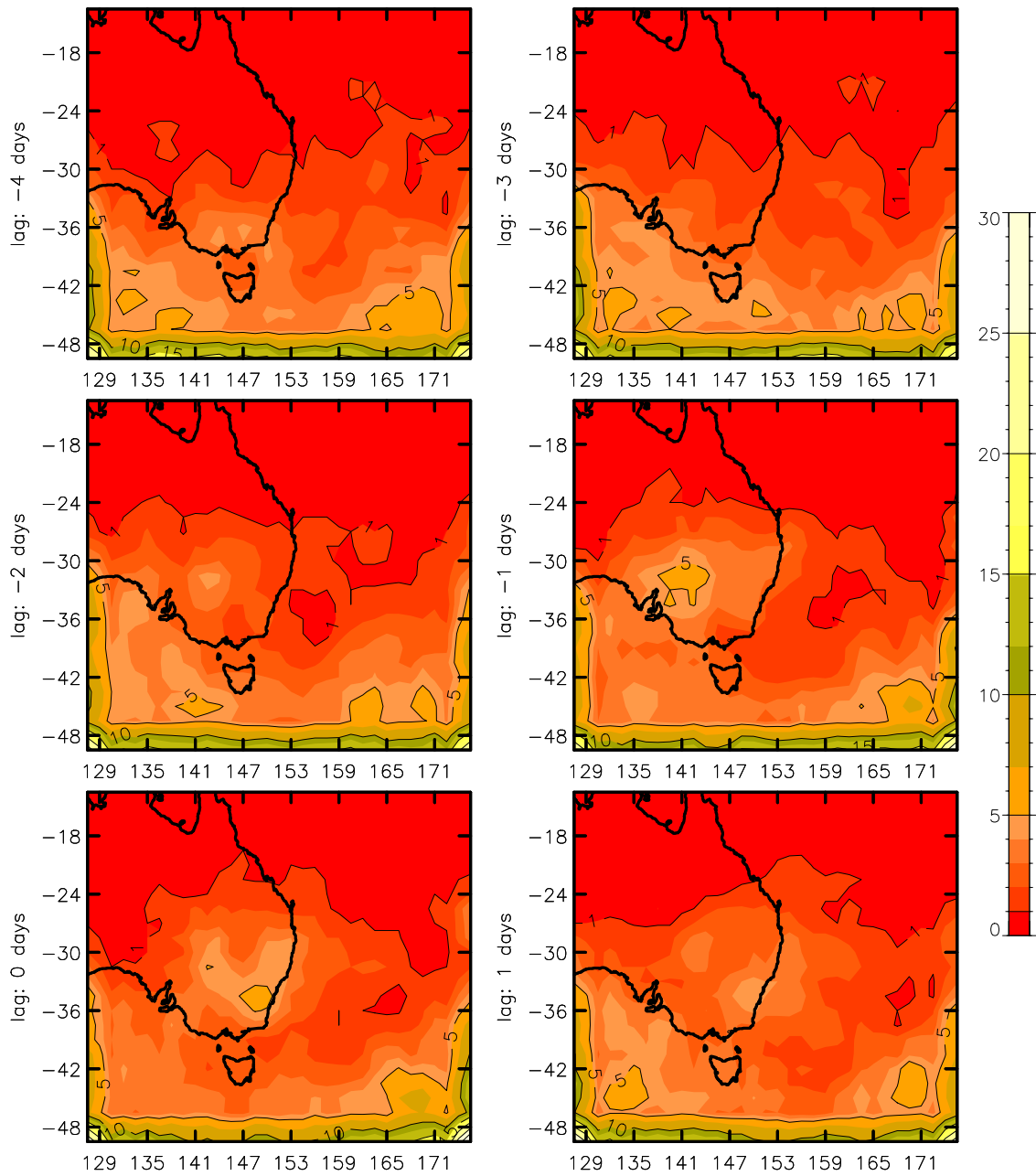


**Fig. B32As** for Fig. 9, but for the 400 hPa forcing term as an indicator of heavy widespread rain events.

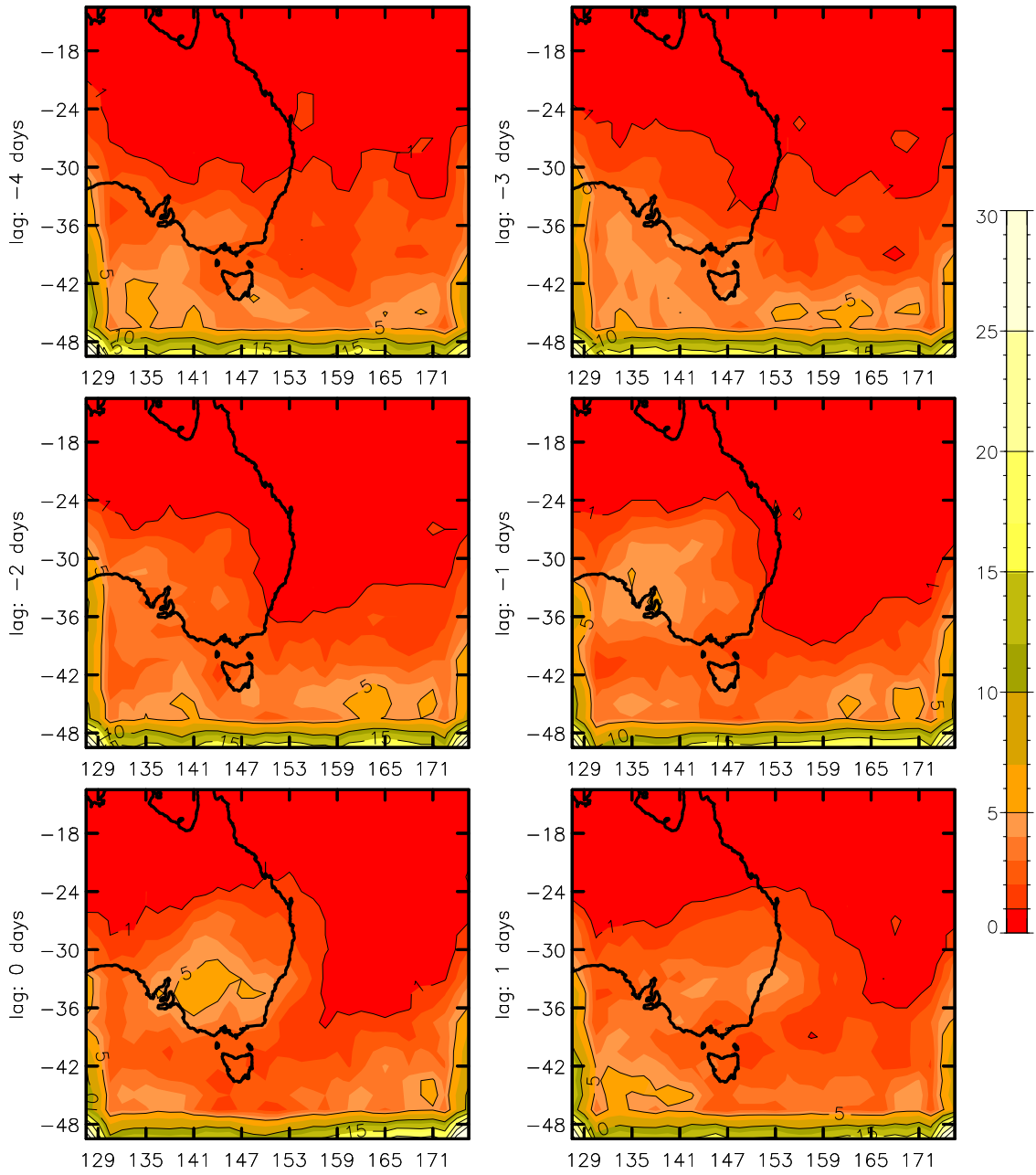


**Fig. B33As** for Fig. 9, but for the 500 hPa forcing term as an indicator of heavy widespread rain events.

## APPENDIX C - GRAPHICAL PERFORMANCE MEASURES

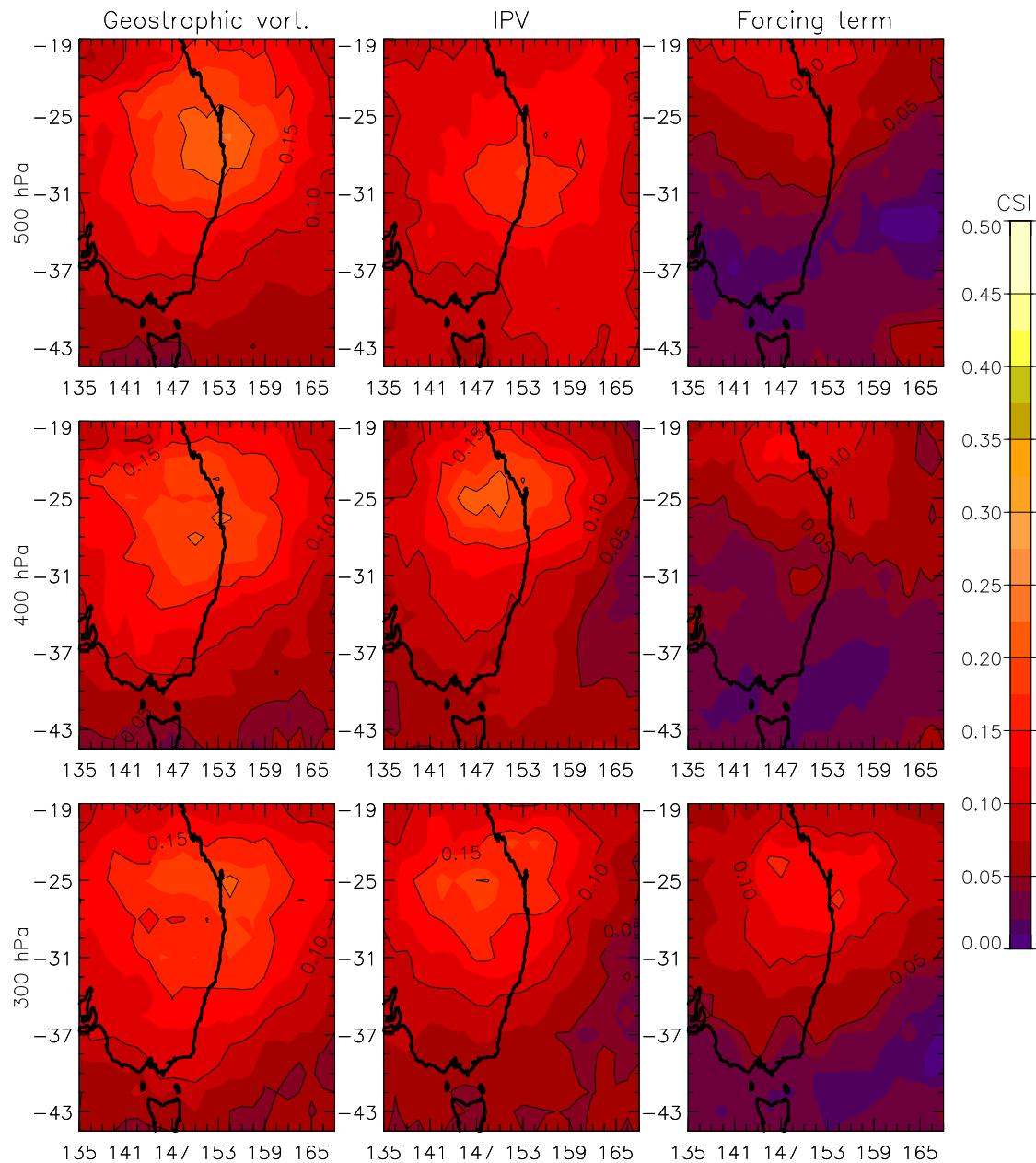


**Fig. C1** As for Fig. 13, but for strong wind events during summer.

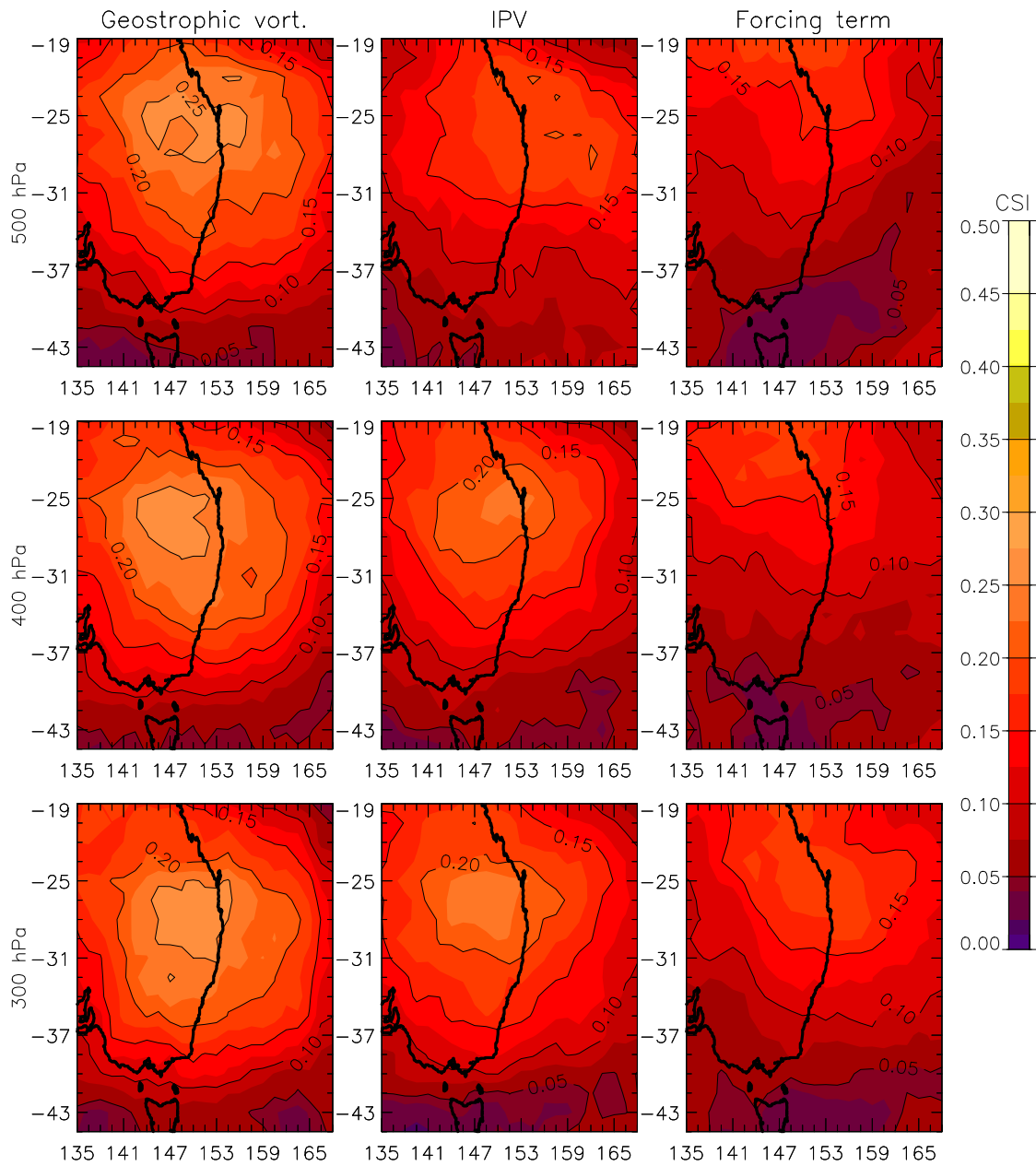


**Fig. C2** As for Fig. 13, but for strong wind events during winter.

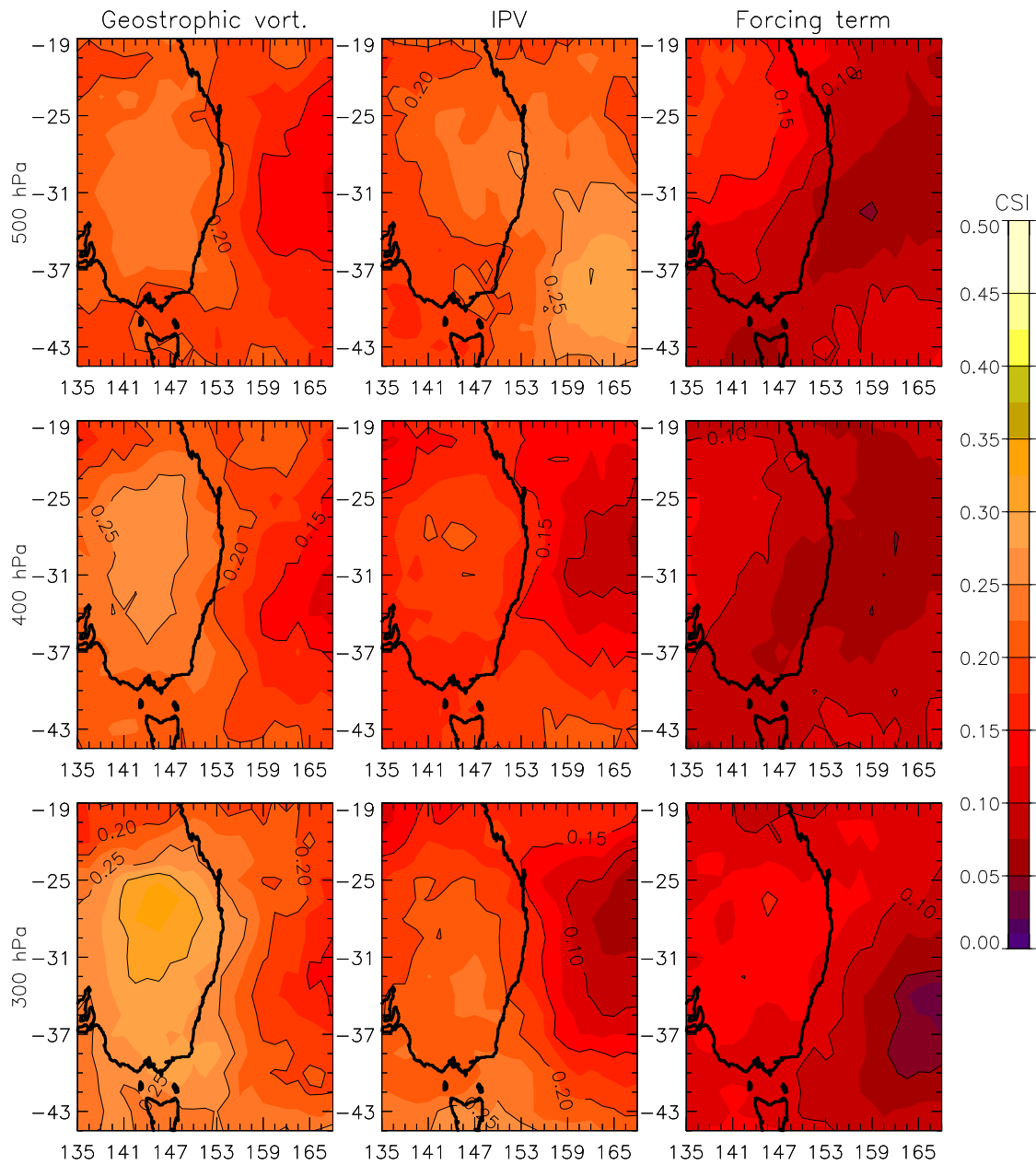


**Fig. C3** As for Fig. 13, but for heavy localised rainfall events during summer.

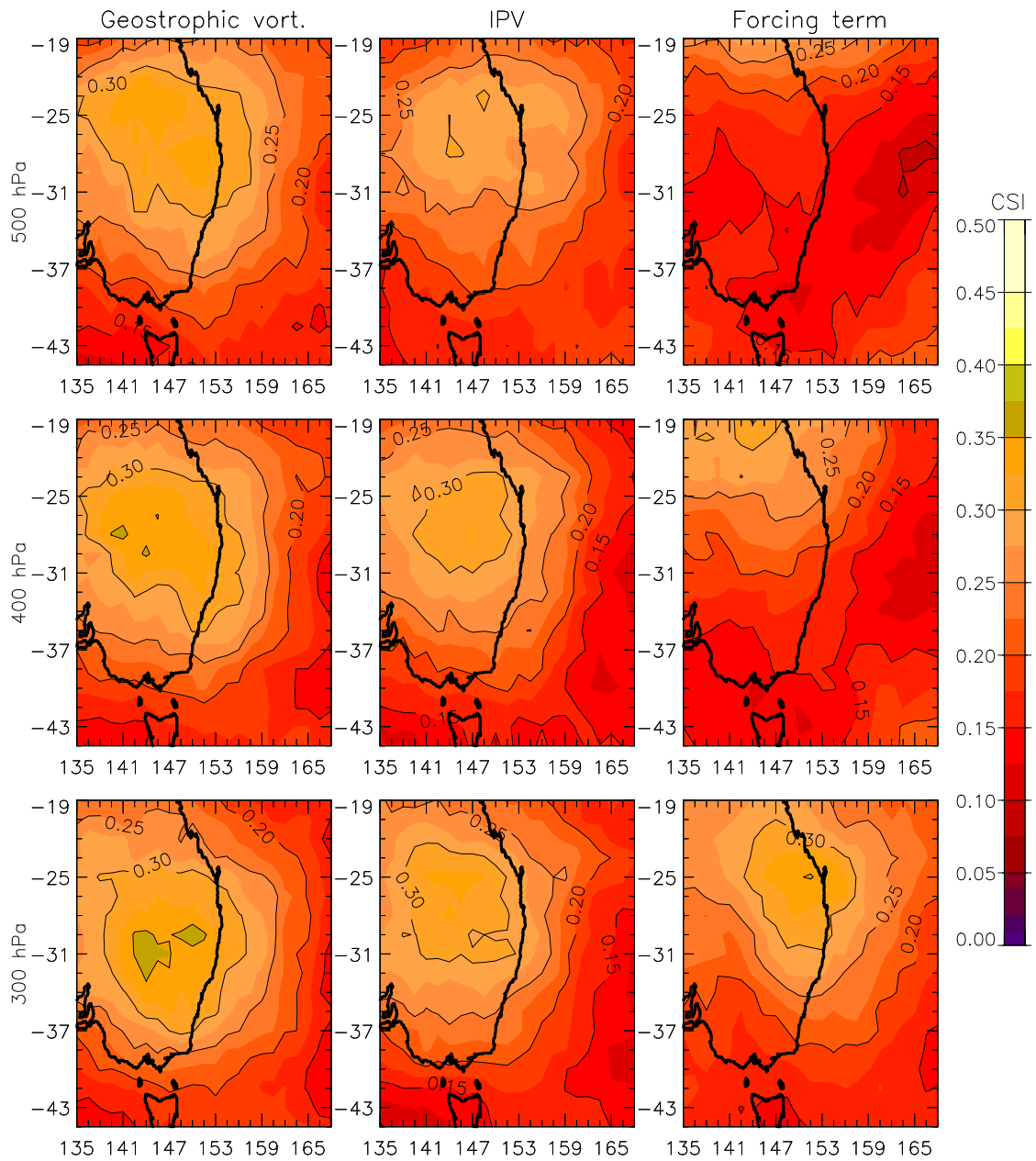


**Fig. C4** As for Fig. 13, but for heavy localised rainfall events during winter.

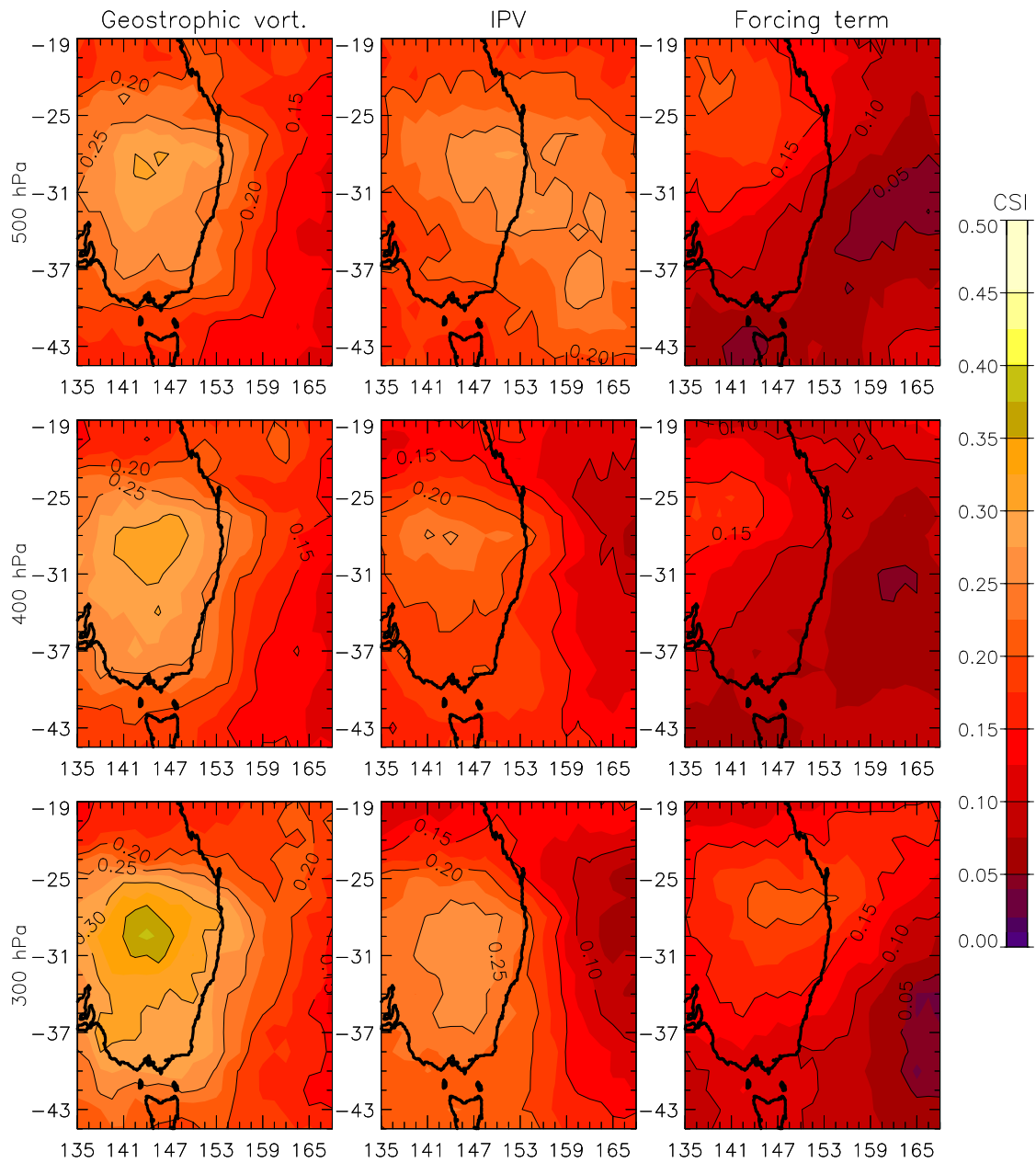


**Fig. C5** As for Fig. 13, but for heavy widespread rainfall events during summer.

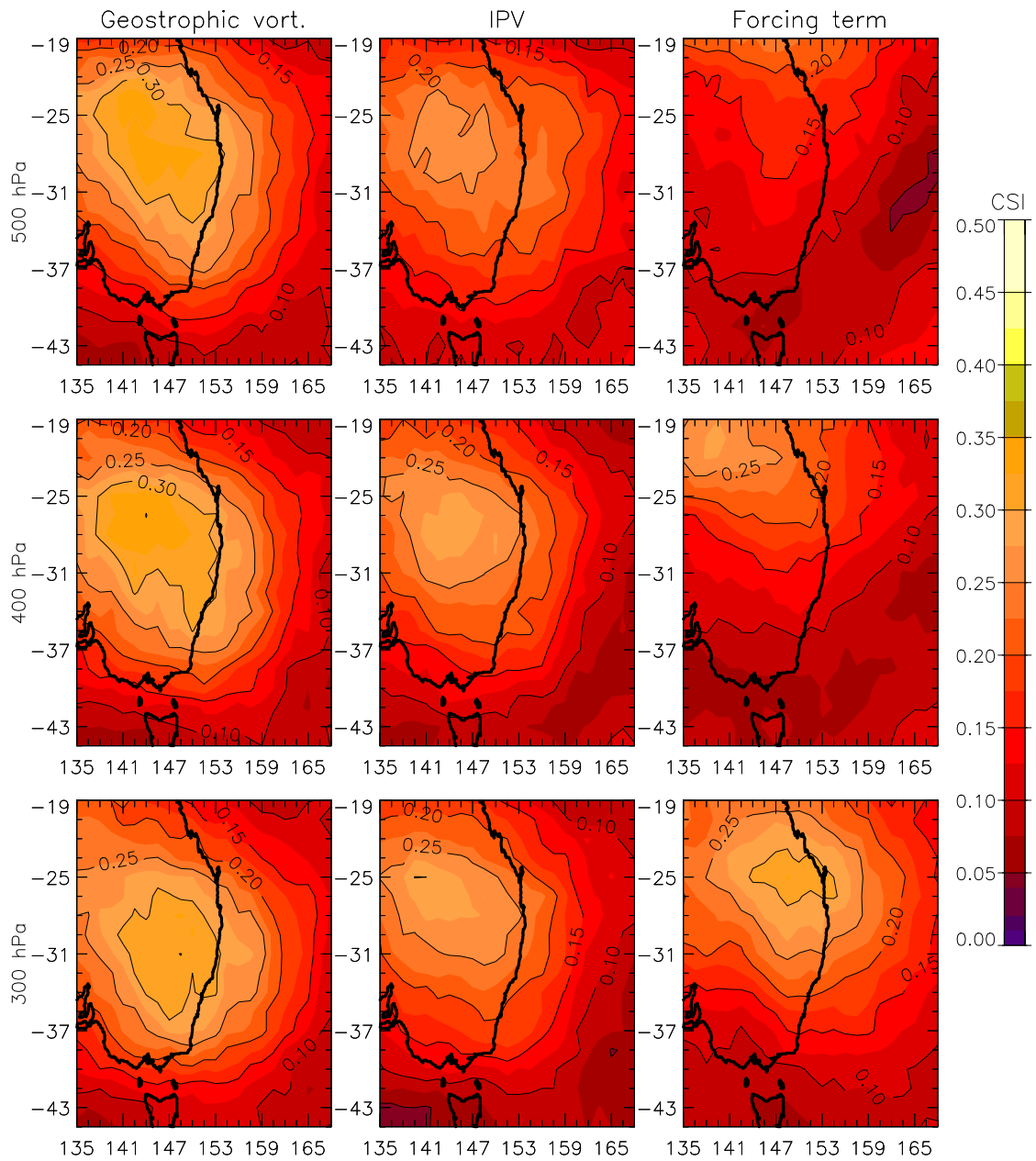


**Fig. C6** As for Fig. 13, but for heavy widespread rainfall events during winter.

## APPENDIX D - TABULAR PERFORMANCE MEASURES

**Table D1** As for Table 2, but for strong wind events only using data for summer.

Diagnostic	Pressure level (hPa)	Max. CSI	Hits	Misses	False alarms	Latitude (°S) of max. CSI	Longitude (°E) of max. CSI
Geostrophic vorticity	300	0.21	31	21	96	25.0	154.5
	400	0.21	29	23	85	26.0	153.0
	500	0.23	30	22	82	26.0	154.5
Isentropic potential vorticity	300	0.20	25	27	72	25.0	148.5
	400	0.22	23	29	52	25.0	145.5
	500	0.18	30	22	111	29.0	153.0
Forcing term	300	0.16	19	33	67	23.0	147.0
	400	0.13	15	37	62	22.0	148.5
	500	0.13	17	35	82	19.0	147.0

**Table D2** As for Table 2, but for strong wind events only using data for winter.

Diagnostic	Pressure level (hPa)	Max. CSI	Hits	Misses	False alarms	Latitude (°S) of max. CSI	Longitude (°E) of max. CSI
Geostrophic vorticity	300	0.27	48	18	115	28.0	148.5
	400	0.27	50	16	119	25.0	147.0
	500	0.26	50	16	124	25.0	156.0
Isentropic potential vorticity	300	0.25	50	16	136	25.0	148.5
	400	0.24	52	14	152	25.0	151.5
	500	0.21	39	27	124	22.0	150.0
Forcing term	300	0.20	45	21	162	25.0	153.0
	400	0.19	45	21	169	22.0	148.5
	500	0.19	39	27	137	19.0	144.0

**Table D3** As for Table 2, but for heavy localised rainfall events only using data for summer.

Diagnostic	Pressure level (hPa)	Max. CSI	Hits	Misses	False alarms	Latitude (°S) of max. CSI	Longitude (°E) of max. CSI
Geostrophic vorticity	300	0.34	107	172	37	26.0	147.0
	400	0.27	87	192	40	26.0	147.0
	500	0.25	82	197	49	29.0	147.0
Isentropic potential vorticity	300	0.28	109	170	115	44.0	151.5
	400	0.21	68	211	41	28.0	145.5
	500	0.30	117	162	109	37.0	162.0
Forcing term	300	0.16	54	225	62	26.0	145.5
	400	0.14	48	231	64	29.0	135.0
	500	0.18	65	214	74	20.0	138.0

**Table D4** As for Table 2, but for heavy localised rainfall events only using data for winter.

Diagnostic	Pressure level (hPa)	Max. CSI	Hits	Misses	False alarms	Latitude (°S) of max. CSI	Longitude (°E) of max. CSI
Geostrophic vorticity	300	0.36	112	139	58	29.0	150.0
	400	0.36	116	135	73	28.0	141.0
	500	0.35	113	138	73	28.0	151.5
Isentropic potential vorticity	300	0.33	115	136	95	28.0	144.0
	400	0.33	114	137	98	28.0	147.0
	500	0.31	108	143	98	23.0	148.5
Forcing term	300	0.35	120	131	90	25.0	151.5
	400	0.31	114	137	116	19.0	142.5
	500	0.29	97	154	88	19.0	142.5

**Table D5** As for Table 2, but for heavy widespread rainfall events only using data for summer.

Diagnostic	Pressure level (hPa)	Max. CSI	Hits	Misses	False alarms	Latitude (°S) of max. CSI	Longitude (°E) of max. CSI
Geostrophic vorticity	300	0.38	101	155	49	29.0	144.0
	400	0.32	83	133	41	28.0	147.0
	500	0.31	80	136	45	29.0	144.0
Isentropic potential vorticity	300	0.27	72	144	49	31.0	147.0
	400	0.26	65	151	36	28.0	144.0
	500	0.28	84	132	85	32.0	154.5
Forcing term	300	0.22	60	156	55	26.0	145.5
	400	0.18	50	166	66	26.0	136.5
	500	0.22	67	149	189	23.0	138.0

**Table D6** As for Table 2, but for heavy widespread rainfall events only using data for winter.

Diagnostic	Pressure level (hPa)	Max. CSI	Hits	Misses	False alarms	Latitude (°S) of max. CSI	Longitude (°E) of max. CSI
Geostrophic vorticity	300	0.33	73	53	97	28.0	148.5
	400	0.35	82	44	108	26.0	144.0
	500	0.34	77	49	99	29.0	144.0
Isentropic potential vorticity	300	0.30	73	52	120	25.0	139.5
	400	0.29	75	51	130	26.0	144.0
	500	0.27	67	59	125	25.0	142.5
Forcing term	300	0.33	82	44	124	25.0	148.5
	400	0.29	76	50	136	20.0	139.5
	500	0.24	62	64	134	19.0	147.0





The Centre for Australian Weather and  
Climate Research is a partnership between  
CSIRO and the Bureau of Meteorology.